

University of Reading

Department of Meteorology

The North East Pacific Warm Blob; past, present
and future

Samantha Elizabeth Dickens

A dissertation submitted in partial fulfilment of the requirement for the degree
of Applied Meteorology MSc, August 2020.

i) Acknowledgements

First and foremost, I would like to thank Richard Allan and Ryan Jones for their continuous support, optimism and enthusiasm throughout this project. Within the duration of this project they made me feel part of a team and helped to keep me motivated, by constantly inspiring new pathways this project could take.

I would also like to thank Niamh Murray, a fellow student and friend, who always supports me in everything I do and always reassures me with her positivity and intelligence. Additionally, Kanzis Mattu, who alongside Niamh, has helped make my postgraduate year immensely enjoyable.

Working on this project in these difficult times was made easier by my hugely supportive family, friends and boyfriend Matt, who never fail to cheer me up and radiate kindness. A special thank you to my sister Francesca, who aided me with edits and read this extremely long project multiple times. As well as, Daisy and Charlotte who helped proof-read and motivate me. Additional thanks to my best friends Alice and Elysia who inspire me every day.

ii) Abstract

This study examines the characteristics, morphology, and incidence of a persistent positive sea surface temperature (SST) anomaly previously identified over the North East Pacific Ocean colloquially termed the "Warm Blob". Observations from the Hadley Centre Sea Ice and Sea Surface Temperature data set (HadISST) are employed to identify and assess the historical variability of the Warm Blob, focused on the 155-142.5°W and 37.5-45.5°N region off the Gulf of Alaska. Blob events are defined where SST anomalies exceed 1°C in magnitude. In addition, a corollary "Cold Blob" is identified as negative SST anomalies affecting this region are analysed for the first time. The most intense Warm Blob events are identified in 1986, 1989, 1991, 2000 and 2014 and Cold Blob events in 1987, 1998, 2007, 2016 and 2017. Warm Blobs are more homogenous in shape, size and location in comparison to the Cold Blob events. Warm Blobs are also more frequent, with 13 Cold Blob events having occurred since 1950 and 22 Warm Blobs, using a base period of 1981-2020. A relationship with anomalous sea surface temperatures in this region and various atmospheric teleconnection patterns is assessed. The Pacific Decadal Oscillation index is weakly negatively correlated with Warm Blob region SST anomalies ($r=-0.2$). A lag-lead analysis finds a maximum correlation between SST anomalies and El Niño Southern Oscillation 9 months later ($r=+0.39$). Future responses in the Warm and Cold Blob are investigated using 3 CMIP5 simulations assessing historical and a future high emissions scenario (RCP8.5). To account for global warming, a 5-year running average is removed. Warm Blob events are predicted to increase in frequency from 2050-2100 in comparison to 1950-2000, particularly for the IPSL-CM5B-LR model. The intensity of these Blobs will also increase in this later period as global SSTs increase due to climate change. Anomalies as large as $>+3^{\circ}\text{C}$ by 2080-2100 are identified, in comparison to a $\sim+2^{\circ}\text{C}$ anomaly maximum between 1980-2000. The standard deviation between these time periods increases by an average of 0.15°C . This occurrence will be mirrored by corresponding changes in negative temperature anomalies, suggesting the frequency of Cold Blob events will also increase. Further work can assess the development of the current 2019/2020 Warm Blob and the impacts of future Warm Blob events in a warmer climate.

Table of Contents

| | | |
|-------|--|----|
| i. | Acknowledgements | |
| ii. | Abstract | |
| 1.0 | Introduction..... | 1 |
| 1.1 | What is the Warm Blob? | 1 |
| 1.2 | Is there a Corollary of the Warm Blob?..... | 3 |
| 1.3 | Motivation..... | 4 |
| 1.4 | Project aims..... | 6 |
| 1.5 | The Phases of the Warm Blob..... | 6 |
| 1.6 | Links to Teleconnection Patterns..... | 8 |
| 1.6.1 | The El Niño–Southern Oscillation..... | 9 |
| 1.6.2 | The Pacific Decadal Oscillation..... | 11 |
| 1.6.3 | The Arctic Oscillation..... | 12 |
| 1.6.4 | The Madden Julian Oscillation..... | 13 |
| 1.6.5 | The North Atlantic Oscillation..... | 13 |
| 2.0 | Methodology and data | 15 |
| 2.1 | Data..... | 15 |
| 2.1.1 | The KNMI Climate Explorer..... | 15 |
| 2.1.2 | Observational datasets..... | 15 |
| 2.1.3 | Assessing the future of the Warm Blob..... | 17 |
| 2.2 | Methodology..... | 22 |
| 2.2.1 | Establishing the location of the Warm Blob..... | 22 |
| 2.2.2 | Analysing the years with the highest anomalies..... | 23 |
| 2.2.3 | Links to Teleconnections..... | 24 |
| 2.2.4 | Changes in the future..... | 24 |
| 3.0 | Results and Discussion..... | 25 |
| 3.1 | Morphology, development and characteristics of the Blob..... | 25 |
| 3.2 | Occurrence of warm and cold events in the historical period..... | 29 |
| 3.3 | Occurrence of warm and cold events in with global temperature anomalies removed..... | 31 |
| 3.4 | Comparison of Warm Blob events..... | 33 |
| 3.5 | Comparison of Cold Blob events..... | 36 |
| 3.6 | Comparison of sea surface temperature anomalies and mean sea level pressure..... | 39 |
| 3.7 | Change in frequency and intensity of Warm and Cold Blobs..... | 43 |
| 3.8 | Links to atmospheric teleconnection patterns..... | 44 |
| 3.8.1 | El Niño Southern Oscillation..... | 46 |
| 3.8.2 | Pacific Decadal Oscillation..... | 49 |

| | | |
|-------|---|----|
| 3.8.3 | Arctic Oscillation..... | 51 |
| 3.8.4 | Madden Julian Oscillation..... | 52 |
| 3.8.5 | North Atlantic Oscillation..... | 53 |
| 3.9 | How will the Blob respond to climate change?..... | 59 |
| 4.0 | Conclusions..... | 61 |
| 4.1 | Summary..... | 61 |
| 4.2 | Limitations..... | 62 |
| 4.3 | Future Work..... | 64 |
| iii) | References | |

The North East Pacific Warm Blob; past, present and future

1.0 Introduction

1.1 What is the Warm Blob?

In 2015 Bond *et al.* identified an anomalously warm region of sea surface temperatures (SSTs) in the North East Pacific. In recognition of this abnormal feature, its persistence, and its potential for impacting both the regional weather and marine life, they titled the phenomenon the “Warm Blob” (Bond *et al.*, 2015).

The North East Pacific Warm Blob is a warm region of sea surface temperatures located off the Gulf of Alaska that stretches along the coast of California and extends from 40°–50°N and 150°–135°W (Bond *et al.* 2015). It has appeared periodically since 2013; however, data between 2013 and 2015 has found that the highest anomalies occurred during the winter of 2014 and the summer of 2015; reaching +2°–3°C (Liang *et al.*, 2017; Bond *et al.* 2015; Hu *et al.*, 2017). These large surface anomalies in temperature are also characterised by sub-surface temperature anomalies (see Figure 2).

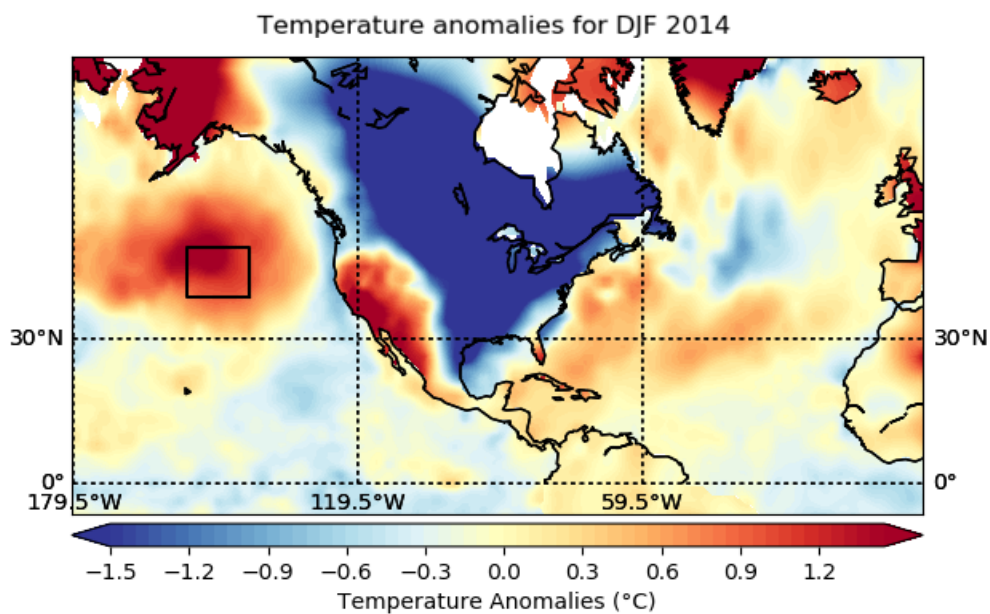


Figure 1: A plot to show the Sea Surface Temperature Anomalies, seasonally averaged over the monthly data for December (2013), January and February of 2014. Using the HadISST1 SST anomalies dataset minus the HadSST global temperature anomaly data set (SST anomalies). The average land temperature anomalies are from the Berkley dataset. Anomalies were calculated with the base period 1981-2020. The black box here indicated the Warm Blob region of interest 155-142.5°W and 37.5-45.5°N.

This map identifies the 2014 Warm Blob and displays its common characteristics. It is circular in shape and is located within the Gulf of Alaska, around 1000km from the coast of California. The box marks the region of the Blob, temperatures are intensified in the centre and are then seen to dissipate outwards. Although warm SST anomalies (SSTa) cover a wider region than just the area bounded by the box, the

main point of focus is the highest SSTa concentrated in the centre. Within the area bounded by the box, temperatures appear to have a maximum SST anomaly $>+1.5^{\circ}\text{C}$.

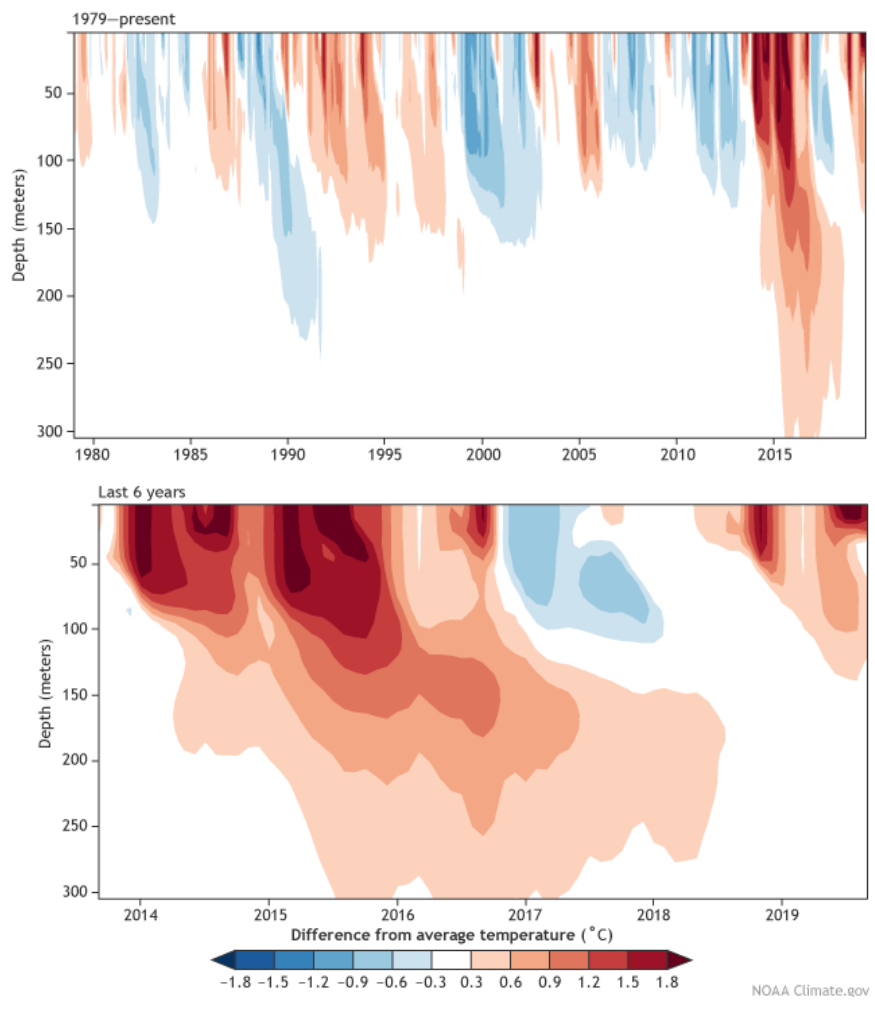


Figure 2: An averaged depth profile of temperature anomalies in the North Pacific in the region occupied by 150°W - 130°W , 40°N - 50°N . This includes data from 1980-2020 and is constructed using an ensemble of ocean reanalysis from NOAA (NOAA, 2019).

Figure 2 shows that the warm temperatures are limited to the upper 300m of the surface waters (Hu *et al.*, 2017), suggesting that more heat is trapped in the upper water column of a shallower mixed layer, resulting in higher temperatures that sustain the surface warming (Zhi *et al.*, 2019). This Figure identifies that the Warm Blob was persistent through 2013-2015 in the surface waters (upper ~150m). Also observed is an anomalous Cold Blob in 2017, with temperature anomalies reaching as cold as -1.2°C .

The Warm Blob has reappeared, in the Pacific, from the beginning of 2020 (Amaya *et al.*, 2020). This is supported by the higher temperatures shown in Figure 2 which begin to develop at the end of 2019.

SST Anomalies for April 2020

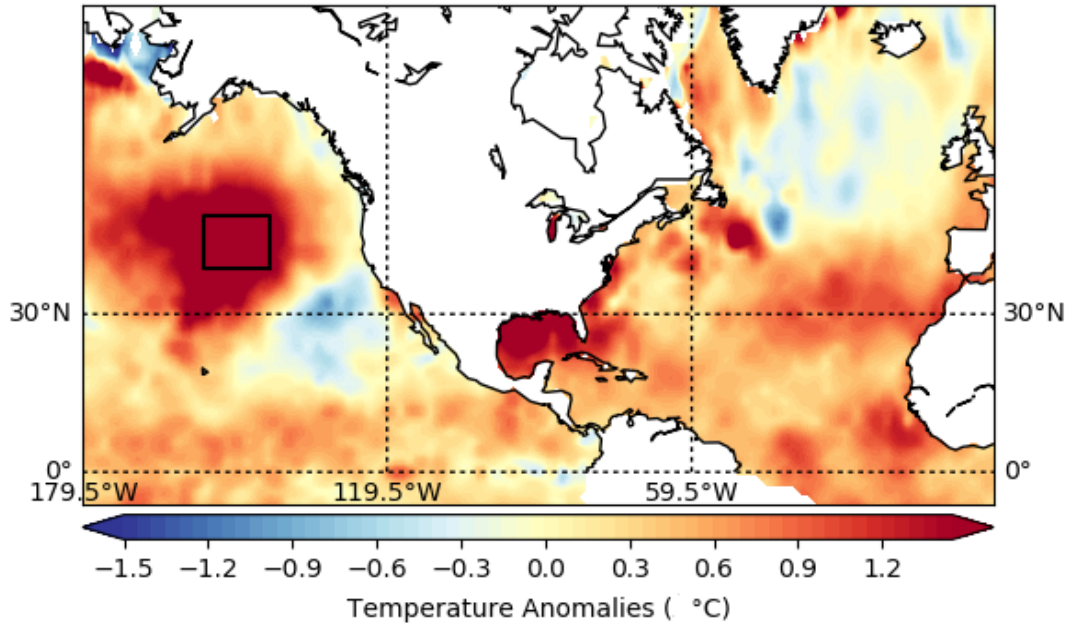


Figure 3: A plot to show Sea Surface Temperature Anomalies for April 2020 demonstrating the redevelopment of the North East Pacific Warm Blob. Using the HadISST1 SST anomalies data set minus the HadSST global temperature anomaly data set (SST anomalies). Anomalies were calculated with reference to the base period 1981-2020. The black box here indicated the Warm Blob region of interest 155-142.5°W and 37.5-45.5°N.

Figure 3 demonstrates the redevelopment of the Warm Blob in 2020. In the region bounded by the black box, temperature anomalies reach as high as $>+1.5^{\circ}\text{C}$. The concentrated region of high SST anomalies in Figure 3 are also supported by data in Figure 2 which shows that in 2020, warm subsurface waters occur reaching $\sim+1.8^{\circ}\text{C}$. Data is limited for this period; however, a greater understanding of this Blob could be established over time.

1.2 Is there a Corollary of the Warm Blob?

The North East Pacific Warm Blob has a key identity in the scientific community; however, as demonstrated in Figure 2, this region experiences both above average positive anomalies and negative anomalies of the same magnitude. This means that it has experienced extreme cold SST anomalies in relation to the surrounding area and seasonal average and suggests that not only does this region experience a Warm Blob but a potential Cold Blob too.

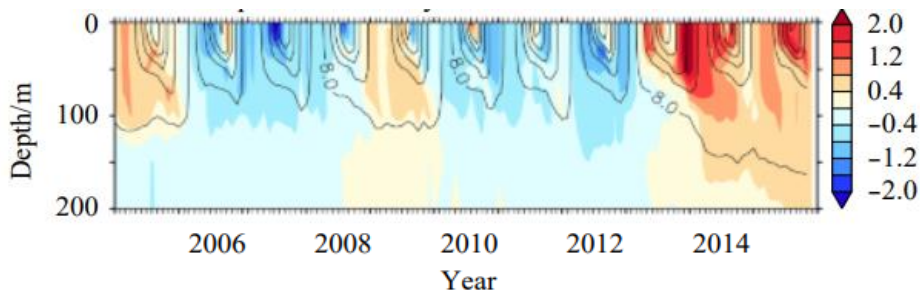


Figure 4: The time-depth profiles of the regionally averaged temperature anomalies of the Warm Blob using the location averaged area data for 40° – 50° N, 155° – 140° W. Using data acquired from the Array for Real-time Geostrophic Oceanography (Argo) provided by the International Pacific Research Centre (IPRC)/Asia-Pacific Data-Research Centre (APDRC) (Hai *et al.*, 2019)

Figure 4 demonstrates this clearly highlighting warming and cooling phases in comparison to the seasonal average, as well as anomalous extremes $>+/-2^{\circ}$ C. This depth profile shows that the largest cold anomaly was experienced in 2007, $\sim -2^{\circ}$ C in this specific location (40° – 50° N, 155° – 140° W).

Although the Cold Blob is not as widely researched as the Warm Blob, large anomalously cold temperatures can be identified intermittently in Figure 4 in 2007, 2008, and 2012. These extreme temperatures can also be seen in Figure 2 from Zhi *et al.*, (2019), which demonstrates the negative anomalies in the sub-surface profile.

The Cold Blob can be identified within the timeseries of SSTa when investigating the Warm Blob in studies by Yu-Heng Tseng *et al.*, (2017), as well as in mapped anomalies by Hu *et al.*, (2017). In these investigations the magnitude of the Cold Blob matches that of the Warm Blob (as large as $+/-2^{\circ}$ C), this suggests that the Cold Blob is as significant as the Warm Blob; however, it has not been as common in recent years.

1.3 Motivation

It is to be noted that this phenomenon is often referred to as a ‘marine heatwave’ (Di Lorenzo and Mantua, 2016). This is due to record-breaking high temperatures experienced in this region and the multi-year persistence of this warm anomaly. However, the effects of the Warm Blob have been speculated to influence not only the marine environment, but the surrounding land. It is currently unknown why and on what time frame this anomalous Blob appears and whether it can be forecasted (Hu *et al.*, 2017).

Initially in 2013, the Blob was not predicted even a couple of months in advance and neither was the ongoing heatwave in the North East Pacific. However, a marine heatwave that results from a strong El Niño event has much greater potential to be predicted (>6 months in advance), in comparison to the predictability of SST anomalies in the tropical Pacific which cannot be explained by the El Niño Southern Oscillation (ENSO) (Xue *et al.*, 2013). This is due to weaker prediction skills in the extratropical northern atmosphere and ocean (Wen *et al.*, 2012; Hu *et al.*, 2013, 2014; Hu and Huang,

2006), meaning that it is more challenging to successfully predict SST anomalies in the midlatitude oceans.

The forecast ability of this phenomenon will be largely dependent on the ocean- atmospheric interactions, as well as global teleconnection links. However, the purpose of the present analysis is to characterise and understand the evolution of comparable Warm Blob events over a longer period.

Atmospheric circulation anomalies played a key role in initiating and maintaining the North Pacific Warm Blob (Bond *et al.*, 2015). In certain periods when this Blob is apparent, unusually high pressures off the Gulf of Alaska reduce heat loss to the atmosphere and cold advection over the region. Forcing of the atmospheric anomalies have been linked to SST anomalies in the western tropical Pacific Ocean (Seager *et al.*, 2015) and to decadal-scale variability in North Pacific Ocean modes (Di Lorenzo and Mantua, 2016). According to the mixed layer temperature budget, these anomalies were caused by a lowering of heat loss from the ocean to the atmosphere alongside relatively weak, cold advection in the upper ocean (Bond *et al.*, 2019). An unusually strong and persistent weather pattern relate these fluxes where a resilient ridge of high mean sea level pressure (MSLP) anomalies existed over the region of interest (Yang *et al.*, 2019).

By assessing these various interactions, it will be determined whether the Blob can be understood both temporally and spatially, and whether the Blob occurs intermittently over a specific time frame. Although this topic is widely researched, there is little information regarding how this Blob will change in the future. Due to the large impacts this Blob has on weather and climate, which will be later addressed, being able to forecast this anomaly could save both money and livelihoods.

The effects of the Warm Blob are extensive, affecting the marine ecosystem and, the meteorology and climate in the area. Studies by Bond *et al.* (2015) discuss how the presence of this anomalous Blob can be explained in relation to various teleconnections. A teleconnection is a climatic or meteorological connection or correlation between two phenomena which rarely occur in the same region, for example a phenomenon in the Pacific may affect, and be affected by, weather patterns in the Atlantic. Teleconnections of possible relevance to the Warm Blob include the North Atlantic Oscillation (NAO), El Niño Southern Oscillation (ENSO), Pacific Decadal Oscillation (PDO), the Madden Julian Oscillation (MJO) and the Arctic Oscillation (AO). Studies claim the Blob holds influence over the drier, winter cold outbreaks across North America (Wang *et al.*, 2014) and enhanced summer warm outbreaks (Kintisch, 2015). Additionally, it was found that this warming has more remote effects. In 2013-2014, while most countries in Europe experienced a milder winter, the UK experienced its wettest winter on record (Lee *et al.*, 2015). It has been discussed that this impact on the UK is a result of the North Atlantic Oscillation as well as effects of the Warm Blob; these teleconnection links will be later discussed.

1.4 Project Aims

This project aims to investigate the environmental conditions surrounding each instance when the Warm Blob and Cold Blob are identified. The project also looks to explore:

- i) Its characteristics - the morphology, development and influence of this sea surface temperature anomaly on regional climate using observations and simulations.
- ii) Links to teleconnections - whether the presence and strength of the sea surface temperature anomalies are associated with atmospheric circulation patterns.
- iii) The ability to forecast - using linear regression to investigate whether teleconnections can be used to predict the development of this Blob effectively.

Within these subcategories, there will be more specific aims within this project including:

- a) How often do the Warm and Cold Blobs occur and is the period between the Blobs constant or has a pattern developed?
- b) What is the spatial structure of sea surface temperature anomalies over the Warm/Cold Blob periods?
- c) What surface pressure systems are associated with the Warm and Cold Blobs?
- d) Which teleconnection pattern displays the strongest correlation with the Warm/Cold Blob events?
- e) Is there a lagged relationship between the sea surface temperature anomalies and global teleconnections?
- f) How will the appearance of these Blobs change in the future as well as their frequency and intensity?

1.5 The Phases of the Warm Blob

The Warm Blob has been identified at several time points throughout history. These are often called “phases” of the Blob. In the first phase, the Blob appeared off the southern coast of Alaska in 2013 and persisted for around 8 months, reaching nearly 2000km wide and 100m deep in size (Kintisch, 2015). During this time, SSTs offshore in the North East Pacific were remarkably warm. It has been suggested that this was a result of a resilient ridge of high pressure and warming off the Gulf of Alaska (Amaya *et al.*, 2020).

This resilient ridge of high pressure and warming, partnered with deflected wintertime storms north off California, led to an intensifying “Mega Drought” (Swain *et al.*, 2014). This ridge was a result of the high geopotential height (GPH) anomalies, which occurred in the North East Pacific during this time. This resulted in anomalous geostrophic flow occurring as a result of the large GPH gradients. Over the Pacific, these gradients were characterised by weakened westerly zonal winds. These winds strengthened zonal flow over Alaska and a pair of meridional wind anomalies centred in the North

Eastern Pacific around 135°W occurred in Polar and equatorward regions. This atmospheric anomaly displaced the jet stream north, which led to minimal storm activity and record-low precipitation in California (Swain *et al.*, 2014).

It has been suggested that the jet stream perturbations within this period, contributed to a historically cold North American 2013/2014 winter (Hartmann, 2015) and was the main forcing mechanism for the Gulf of Alaska Warming (Bond *et al.*, 2015).

This ridge of high surface pressure was highly resilient due to three main factors (i) teleconnections to the North Pacific from the western tropical Pacific (Seager *et al.*, 2015) (ii) loss of Arctic sea ice (Lee *et al.*, 2015) and (iii) internal variability (Seager *et al.*, 2015). From October 2013 through January 2014, mean sea level pressure anomalies (MSLPa) were much higher than normal “with a peak magnitude approaching +10 hPa” (relative to the base period of 1981-2010) (Bond *et al.*, 2015). Bond *et al.* (2015) concluded that the Gulf of Alaska Warming was a result of a lack of seasonal cooling. This was a result of a significant reduction in energy imparted by the atmosphere into the ocean for wintertime mixing processes due to this resilient high ridge.

The Blob re-intensified in the spring of 2014. In this instance peak temperature anomalies in the upper 100m of the surface waters were greater than +2.5°C, in respect to the base period 1981-2010 (Bond *et al.*, 2015). In the Boreal winter, at the same time the Blob was visible, many anomalous weather and climatic events were recorded in the extratropical Northern Hemisphere. This includes an unusually warm winter in Alaska and the Bering Sea, with anomalies as large as +2°C, wildfires and severe droughts in California and intense snowstorms and cold temperatures in eastern North America (Lee *et al.*, 2015). It was thought that these weather events occurred as a result of El Niño warming, yet the ENSO index demonstrates that an El Niño event did not occur until the end of 2014-2016. Although an El Niño warming phase did not occur through 2013-2014, the Warm Blob may have been intensified in 2014 due to this effect (Lee *et al.*, 2015).

It has been suggested that the second phase of the Blob occurred as a result of the dissipation of a high-pressure ridge. The ridge led to patches of warm water spreading along the coast from Alaska to central Mexico, under wind driven processes. During the summer of 2014, the Blob was kept well offshore as a result of Ekman transport associated with coastal upwelling (Kintisch, 2015).

This anomalous ridge of high pressure was observed over the west coast of North America, Alaska and at high latitudes in the North Pacific extending northwards into the Arctic. The high pressure was associated with a dipole low pressure system over eastern North America and the extratropical North Atlantic. A positive pressure anomaly was also observed over the subtropical North Atlantic (Lee *et al.*, 2015). These anomalous pressures over America have been linked to a reduction in sea ice extent and concentration, both of which are a predicted result of the warmer SSTs (Gastineau and Frankignoul,

2015). The overall background warming is a result of the increasing atmospheric temperature attributed to increased greenhouse gas concentrations (Lima and Wethey, 2012). However, the removal of global temperature anomalies alone does not sustain as evidence for the SST anomalies of the Warm Blob.

While long-term trends in global SSTs are moderately well known, an overview of historical occurrences of marine heatwaves, as well as the mechanistic understanding of their associated processes is currently unclear (Frölicher and Laufkötter, 2018). Individual studies note exceptions, indicating that marine heatwaves have become more common in more than one-third of the world's coastal oceans (Lima and Wethey, 2012).

By the summer of 2014, this area of anomalously warm SSTs in the North Pacific extended into the coastal region and persisted through to the spring of 2015 (Bond *et al.*, 2015). The Warm Blob continuously developed into a strong El Niño, which due to the phase locking to the seasonal cycle, reached its mature phase by the end of 2015 (Yu-Heng Tseng *et al.*, 2017). An El Niño phase was observed between 2014-2016 and has been recognised as one of the strongest on record (Tseng *et al.*, 2017).

1.6 Links to teleconnection patterns

In a study by Lorenzo and Mantua (2016) it was stated that the development and persistence of the original 2013 Warm Blob displayed a relationship between the North Pacific and the Tropical Pacific, as a result of long-distance teleconnections. This is supported by current literature which linked these anomalous temperature events with an unusually warm winter in Alaska and the Bering Sea, as well as, wildfires and severe drought in California (Swain *et al.*, 2014).

The Blobs have also been linked to the boreal winter of 2013/2014 where severe snowstorms and cold temperatures occurred in eastern North America (Lee *et al.*, 2015). Through investigations into this Blob, its occurrence has been explained as a mixture of other phenomena including: the El Niño–Southern Oscillation, the Pacific Decadal Oscillation, the Arctic Oscillation, the North Pacific Gyre Oscillation, the Madden Julian Oscillation as well as the North Atlantic Oscillation.

The role of climate feedbacks should be emphasised, as they are responsible for amplifying the initial SST anomalies and the eventual negative feedbacks that reduce these anomalies. Not only may feedbacks play a part in the initial generation of the Blob but they are also involved in generating the development and sustaining the Warm Blob. For example, cloud feedbacks are identified to be important in amplifying warming in this and other stratocumulus regions (Loeb *et al.*, 2020). It has been analysed that increased SSTa in this region reduces cloud cover, thus further decreasing the short-wave radiation flux, altering the radiation budget. The radiation budget is vital when investigating SST anomalies and thus, consequent changes in the net heat budget. The Earth's radiation budget depicts the balance between incoming solar radiation absorbed by Earth and the resultant radiation reflected back

to space (Loeb *et al.*, 2020). Various teleconnections alter variables including SSTs, land temperatures and pressure, which in turn modify the radiation budget.

1.6.1 The El Niño–Southern Oscillation

The first phenomenon of interest in this investigation is the El Niño–Southern Oscillation (ENSO). ENSO is a coupled ocean-atmosphere phenomenon with global influences. It is an important mode of variability in the climate system (Chen *et al.*, 2019). An increased understanding of the ENSO has enabled the creation of useful forecasts of seasonal weather and climate conditions, a season or more in advance (Hartmann, 2015). This global oscillation has two phases, a warmer phase called the El Niño and a colder phase called the La Nina. Both phases of the ENSO have a large impact on weather and climate in North Pacific.

Lau and Nath (2001) reported that ENSO events coincide with noticeable changes in the midlatitude SST patterns in the North Pacific and North Atlantic. Their research concludes that multiple processes may be in action including the extratropical atmosphere response to disturbances in tropical forcing during ENSO events. Midlatitude atmospheric anomalies, incur local disturbances on the underlying ocean through changes in the energy flux across the sea–air interface. This leads to subsequent extratropical SST anomalies (Lau and Nath, 2001).

It has been concluded that changes in the tropical cyclone activity in the Western North Pacific are associated with the warm phase of the ENSO, a consequence of longitudinal changes in the rising and sinking branches of the Walker Circulation (Chan, 2000). Chan (2000) states that a year after the mature phase of the warm ENSO, this tropical cyclone activity over the ocean basin tends to be below normal. These tropical cyclones occur when sea temperatures are at their highest, usually in autumn after temperatures have built up over the summer. When ocean temperatures reach at least 27°C, the warm air rises and evaporates quickly, causing an area of very low pressure. Therefore, the increased frequency of tropical cyclones acts as a key indicator that the SSTs in this region are very warm, translating the link between ENSO and SSTs in the Warm Blob region.

ENSO events are related to an anomalous zonal SST gradient over the west Pacific Ocean (Hoell and Funk, 2013). Various investigations involve research on SST-forced teleconnections to the North Pacific during boreal winter when important climatic phenomena, like the ENSO, tend to peak (Howell and Funk, 2013). The intermittent phases between ENSO variations over the North East Pacific can be large and therefore the predictability of the regional climate is difficult (Hoell and Funk, 2013).

Feng *et al.* (2014) has demonstrated that the 2014 marine heatwave enhanced the El Niño event in the following year. This is a result of air-sea interaction resulting in the warm temperatures near the coast of Hawaii. These migrate southward to reach the equator. This means that the Blob likely contributed to the El Niño event which occurred in 2015/16 (Jacox *et al.*, 2019).

Although El Niño events occur in the tropical Pacific, the effects of this teleconnection are global, and this phenomenon influences the SSTs in the North Pacific. This is a result of the winds coming from the southwest near to the West coast of the US during an El Niño event which warm the ocean underneath: through downwelling. The ocean then pushes the colder denser water deeper and the warmer water rises, this warms a very narrow region adjacent to the coast (Bylhouwer *et al.*, 2013). In 2014, an El Niño did not occur until the end of the year; this likely contributed to the persistence of the Warm Blob (Newman *et al.*, 2003; Alexander *et al.*, 2010)

Jacox *et al.* (2019) states that the El Niño is a very common cause of warm water anomalies in the Pacific, as a result of heat flux exchanges in the surface waters which induces changes in climate patterns. The Niño of focus in this area is Niño3.4 and located in the region 5°N-5°S, 120°-170°W (Cheng *et al.*, 2020). El Niño events tend to produce ocean warming at the international date line, and the Pacific basin, by changing the wind patterns off the US west coast, these winds typically cool the coastal ocean. This occurs through oceanic teleconnections, in which coastally trapped kelvin waves propagate northward along the North American west coast (Jacox *et al.*, 2019). Aforementioned by Newman *et al.* (2003), the original Blob wasn't necessarily caused by an El Niño event, but the presence and enhancement of this ENSO is what likely caused the Blob to persist and extend in size.

The formation of the 2014 Blob occurred under a strong, stationary, blocking atmospheric high-pressure system. The near-surface ocean heated rapidly, associated with weak winds and warm air temperatures caused by the blocking. These blocking events over the North Pacific are normally common during a La Nina phase of the ENSO. Weather patterns like blocking can occur randomly due to the chaotic nature of the atmosphere so may not necessarily be a result of ENSO influences. This warming may also be related to changes in ocean currents such as the Gulf Stream in the Atlantic and the Kuroshio current which may have a large influence over longer periods of time (Grossil *et al.*, 2017).

Feng *et al.*, (2014) claim that both the ENSO and the warm water anomalies are likely to be interlinked, yet it is not clear which is the cause, and which is the effect. Scientific conclusions in relation to the impacts of the Blob on the weather (e.g. Bond *et al.*, 2015; Hartmann, 2015) and how a strong ENSO phase and strong Blob are linked should be handled with discretion. Particularly in the North Pacific, due to the complicated ocean-atmosphere relationship. This teleconnection relationship discussed played a key role in 2014, maintaining the persistence of the North Pacific atmosphere from 2013-2015 (Di Lorenzo and Mantua, 2016); however, the relationship between the Blob and the 2015/16 El Niño has not yet been addressed.

1.6.2 The Pacific Decadal Oscillation

Connected to ENSO, another phenomenon of interest is the Pacific Decadal Oscillation (PDO). The PDO is often described as either a long-lived El Niño-like pattern of Pacific climate variability (Zhang *et al.* 1997) or a combination of two occasionally independent modes, which have very distinct spatial and temporal characteristics in SST variability (Hare and Mantua, 2000).

The PDO can be identified by widespread fluctuations in both the Pacific Basin and the North American Climate. The PDO appears to function in parallel with ENSO where extreme phases can be classified as being warm or cold. These phases can be based on SST anomalies in the northeast and tropical Pacific Ocean (Mantua *et al.*, 1997). The PDO has a positive value when SSTs are anomalously cool in the North Pacific and warm across the Pacific coastline and when sea level pressures are below average. Alternatively, the PDO has a negative value when the climate anomaly patterns are reversed. When SST anomalies are warm offshore in the North Pacific and cold along the Californian coast, as well as positive anomalies in sea level pressures (Mantua *et al.*, 1997).

The PDO is defined only by the SSTs in the North Pacific region poleward of 20°N (Mantua *et al.*, 1997; Zhang *et al.*, 1997). The spatial pattern of the PDO resembles an arc, with opposing SST anomalies in the central North Pacific in relation to those in the Gulf of Alaska. The phase period of the PDO is between 20 to 30-years (Jo *et al.*, 2013) which can be studied in relation to the SST anomalies in the Warm Blob to test for correlation.

Widespread impacts occur as a result of interdecadal changes in Pacific climate including land temperatures and marine environment conditions in the North Pacific. This explanation, as well as, the effects of ENSO could support the reason the warm water anomaly develops in the North Pacific. This will be later assessed in the results and discussion section of this project.

In the period of 2013-2015, where the Warm Blob was identified, the eastern movement of the Blob closer to the coastline and the cooling in the Central Pacific produced a spatial distribution of SST that resembled a positive PDO pattern. During this time frame, the PDO index was the highest positive ever recorded for winter months. The values reached +2.51 in December 2014 and +2.45 in January 2015 (Peterson *et al.*, 2015). This demonstrates that when this Warm Blob was prevalent, the positive PDO phase strengthened as the SST pattern in this region, at this time, symbolised the anomalies which occur in a positive phase (Jacox *et al.*, 2015). This suggests that Warm Blobs are linked to a positive PDO phase (Peterson *et al.*, 2015).

Closely related, the North Pacific Gyre Oscillation (NPGO) describes periodic variability related to the PDO. This fluctuation occurs on decadal time scales and affects multiple variables including salinity, nutrients and subsequently marine life (Di Lorenzo *et al.*, 2008). The PDO correlates with the NPGO as it is the result of the large-scale climate variability in the region driven by the PDO. Fluctuations in

the NPGO are driven by regional and basin-scale variations in wind-driven upwelling and horizontal advection (Di Lorenzo *et al.*, 2008). This wind driven variability can also lead to temporal changes in surface waters (Di Lorenzo *et al.*, 2008) resulting in the transport of warm sea surface temperatures resulting in anomalous warming effects such as the Blob.

1.6.3 The Arctic Oscillation

Although global atmospheric circulations influence the presence of the Warm Blob, more local scale influences on the North Pacific can have a substantial impact. Recent warming in the Arctic regions is thought have strong impacts on midlatitude weather patterns (Cohen *et al.* 2012, Lee *et al.* 2015; Yu *et al.* 2017). The potential factors for the phase-locking of the Tropical Northern Hemisphere pattern may stem from the forcing related to specific Tropical Pacific Ocean or polar conditions (Liang *et al.*, 2017).

It is useful to distinguish between unforced variability and variability forced by natural or anthropogenic causes. Unforced variability arises from the internal dynamics without any specific cause. Whereas, forced variability can be associated with some change in the boundary conditions of the climate system, such as changes in the radiation budget on the natural side or increased carbon dioxide (CO₂) emissions on the anthropogenic side. A forced response is defined as the variable's total response to external forcing i.e. in this case, the Arctic Oscillation's (AO) forced response is Arctic warming which occur as the result of global warming and increased SST (Sipple *et al.*, 2019). However, unforced effects on the AO could be influences of the ENSO.

Internal variability also strongly affects polar conditions which can be largely characterised by the Arctic Oscillation. The AO is a large-scale mode of climate variability, it is a climate pattern by which winds circulate around the Arctic at a latitude ~55°N latitude, in an anti-clockwise motion. In a positive phase, colder air across polar regions is more confined as a result of a ring of strong winds circulating the North Pole. In the negative phase, the winds weaken, and the belt becomes more distorted. This allows for an easier southward infiltration of colder, arctic airmasses and increased storminess into the midlatitudes (Grossi *et al.*, 2017).

Careful monitoring of the Arctic is of great importance to the scientific community due to amplification in the Arctic. This involves temperatures in the Arctic increasing at more than twice the rate of the Northern Hemisphere (Serreze *et al.*, 2009; Cohen *et al.*, 2014). This Warm Blob could be related to the significant warming, intensifying the rate at which the Arctic warms through the transportation of the Warm Blobs anomalously warm SSTs via the Alaskan current (Serreze *et al.* 2009).

An assessment of this suspected relationship can be provided in 2013-2015 where the Warm Blob occurrence was coupled with a strong positive AO year which occurred in 2013. This correlation implied a “blocking regime with a wavy jet stream pattern”, where cold north westerly winds penetrated into Central America (Overland and Weng, 2016). In 2014, a negative phase of the AO occurred, this

contributed to the formation of positive temperature anomalies in the central Arctic. The timing of these events could suggest that the two are linked; the Warm Blob occurred in a negative AO phase (2014), as a result of changes in pressure and therefore changes in the wind pattern (Overland and Weng, 2016). Subsequently, the Arctic saw widespread regions of temperature amplifications in the winter of 2016, related to extensive low geopotential heights at 700 hPa extended over south eastern America (Overland and Weng, 2016). An investigation of the relationship between SSTs in the Warm Blob region and sea level pressure (SLP) would prove useful in relating the AO with the Warm Blob.

1.6.4 The Madden Julian Oscillation

The Madden Julian Oscillation (MJO) is a global teleconnection pattern which propagates eastwards concentrated around the equator. It is a migrating assembly of clouds, rainfall, winds and pressure that rotates longitudinally around the planet in the tropics, returning to its initial location. Its oscillation period is uncertain and can be seen on a timescale of 30-60 days (Maloney and Hartmann, 2000). It controls tropical weather however, through atmospheric-ocean interactions it could have an impact on the warming of SSTs. In comparison to ENSO, which can last several seasons over the Pacific Ocean basin, there can be multiple MJO events within a season. The MJO consists of two phases; a convective and suppressed phase. The convective phase enhances rainfall while the suppressed phase reduces rainfall.

The MJO can influence both the frequency and strength of tropical cyclones in the Pacific ocean basin through the transportation of heat and moisture (Maloney and Hartmann, 2000). It can cause changes in the jet stream that lead to cold air outbreaks, as well as extreme heat events and flooding rains over North America (Riddle *et al.*, 2013; Johnson *et al.*, 2014).

Warming of the tropical Pacific can also lead to the development of this marine heatwave through atmospheric-ocean interactions and teleconnections. Atmospheric intra-seasonal oscillations such as the MJO serve as the major source of intra-seasonal westerly wind events during El Niño events (Lyu *et al.*, 2018). This was evident during the early onset of the 2015/2016 El Niño, where the MJO induced Westerly Wind Events in the equatorial Pacific (Hong *et al.*, 2017).

1.6.5 The North Atlantic Oscillation

Another teleconnection inducing the seasonal and intraseasonal changes in this region is the North Atlantic Oscillation (NAO). This involves a positive and negative pressure dipole over the North Atlantic, resulting in extreme changes in surface pressure off the Azores and Iceland. Although this phenomenon has a more obvious effect on the North Atlantic than the North Pacific, teleconnections link the two oceans through the global ocean conveyor belt. The NAO is simply a regional manifestation of the larger scale AO pattern (Thompson and Wallace, 1998).

As well as the Warm Blob in the North Pacific, an opposing Cold Blob was identified in the North Atlantic. This is also known as ‘the Atlantic warming hole’ (Rahmstorf *et al.*, 2015). The North Pacific Warm Blob and the North Atlantic Cold Blob have been seen to be concurrent: in 2013-2015 the appearance of the Warm Blob coincided with persistently cold SSTs in the North Atlantic (Liang *et al.*, 2017).

The cause of the Atlantic Cold Blob is unclear: multiple mechanisms have been used to explain this anomaly including atmospheric forcing associated with the NAO (Delworth *et al.*, 2016). This phenomenon is connected to the Atlantic meridional overturning circulation (AMOC) (Rahmstorf *et al.*, 2015), whereby warm salty water is transported northwards in the upper layers of the Atlantic, accompanied by a deep southward flow of colder, denser water - all part of the thermohaline circulation (Rahmstorf *et al.*, 2015). The AMOC is also associated with the melting of the Greenland ice sheet (Bakker *et al.* 2016).

There is limited evidence regarding the co-existence of the Atlantic and Pacific Blobs indicating that scientists consider them separate. This is supported by evidence also suggesting they are driven by differentiating mechanisms (Liang *et al.*, 2017). However, there is a possibility that the two phenomena relate and may be linked by atmospheric circulation patterns.

In this dissertation, the relationship between the Pacific Warm/Cold Blob and the NAO will be statistically analysed to determine whether these are related. If a significant conclusion is reached, this connection between oceans can be used as a mechanism to explain climate connectivity between the North Pacific and North Atlantic. This could prove useful as a valuable forecasting tool, establishing the occurrence of the Pacific and Atlantic Blob events (Liang *et al.*, 2017).

As discussed, multiple phenomena could be the driving mechanisms behind the presence of the Warm and Cold Blob, each of these teleconnections will be investigated statistically in Section 4.2.

2.0 Data and Methodology

2.1 Data

2.1.1 The KNMI Climate Explorer

The KNMI Climate Explorer is a web application which analyses climate data statistically and is available from the following link: <https://climexp.knmi.nl/start.cgi> (Oldenborgh and Burgers, 2005).

This explorer contains various weather and climate variables in the form of; observations, simulations, and reanalysis data, as well as CMIP models. The site is maintained by a single member of the Royal Netherlands Meteorological Institute (KNMI) and all data is freely available. Within this site one can use statistical analysis and format the data in the desired format required. Many of the variables used in this report investigate anomalies, which were calculated by the KNMI explorer with a chosen base period. Plots created in this report were also cross-checked using the mapping tool on this site to ensure data was read in and mapped correctly.

2.1.2 Observational datasets

This project begins looking at observations in the form of monthly data delivered in a latitude/longitude grid, with 1.0° resolution. Prior to using this data, an area of focus in the north-east Pacific was determined, as discussed in Section 3.2.1. The main variable of focus throughout this project is sea surface temperature anomalies (SSTa). The observational SST anomalies were derived using the base period of 1981-2020, this has been used for every anomaly variable in this investigation unless stated otherwise. Certain variables have been investigated in the form of anomalies, in order to identify relationships between extremes.

One of the most frequently used SST datasets is derived from the UK Met Office's Hadley Centre: the HadISST1 dataset (Rayner *et al.*, 2003). It has a horizontal resolution of $1.0^\circ \times 1.0^\circ$ and a time span from 1870 to the present day. The high grid resolution means the Blob could be accurately mapped in a latitude/longitude grid, as well as having a large historical record. This record meant that the Blob could be investigated further into the past than has been examined according to literature. This dataset is based on carefully homogenised observations and gaps in the data are filled through interpolation. HadISST1 corroborates well with other published analyses, including trends in SSTs successfully at different spatial scales; global, hemispherical, and regional, comprising SST fields with more homogenous variance overtime and improved monthly persistence than other SST models (Rayner *et al.*, 2003).

There are limitations in the HadISST1 dataset and care should be taken when analysing this data for investigations of observed climatic variability, particularly if data is sparse in some regions. This is a result of limitations within the interpolation techniques (Sheppard and Rayner, 2002). It is recommended that the HadSST dataset be used in conjunction with HadISST1 in order to include the

effects of climate change (Jones *et al.*, 2001). This collaboration of datasets was used in the Third Assessment Report of the Intergovernmental Panel on Climate Change (IPCC) (Folland *et al.*, 2001). This is why analysis of the global temperature anomalies dataset from the HadSST 3.1.1.0 northern hemisphere averaged SST anomalies occurred, in certain aspects of this project, in an attempt to remove the global warming pattern.

Additionally, early observations of the HadISST1 dataset, i.e. in 1880, were made by collecting water samples in poorly insulated buckets. This data incurs systematic error as the buckets lose heat as they were brought up to the deck, therefore introducing a continuous cold bias into the early SST records (Smith and Reynolds, 2002).

The variables used within this report were not all available for the same time period. The observational data including the SST anomalies (HadiSST1) as well as the global temperature anomalies (HadSST 3.1.1.0), average land temperature anomalies (Berkley) and mean sea level pressure anomalies (HadSLP2r) were available from 1880. However, as stated in Table 1, the teleconnection variables were only available from 1950, with the exception of the MJO dataset which was only available from 1979. For this reason, initially the period of 1880-2020 is assessed only involving the: SST anomalies, global temperature anomalies, land temperature anomalies and mean sea level pressure anomalies. However, as discussed, this early period is not necessarily the most reliable due to poor apparatus so when correlation coefficients are examined the period of 1950-2020 is used instead in order to minimise skewness of the cold bias in the early period.

When comparing the SST anomalies to the teleconnection variables, the period of 1950-2020 and the period of 1979-2020 were assessed. This was because, as stated, the MJO data was only available from 1979 however, for the other variables the longer time period was also assessed as the more data available the more statistically significant the result would be. When assessing the relationship between the SST anomalies and the teleconnection variables, the effects of global temperature anomalies are not removed. This is because the datasets are calculated in relation to the raw SST data so therefore this would mean that the two datasets would not be comparable if the warming effect was removed. This conclusion was deduced through the examination of the relationship between the SST anomalies and the global temperature anomalies which had very low significance.

When comparing the morphology and characteristics of specific Warm and Cold Blob events, the global temperature anomalies were removed from the raw SST anomalies in order for the magnitudes of the anomalies in these time frames to be more comparable. This meant that, the effects of increasing temperatures under global warming would be negligible.

The raw variable data could be extracted in the form of a latitude/longitude grid meaning the variables are specific to location. However, when looking at the global temperature anomaly data, this is given in the form of an average global monthly value. For this reason, this dataset is not location specific

meaning error could occur as warming in this region (155-142.5°W and 37.5-45.5°N) may not match the global average, as global warming is not spatially homogenous. When the monthly relationship between global temperature anomalies and the SST anomaly timeseries were compared the r value was only 0.09, for this reason the global temperature were not always removed as this relationship was not deemed significant. Further detail of the observational datasets used are described in Table 1.

2.1.3 Assessing the future of the Warm Blob

It is unclear how this Blob will change in both intensity and frequency with time as well as the potential for impacts to alter in position or variability and become more severe. Using Coupled Model Intercomparing project 5 (CMIP5) simulations (Taylor *et al.*, 2012), future projections under a specific emission pathway can be evaluated over time. The assessed pathway is RCP8.5 (Representative Concentration Pathway 8.5) (Riahi *et al.*, 2011). This is a pathway that leads to CO₂ concentrations in 2100 that produces a change in forcing of 8.5W/m². This concentration is what would occur if emissions continue to rise at the same rate throughout the 21st century.

Through this RCP pathway, relative to the present, these anomalies will become more frequent, due to expected rising SSTs. However, if a heatwave is defined as a short-lived event with temperatures relative to the mean climate at that time, the frequency of marine heatwaves could stay the same but just happen in an overall warmer climate. In this investigation the base period of 1981-2020 continued, for this reason, a running 5-year mean was removed from its corresponding period, in an attempt to remove the effects of global warming so that the data is more comparable with the observational dataset. Further detail of the CMIP5 datasets used are described in Table 2.

Table 1: A table to summarise the variables (and associated dataset details) used in this report, which have been downloaded via the KNMI explorer.

| Variable | Name of Dataset | Period Available | Base Period And reference | Description of Dataset |
|-----------------------------------|---|------------------|--|--|
| Sea Surface Temperature Anomalies | HadISST1 SST 1° reconstruction | 1870-2020 | 1981-2020 (for anomalies) Rayner <i>et al.</i> , 2003 | Hadley Centre sea ice and sea surface temperature data set version 1 (HadISST1), is a constructed dataset from the Met Office Hadley Centre. HadISST1 is an advancement upon previous global sea ice and SST datasets (such as the GISST). It has been made complete but using interpolations to eradicate gaps in the SST dataset. |
| Global Temperature Anomalies | HadSST 3.1.1.0 northern hemisphere averaged SST anomalies | 1850-2020 | 1981-2020 (for anomalies) Kennedy <i>et al.</i> , 2011a,2011b | This dataset identifies changes in SSTs at global and regional levels. This dataset is focused on the ocean in the northern hemisphere. With a chosen base period and is averaged monthly. |
| Land Temperature Anomalies | Berkeley average land temperature 1° resolution | 1750-2020 | 1981-2020 (for anomalies) Oyler <i>et al.</i> , 2014 | Berkley average land temperature is a global temperature dataset that uses a statistical analysis to account for inhomogeneities in the dataset (Rohde <i>et al.</i> , 2013). |
| Sea Level Pressure Anomalies | HadSLP2r SLP | 1850-2020 | 1981-2020 (for anomalies) Allan and Ansell, 2006 | HadSLP2 is based on a number of terrestrial and marine data collations. Each terrestrial pressure sequence used undergoes a quality control process and inaccurate or dubious values were either corrected or removed. The concluding dataset is presented in a latitude longitude grid by combining together the processed terrestrial and gridded marine mean sea level pressure data. It is said that “these fields were made spatially complete using reduced-space optimal interpolation” (Allan and Ansell, 2006). |

| | | | | |
|------------------------------------|---|-----------|--|--|
| El Niño Southern Oscillation Index | HadISST1 Niño3.4 index | 1870-2020 | Linear regression period (1880-2020) Rayner <i>et al.</i> , 2003; Jin <i>et al.</i> , 2008 | The HadISST Niño 3.4 Index takes a monthly average of the sea surface temperature component bounded by the NIÑO3.4 region: Longitude: -170.000 -120.000°E Latitude:-5.000 5.000°N. The anomalies are then calculated with reference to a chosen base period. This ENSO index was chosen as it is optimally comparable to the SST anomaly HadISST1 dataset as the two are the same. These anomaly values are absolute without the effects of global temperature increase removed so are compared to the raw SST dataset. |
| Pacific Decadal Oscillation Index | Pacific Decadal Oscillation index, from SWFSC | 1900-2020 | Linear regression period (1900-2020) Mantua <i>et al.</i> , 1997 | This PDO dataset is from the Southwest Fisheries Science Centre. The PDO is derived as the principle component of monthly SST anomalies in the North Pacific Ocean, pole-ward of 20°N (Zhang <i>et al.</i> , 1997). This dataset is also absolute so again is compared to the raw SST values. |
| Arctic Oscillation | Monthly AO CPC | 1950-2020 | Linear regression period (1950-2020) Overland and Wang, 2005 | The AO index is derived from the National Centre for Environmental Prediction reanalysis (Kalnay <i>et al.</i> , 1996). The index is calculated as the first Empirical Orthogonal Function (EOF) for height anomalies poleward of 20°N. The aim of this process is to identify the maximum amount of deviation in the “circulation fields” (NOAA, 2017). |
| Madden Julian Oscillation | Monthly MJO 06 CPC 120°W | 1978-2020 | Linear regression period (1979-2020) Zhang <i>et al.</i> , 2007 | The CPC MJO index is calculated by conducting an EOF analysis using 200-hPa velocity potential for the region equatorward of 30°N from the NCEP/NCAR Reanalysis (Kalnay <i>et al.</i> 1996). This is only determined during the ENSO neutral and weak ENSO winters (November-April) in 1979-2020. An extended EOF analysis is used to identify ten time-lagged patterns correspondence with longitudinal locations. In this case 06 CPC is for the region 120°W (Xue <i>et al.</i> 2002). |

| | | | | |
|--------------------------------|--|-----------|---|--|
| The North Atlantic Oscillation | Monthly CPC North Atlantic Oscillation (NAO) | 1950-2020 | Linear regression period (1950-2020) Feldstein and Franzke, 2006 | The NAO index used by the CPC was based on the methodology of Barnston and Livezey (1987), which determined teleconnections by applying a rotated principal component analysis of the 500-hPa geopotential height field anomalies from the period 1950-2000 (Feldstein and Franzke, 2006), These anomalies were then recentred for the chosen base period (1981-2020). Calculating the NAO index using the RPCA approach is a complicated process and the NAO index is not derived independently of any other extra tropical teleconnection index. |
|--------------------------------|--|-----------|---|--|

Table 2: A table to summarise the Coupled Intercomparison Models (CMIP5) (Taylor et al., 2012) datasets used in Section 3.10 of the Results Section available via the KNMI explorer.

| Name | CMIP5 Pathway | Description | Data Available | Description of Dataset |
|--------------------|---|---|--|--|
| IPSL-CM5B-LR model | Output prepared for CMIP5 RCP8.5 r1i1p1 | <i>The Institut Pierre Simon Laplace (IPSL)(France)</i> The atmospheric model only has a low-resolution model. Spatial Resolution: 1.9° latitude, 3.75° longitude | 1861-2100 Ying <i>et al.</i> , 2016 | The IPSL is a full earth system model, the specific dataset used in this report is the CM5B model which is the latest version. This model is constructed on an atmosphere-land-ocean-sea ice model, including a full depiction of the carbon cycle as well as the chemical influences of aerosols. |
| GISS-E2-H model | Output prepared for CMIP5 RCP8.5 r1i1p2 | <i>NASA Goddard Institute for Space Studies</i> Coupled Ocean-Atmosphere model ModelE (Atmosphere)/ Hycom(Ocean) Spatial Resolution: 2° latitude, 2.5° longitude | 1861-2100 Shindell <i>et al.</i> , 2013 | NASA/GISS, New York. The GISS-E2-H is the newest GISS climate model. The model takes into consideration chemistry related ozone with a large focus on methane concentrations in future simulations. |
| GFDL-ESM2G model | Output prepared for CMIP5 AR5 r1i1p1 | <i>Geophysical Fluid Dynamics Laboratory</i> <i>An Earth System Model (NOAA)</i> Spatial Resolution: 2.0225° latitude, 2° longitude | 1861-2100 Taylor <i>et al.</i> , 2012 | The GFDL model is constructed with a focus on the Earth's biogeochemical cycle. This includes both anthropogenic influences and their effects on the climate system. The ocean aspect has a focus on ocean mixing as well as biogeochemistry. |

2.2 Methodology

2.2.1 Establishing the location of the Warm Blob

When looking at SSTa data, the region of focus is off the Gulf of Alaska in the North East Pacific (Bond *et al.*, 2015). However, when assessing seasonal changes in land temperatures, a focus is also required for the North American land mass.

To identify the region of focus, the standard deviation of the raw SSTa (HadISST1 anomalies) over the course of 1981-2020 were plotted to identify where the largest variability occurred (using a base period of 1981-2020). This was achieved by calculating the standard deviation value for each grid point for the given time period. From this, the region of focus in the North East Pacific, resembling the Warm Blob could be refined and defined.

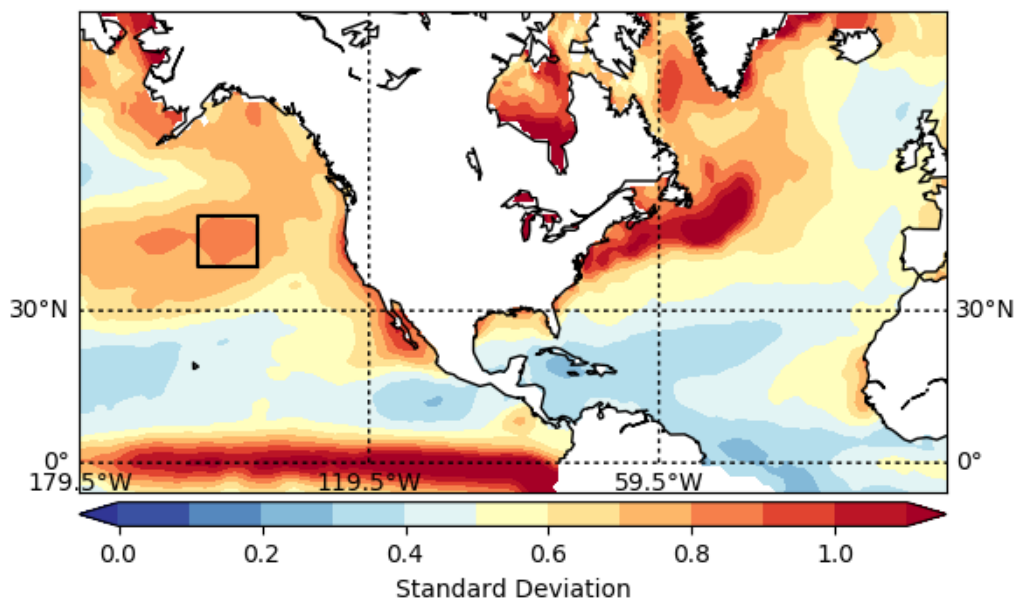


Figure 5: A map to show the standard deviation of SST anomalies ($^{\circ}\text{C}$) over monthly data for the period 1981-2020 for each grid point using the HadISST1 dataset minus the effects of global temperature using the HadSST dataset, using a base period of 1981-2020. The black box marks the region of interest $155\text{-}142.5^{\circ}\text{W}$ and $37.5\text{-}45.5^{\circ}\text{N}$

From this investigation it was concluded that the region of focus would be $155\text{-}142.5^{\circ}\text{W}$ and $37.5\text{-}45.5^{\circ}\text{N}$, as this was where the standard deviation values were largest in this region ($>0.8^{\circ}\text{C}$). In comparison to deviation values off the coast of Florida (deviation of SSTs due to the presence of the Gulf Stream) and around the equator (Niño3.4 region) which are $>1^{\circ}\text{C}$, the standard deviation values bounded by the black box do not stand out as being largely significant. However, after assessing composite plots of the Warm and Cold Blob (Figures 11e and 13e), made using the average value of each grid square at the time frames when the Blob is identified, one concluded this region was appropriate. The region of high standard deviation located near the equator is that of Niño3.4. This

region's SST anomalies will be later compared to the Blob region to test for a statistical relationship between the two warm anomalous modes of water.

The method used to identify this area is not optimal and is a simplified approach. If the standard deviation was higher, this method would have more significance however, concern arises as it is lower than expected for this highly anomalous region. A limitation of this method is that the process of finding the highest region of standard deviation is highly dependent on the dataset and the time period used as a base for the anomalies. However, having mapped the 2014 Warm Blob event in Figure 6, the location of the Warm Blob also corroborated with the location selected.

This area is more refined than investigated by Bond *et al.* (2015), where the region bounded by 40°–50°N and 150°–135°W was used. Bond *et al.* used this region as the standard deviation in this area had a record high value of 2.6 standard deviations in 2014 above the normal (using a base period of 1949–2014). This standard deviation value is much larger than the values experienced in Figure 5, this is likely because Bond *et al.* only looked at the standard deviation of one event, the 2014 Warm Blob, as opposed to the standard deviation across the whole time period. For this reason, the approach taken in this report is an improvement on this method as more warm events are included as well as cold events. Freeland and Whitney (2014), again assessed a slightly larger region, similar to Bond using 40°–50°N, 155°–140°W, which was described to be ~500 km wide and ~100 m deep (Freeland and Whitney, 2014). The area of focus in this report, is likely to be slightly different to the region studied in literature as this report also assesses the Cold Blob not just the Warm Blob so negative anomalies are also important.

Once this location was defined a timeseries of this SSTa data could then be calculated by averaging all the values bounded by this region, to conclude a single value per month. This was referred to by Bond *et al.* (2015) as the Pacific Blob Index.

2.2.2 Analysing the years with the highest anomalies

To analyse how the intensity and frequency of the Warm and Cold Blob change overtime, a seasonal timeseries was constructed of raw SST anomalies and one with the effects of global temperature anomalies removed. This was done by taking a 3 month mean of the timeseries previously explained in Section 3.2.1. Seasons were defined as; winter: December, January, February, spring: March, April, May, summer: June, July, August and autumn: September, October, November. From this seasonal timeseries, the maximum and minimum anomaly years could be identified.

In order to assess the frequency of the Warm and Cold Blobs and to analyse whether a pattern or regular intermittent period was observed, events with anomalies larger than a chosen value were extracted. This was accomplished by characterising a Warm Blob as an anomaly with a value $>+1^{\circ}\text{C}$ and a Cold Blob was an anomaly $<-1^{\circ}\text{C}$, this included the top 15% of anomaly values across the monthly timeseries dataset. This 15% value was produced using the SST minus global temperature anomaly timeseries, all

the anomalies were made positive and the 85th percentile value was calculated. This value was 1.02°C so therefore, +/-1°C was used. In doing this the largest Cold and Warm Blob events could be highlighted.

2.2.3 Links to Teleconnections

In order to establish whether Warm and Cold Blob events are associated with other known atmospheric circulation patterns, linear regression was used to test for a relationship. This was achieved in the form of an *r* value (Pearson product-moment correlation coefficient) (Benesty *et al.*, 2009). In statistics, the *r* correlation coefficient measures the strength and direction of a linear relationship between two variables, ranging between -1 and 1. The -1 value indicates a perfectly negative correlation and +1 indicates a perfectly positive. If the *r* value is close to 0, it indicates that there is no relationship between the variables. These phenomena were compared to the raw SST anomalies, using a base period of 1981-2020.

As well as this, a time lag was investigated between SST anomalies and certain teleconnections in order to distinguish which variable was the cause and which the effect. This was accomplished through understanding which phenomena appeared to occur first. Capotondi *et al.*, (2019) states that for events like the ENSO there will be a delay in the effect on the region of the North East Pacific, due to the time at which it takes for the ocean conveyor to transport water from the Niño3.4 region northwards. This can also be true for events like the PDO. As well as this, events occurring in the Atlantic are deemed to take effect at an even longer time lag due to the distance between where the phenomenon originates and the North Pacific. This time lag was investigated by finding the *r* coefficient between the two variables with increasing monthly delays.

2.2.4 Changes in the future

Three CMIP5 models will be investigated from 1950-2100 in order to identify if the data correlates with the observational anomaly magnitudes as well as, how the Blob will change in intensity and frequency in the future. A raw seasonally averaged SST timeseries is constructed through a 3-month average (seasons as previously defined) and a linear regression trend line will be fitted. Standard deviation will be used to assess changes in frequency within certain time periods of the same duration. As well as this, a five-year mean will be removed from the timeseries (as previously explained in Section 2.2.2) in an attempt to remove the global temperature warming effect overtime. Warm and Cold Blobs will be defined as >+1°C and <-1°C, so that they can be compared to the Blobs defined in the observational dataset. The morphology of future Blobs will be mapped using the raw SST CMIP5 data in order to identify their changed intensity and morphology.

3.0 Results and Discussion

As stated in Section 1, there are three main objectives of this study. The first is to be able to investigate the morphology, development and characteristics of the Blob. This will be presented as a series of maps with seasonally averaged SST and average land temperatures anomalies, and as a comparison with Sea Level Pressure (SLP) anomalies. Additionally, timeseries data will be examined to identify peaks and troughs in the anomaly data. From this, the extent and intensity of the Warm Blob can be characterised. This will be the point of focus in Section 4.1.

The second objective is to assess whether there is a relationship between the Warm and Cold Blobs and various global teleconnections. This was investigated using linear regression, and in some cases a time lag, to statistically investigate correlations in the datasets. This objective will be the point of focus in Section 4.2.

The final objective is an analysis into how the Blob is modelled to change in the future. This will involve using CMIP5 models to investigate how these warm and cold events will alter in both magnitude and frequency. This will be the focus of Section 4.3.

3.1 Morphology, Development and Characteristics of the Blob

The anomalous Blob of 2013-2015 has been widely researched and has been characterised as a 2000km wide and 100m deep circular, concentrated region of above normal SST anomalies (Kintisch,2015). An enhancement of the 2013/2014 event occurred in December 2014, due to the presence of the El Niño (Lee *et al.*, 2015). The winter 2014 Blob will be investigated to analyse these enhanced characteristics of the Blob.

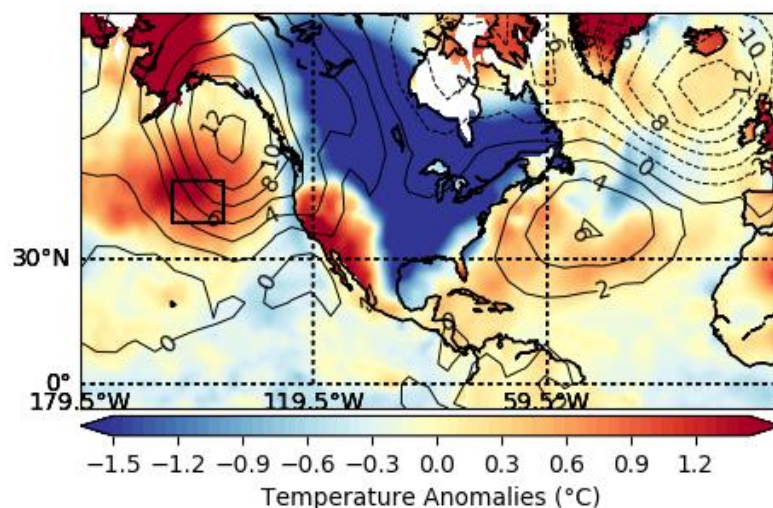


Figure 6: Seasonally averaged sea surface temperature anomalies minus global temperature anomalies for December, January, February for the end of 2013 beginning of 2014. SST data is from the HadISST1 dataset minus the global temperature anomalies from the HadSST anomaly dataset. As well as land temperature anomalies from Berkley. The black box here indicated the Warm Blob region of interest 155-142.5°W and 37.5-45.5°N. An overlay of sea level pressure contours has been added from the HadSLP2r dataset

The Warm Blob can be clearly identified in Figure 6 with temperature anomalies in the centre of this Blob as high as +1.5°C. The Blob can be seen to stretch from 175-130°W and from 30°–55°N with a more concentrated region of higher SST anomalies from 160-145°W and 40°–45°N. The concentrated region represents a Blob with a width of ~1400km. This is on the same scale as the size of the Blob identified by Kintisch (2015). The Blob here is located off the Gulf of Alaska and is circular in shape. In the region bounded by the black box, the SST anomalies are noticeably warmer in comparison to any other oceanic region. It can also be seen that coastal regions, such as the Gulf of Alaska and California, experience very high land temperature anomalies >+1.5°C. As previously stated, this Warm Blob has been said to not only impact marine temperatures but can also influence inland weather and climate (Hartmann, 2015).

It has been stated that the 2013-2015 Warm Blob event occurred as a result of continuous high pressure over the region. From October 2013 through to January 2014, much higher than normal MSLP were present over the North East Pacific, “with a peak magnitude approaching 10 hPa” (Bond *et al.*, 2015). As a result of these large sea level pressure anomalies there was a highly anomalous weather pattern in this region, during this period. This can be supported by Figure 6 where a +12hPa high pressure centre was experienced over the Gulf off Alaska.

This anomalous ridge of high pressure was observed over the west coast of North America, Alaska. Simultaneously, at higher latitudes in the North Pacific a low-pressure system is experienced. Lee *et al.*, (2015) stated that this high pressure was associated with a dipole low pressure system over the extratropical North Atlantic. This is demonstrated by Figure 6 where a low-pressure anomaly of -12hPa is experienced over the north of the UK.

Furthermore, a slight positive pressure anomaly was observed off the coast of Florida. This feature is also evident in Figure 6, where a high-pressure anomaly over the Atlantic is observed with a high of +6hPa. This is slightly smaller than was observed by Bond *et al.*(2015). Over the Atlantic, both a high and low-pressure anomaly is evident. The dipole pressure system can be seen with a low pressure in the north, near to the UK, and a high pressure off the coast of Florida.

The high-pressure system observed over the North Pacific has an associated ridge of high pressure. This feature has been documented in literature, demonstrating that the pressures in this area are much higher than in the surrounding regions. This evidence explains why this region experiences the warm SST anomalies and the surrounding area does not.

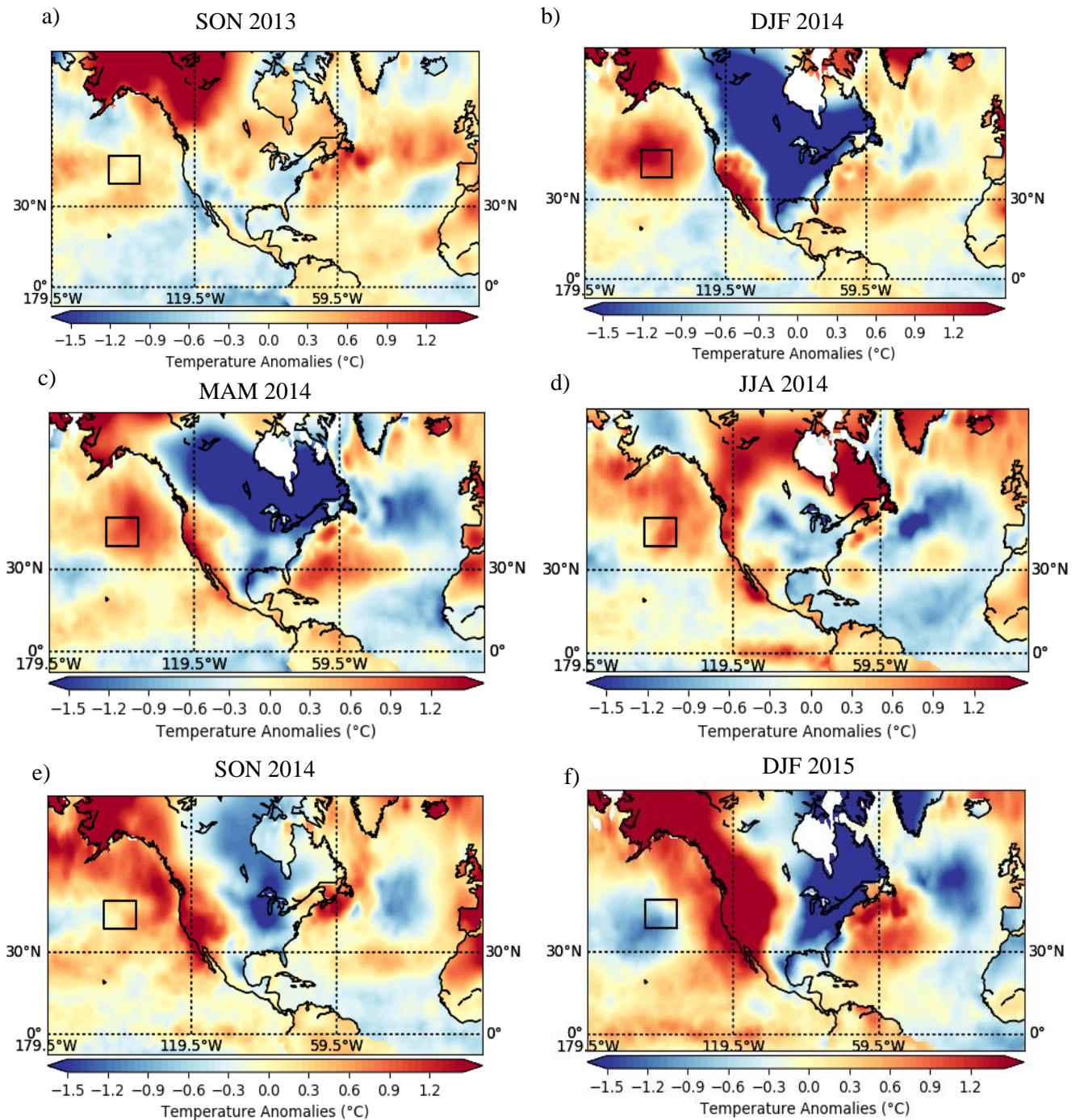


Figure 7: A subplot to show a seasonal averaged time series of the 2013-2015 event mapping the Warm Blob sea surface temperature anomalies overtime a) September, October, November 2013, b) December, January, February 2014, c) March, April, May, 2014, d) June, July, August 2014, e) September, October, November, 2014, f) December, January, February 2015. SST data is from the HadISST1 dataset minus the global temperature anomalies from the HadSST anomaly dataset. As well as land temperature anomalies from Berkley. The black box here indicates the Warm Blob region of interest 155-142.5°W and 37.5-45.5°N.

Figure 7 can be used to understand the characteristics associated with the formation and dissipation of the Blob. In the autumn of 2013, temperatures were close to normal for that season and location; however, it should be noted that land temperatures in Alaska at this time are high with anomalies $>+1.5^{\circ}\text{C}$. Figures 7b and 7c show the peak of the Warm Blob, with a circular feature with warm concentrated SSTs in the centre which are between $+1.2-1.5^{\circ}\text{C}$. In this period the land temperatures are much cooler in the east with anomalies $>-1.5^{\circ}\text{C}$ however, temperatures remain high inland off the Gulf of Alaska and along the Californian coast.

After this 6-month period, Figures 7d and e show a very similar dissipation, in which the warm SSTs disperse and dilute along the North East Pacific coast. In this time land temperatures on the west coast warm significantly, suggesting that the warmth from the Blob is being transported inland. This spread of warm SSTs could be the result of the transportation of warmer waters along the Alaskan and Californian current, north and south. By the winter of 2014/2015, Figure 7f resembles the characteristics of a Cold Blob, with high negative anomalies collating in the Blob region $\sim<-0.9^{\circ}\text{C}$.

The formation and dissipation of this Warm Blob is linked to physical processes, including surface fluxes and atmospheric-ocean circulation. Liang *et al.* (2017), states that prolonged Blob events are induced mainly through anomalies in surface heat fluxes and anomalies in wind-induced ocean advection.

These significant warm and cold SSTs largely associate with positive and negative surface heat flux anomalies (Liang *et al.*, 2017). The positive surface heat flux anomalies here are associated with near surface wind anomalies. In this time period (DJF 2014) this region is dominated by clockwise near-surface wind anomalies relating to the anomalous ridge (Bond *et al.*, 2015). Clockwise wind anomalies dominating in the south and east weaken the prevailing westerlies, which decrease the surface heat flux, leading to this warming. Liang *et al.* (2017) also examined the vertical heat exchange at the bottom of the mixed layer, which occurs due to entrainment processes. This is estimated by the wind stress curl (which determines the rotation a vertical column of air) and in the Pacific Blob region slightly negative anomalies occurred.

3.1 Occurrence of warm and cold events in the historical period

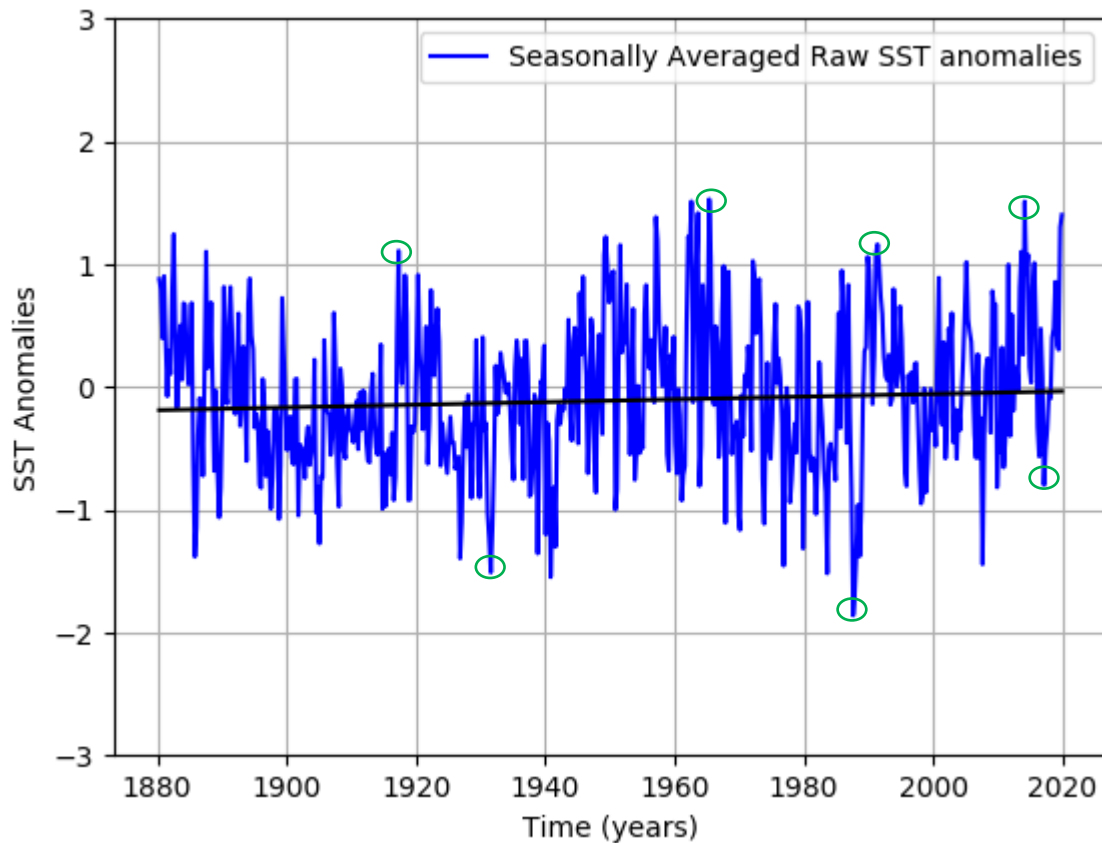


Figure 8: Raw seasonal HadISST1 sea surface temperature anomalies ($^{\circ}\text{C}$) (calculated using a base period of 1881-2020) from 1880-2020 calculated by averaging the data points bounded by the region of interest $155\text{-}142.5^{\circ}\text{W}$ and $37.5\text{-}45.5^{\circ}\text{N}$. Additionally, a line of best fit is evident showing the linear relationship overtime. The green circles highlight datapoints which are discussed below in reference to Warm and Cold Blob events.

From Figure 8, the 2014 boreal winter Warm Blob can be identified as a peak in SST anomalies in 2014 with a value of $\sim +1.5^{\circ}\text{C}$. This Warm Blob event is significant in literature due to its intensity however, it would seem that historically a warming event of this size has occurred before in this region. Although Warm Blobs experienced in this region prior to 2014 have not been widely researched Liang *et al.*, (2017) noted that they identified five prolonged (≥ 24 months) blob events during the period 1948–2015, implying that the 2014 event is not the original.

A large positive anomaly occurred in 1964 where SST anomalies reached close to $+1.6^{\circ}\text{C}$, as well as another warm event of this magnitude seen in 1991, with a positive anomaly of $+1.2^{\circ}\text{C}$. Between 1960-1965 it seems that the appearance of the Warm Blob was a common feature however, this could just be an extended Warm Blob lasting the entire duration of this time.

It can also be concluded that anomalies of the same magnitude, but opposite sign were identified. An opposing Cold Blob is experienced in 1930, 1987 and 2017, these cold anomalies are as large as -1.9°C . Miller and Cheney (1990), stated that the 1987 cold anomaly ($\sim -1.9^{\circ}\text{C}$) was associated with the 1987

El Niño. It can be seen in the timeseries that prior to this event. A warm anomaly was experienced in 1986, with a warming of $\sim +1^{\circ}\text{C}$, Miller and Cheney (1990) that was also related this to the ENSO event.

McPhaden and Picaut (1990) state that warm SST anomalies ($>+1^{\circ}\text{C}$ warmer than climatology in the eastern and central Pacific) experienced in the summer of 1986 occurred in this region as a result of low level 850mb anomalous westerly winds that sustained west of 0° longitude (the date line). By the end of 1986, uncharacteristic deep convection and associated atmospheric warming occurred over the hottest waters in the tropical Pacific as they migrated eastwards towards the equator (McPhaden and Picaut, 1990).

The ENSO index then decreased to a minimum in summer 1987, reaching its lowest value in over 20 years, excluding the 1982-83 ENSO. By early 1988 the ENSO index normalised to near zero and anomalously negatively SSTs and strong trade winds appeared across the Pacific basin (McPhaden and Picaut., 1990), representing the Cold Blob experienced in 1987 in Figure 8. This description corroborates with the data displayed in Figure 8 however, due to the quality of instrumentation at this time, this would be difficult to map and compare to data recorded using the highly advanced equipment of today.

It can be deduced from this timeseries that the region of focus experiences extremes in SSTs with a range of 3.4°C in anomaly values, between 1880-2020. Additionally, the timeseries suggests that the SST anomalies in this region do not remain persistently positive or persistently negative for a period longer than 10 years, as demonstrated by the large fluctuations seen in Figure 8, meaning that this region does not correspond with climatology.

The trend line in Figure 8 demonstrates that there is a warming trend in this period, shown by the positive temperature increase, although it is small. To remove this warming effect, which is likely due to global warming, the next logical step was to remove the effects of global temperature anomalies for the northern hemisphere ocean.

Occurrence of warm and cold events in with global temperature anomalies removed

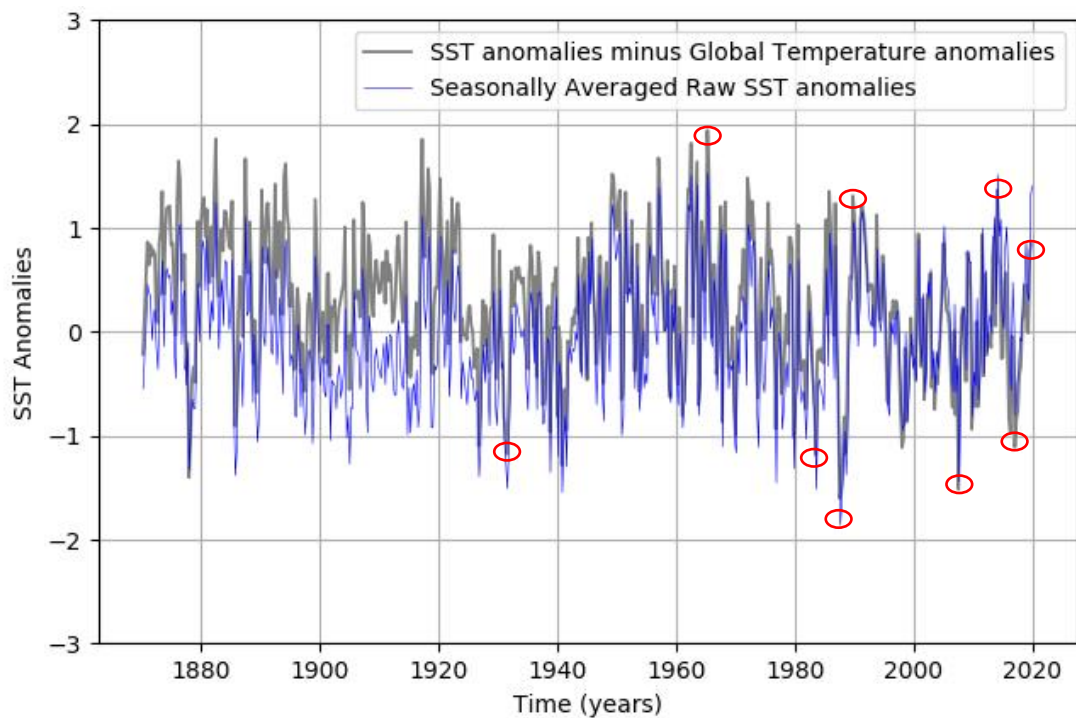


Figure 9: Seasonal sea surface temperature anomalies ($^{\circ}\text{C}$) (raw using HadISST1=blue line) with the effects of seasonal global temperature anomalies removed (global temperature removed using HadISST1 minus HadSST =grey line) (both calculated using a base period of 1881-2020) from 1880-2020. Calculated by averaging the data points bounded by the region of interest $155\text{-}142.5^{\circ}\text{W}$ and $37.5\text{-}45.5^{\circ}\text{N}$. The red circles highlight datapoints which are discussed below in reference to Warm and Cold Blob events.

Figure 9 shows that the peaks between 1880-1940 appear to increase in magnitude on average by $\sim 0.3^{\circ}\text{C}$, despite having removed the effects of the global temperature anomalies. However, between 1940-1980 the adjustments are marginal. In comparison, the troughs appear to decrease in intensity, supporting this $\sim 0.3^{\circ}\text{C}$ warming between 1880-1940.

It is important to note that the earlier Warm Blob events become more apparent and the Cold Blobs reduce in magnitude and frequency, due to warming caused by the removal of global temperature anomalies. This period in relation to the average global temperature experienced between 1981-2020 (base period), is much colder due to recent global warming so in the removal of global temperature anomalies, it is warmed. A significant change is noted in 1917, where the positive SST anomaly has increased by nearly a whole degree. The 2014 Warm Blob anomaly does not appear to change in magnitude with this effect removed (as the base period is set to 1981-2020) however, the more dramatic increases are seen earlier in the timeseries, the largest being between 1880-1920.

The removal of global temperature anomalies has increased the anomaly range marginally to $\sim 4^{\circ}\text{C}$. The peak and trough years identified in the previous plot remain at the same time intervals once global temperature is removed. This suggests that the Warm and Cold Blobs occur independently of global temperature change and are on a much larger scale. This global temperature anomaly dataset removes

the overall monthly warming anomaly for the northern hemisphere ocean, so is not necessarily the best portrayal of background global warming in this specific region.

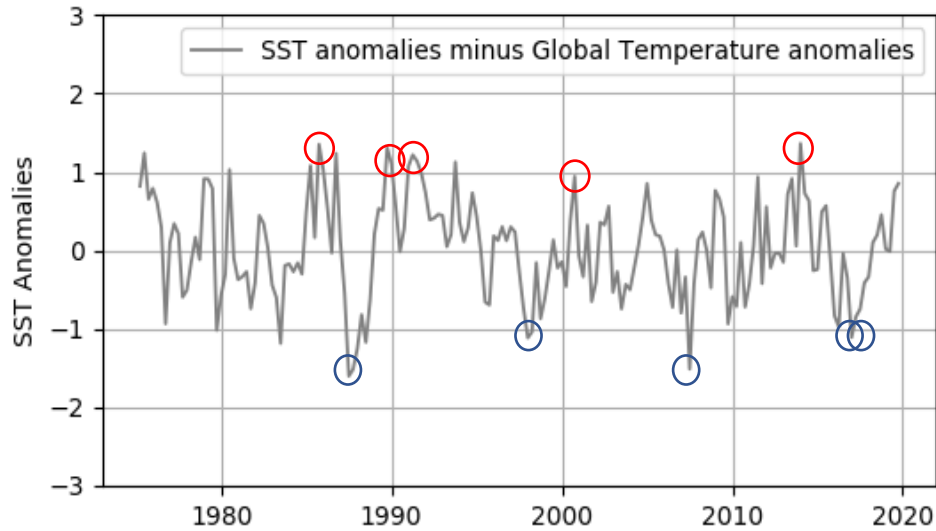


Figure 10: A section of time extracted from Figure 9 using a refined period of 1975-2020. All anomalies are calculated using a base period of 1981-2020 calculated by averaging the data points bounded by the region of interest 155-142.5°W and 37.5-45.5°N. Using HadISST1 data SST anomaly data minus the global temperature anomaly dataset HadSST (°C). The red circles have been identified as chosen Warm Blob years which will be later assessed, and the blue circles indicate chosen Cold Blob years. These points have been selected randomly out of the largest anomaly values to observe the Blob's characteristics in different time frames.

Using the timeseries from Figure 9, but focusing in on the period of 1975-2020, Warm and Cold Blob events can be detected and mapped. The following Blob events have been selected randomly from the maximum anomalies to compare events, and to test for similarities and differences in characteristics and morphology.

3.4 Comparison of Warm Blob events

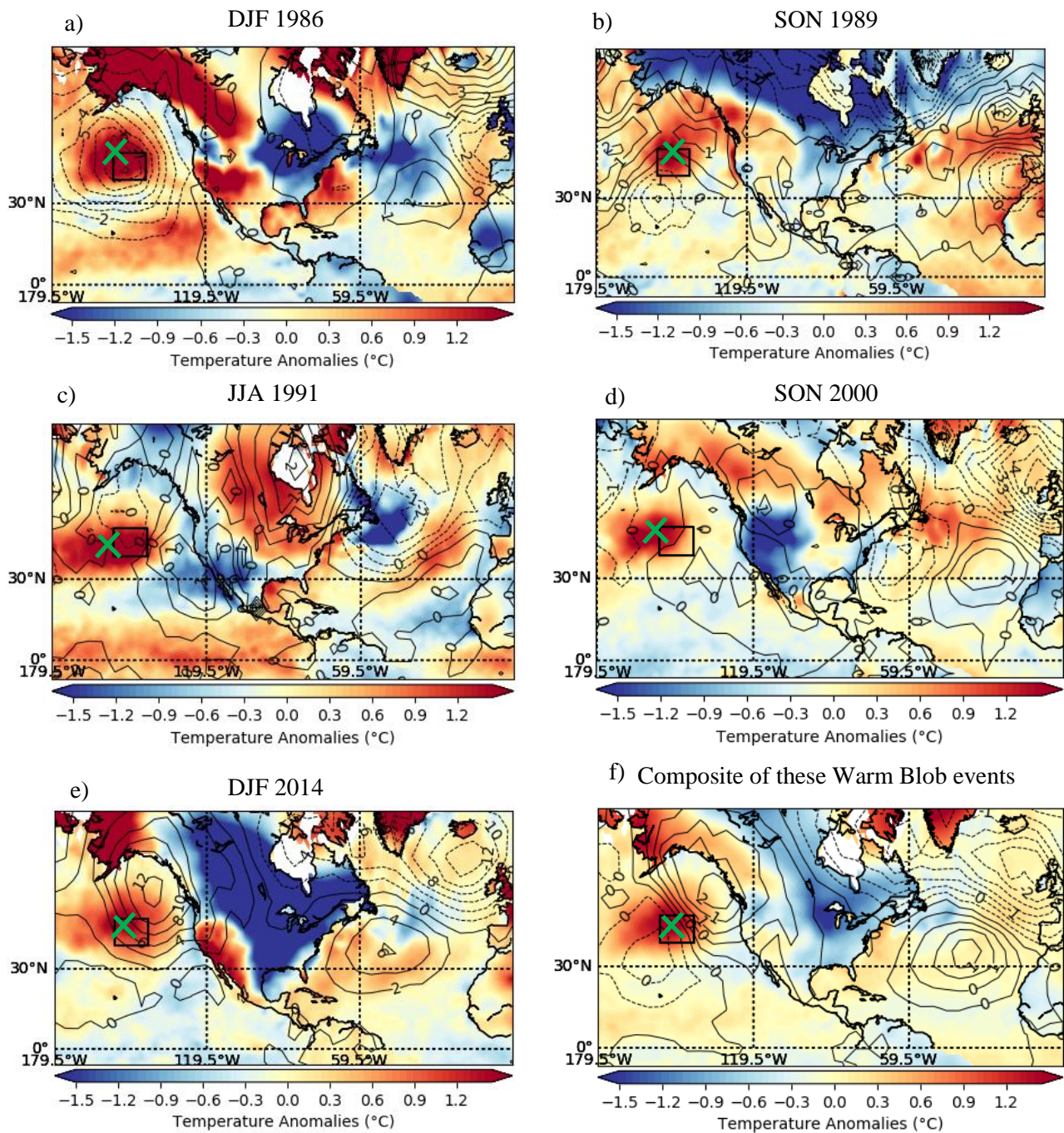


Figure 11: Subplots to show the characteristics of the Warm Blob in maximum SST positive anomaly years. Both land and SST anomaly data are calculated using a base period of 1981-2020. The SSTs are calculated using HadISST1 minus the global temperature anomaly HadSST SST data. The land temperature anomalies are calculated using the Berkeley dataset. Mean Sea Level Pressure contours have also been added using HadSLP2r data. Each map identifies a different timeframe of seasonally averaged data: a) Winter 1986 b) Autumn 1989 c) Summer 1991 d) Autumn 2000 and e) Winter 2014 and f) A composite image of all 5 events averaged. The green crosses represent the centre of the anomalously high warm temperatures. The black box indicates the region bound by 155-142.5°W and 37.5-45.5°N.

Figure 11 highlights the characteristics of the Warm Blob in 5 randomly chosen Warm Blob time frames. These were selected based on having average SST anomalies greater than $+1^{\circ}\text{C}$ in the selected region. It can be concluded that the position of the Blob moves slightly westward in certain time frames, due to the change in location of the green cross. However, the black location box is predominantly located over the maximum anomaly values.

It is evident that the 1986 Blob appears to involve the largest anomalies in the black box region, with temperatures exceeding $+1.5^{\circ}\text{C}$ covering the largest area. This is supported by the timeseries shown in Figure 10. In 4 out of the 5 plots the warm anomalies appear to be fully detached from the coastal region with colder anomalies seen at the coast -0.3 to -0.9°C . However, in the autumn of 1989 (Figure 11b) the warm temperatures extend into the Gulf of Alaska and the warming seems to move inland. Resulting in an area of average land temperatures $\sim+0.6^{\circ}\text{C}$. This difference could be explained by variance in seasonality and surface winds during the 1986 to 1987 Warm Blob-Cold Blob transition, as observed by McPhaden and Picaut (1990).

Both the Blobs identified in the autumn do not appear to be as intense as the summer or winter-time Blobs and the warming is not as concentrated. During the 2014 event (Figure 11e) the Blob was said to have remained offshore as a result of Ekman transport associated with coastal upwelling (Kintisch, 2015). This transport was a result of northerly winds and southward flow that lead to westward movement caused by the Coriolis effect and upwelling which replaced the transported water (Peterson et al., 2015). This feature was associated with the 2014 Warm Blob, however, has not been linked to other Blob occurrences.

The effect that the warm water anomalies have on land temperatures is difficult to deduce. In each event it would appear that the land responds differently. In both the winter seasons (Figures 11a and 11e), the land temperatures warm in correspondence with the Blob. This is most obviously seen along the coast of California and in the more northern regions around the Gulf of Alaska, here average land temperatures are greater than $+1.2^{\circ}\text{C}$.

Ocean currents, warm air and winds advect warmth overland and can cause areas to be affected by the warmer temperatures of the Blob event. The North Pacific current transports these warm temperatures eastward towards the land, then from here the warm water diverges northwards and southwards as a result of the Alaskan and Californian current (Hickney and Royer, 2001). These land anomalies may be warmer than in the other months, as the Blob in these periods have persisted for longer. This means that the land has had time to respond to the ocean warming. Looking at the timeseries in Figure 10, it appears that the 1989 event followed previous warming. This previous warming may explain why the land temperatures are warmest in this plot, as the warm water has had time to be transported along the currents to inland regions.

In comparison, in the summer of 1991 (Figure 11c) coastal land temperature anomalies are negative, again looking at Figure 10 it appears that, prior to this, an extreme cold anomaly was observed. This suggests that the Blob here has only just developed, and the warmer SSTs may not have had the opportunity to impact the land temperatures as the effects of the cold event are still influencing the land.

Figure 11 shows that warm SSTs extended southwards over the summer of 1991. This could be a result of the strong Californian current. The Californian current causes upwelling all year round but is strongest in the summer months (Huyer, 1983). For this reason, these warm SSTs may have been transported southward quickly along this current. This may explain why positive SST anomalies are evident in region such as Central America, $\sim +0.9^{\circ}\text{C}$.

It appears that in the winter and summer seasons the Warm Blob is mirrored by an area of cooler SSTs (-1.2°C) off the east coast of America. This is representative of the North Atlantic Cold Blob which has been previously linked to the Warm Blob (Liang et al., 2017). However, in the autumn, this Cold Blob is not apparent and SSTs in this region are warmer. The relationship between these two anomalous modes will be assessed in relation to the NAO.

It is interesting to note that in relation to pressure both winter events (Figures 11a and 11e) demonstrate significant anomalies in positive MSLP values over the North Pacific. In 1986 positive anomalies are as large as $+6\text{hPa}$ and in 2014 $+12\text{hPa}$. This suggests that if a Warm Blob occurs in the winter, it could be a result of or linked to MSLP. In the other three-time frames, pressure anomalies in this region are negligible. This could suggest that both the characteristics and causation vary seasonally and are not necessarily a consequence of the same mechanisms.

Overall, the Warm Blob effects on the land are quite different in summer and winter. As even if the circulation response is the same, seasons respond differently (i.e. winter cold high pressure, summer hot high pressure, this is due to different seasonal factors).

3.5 Comparison of Cold Blob events

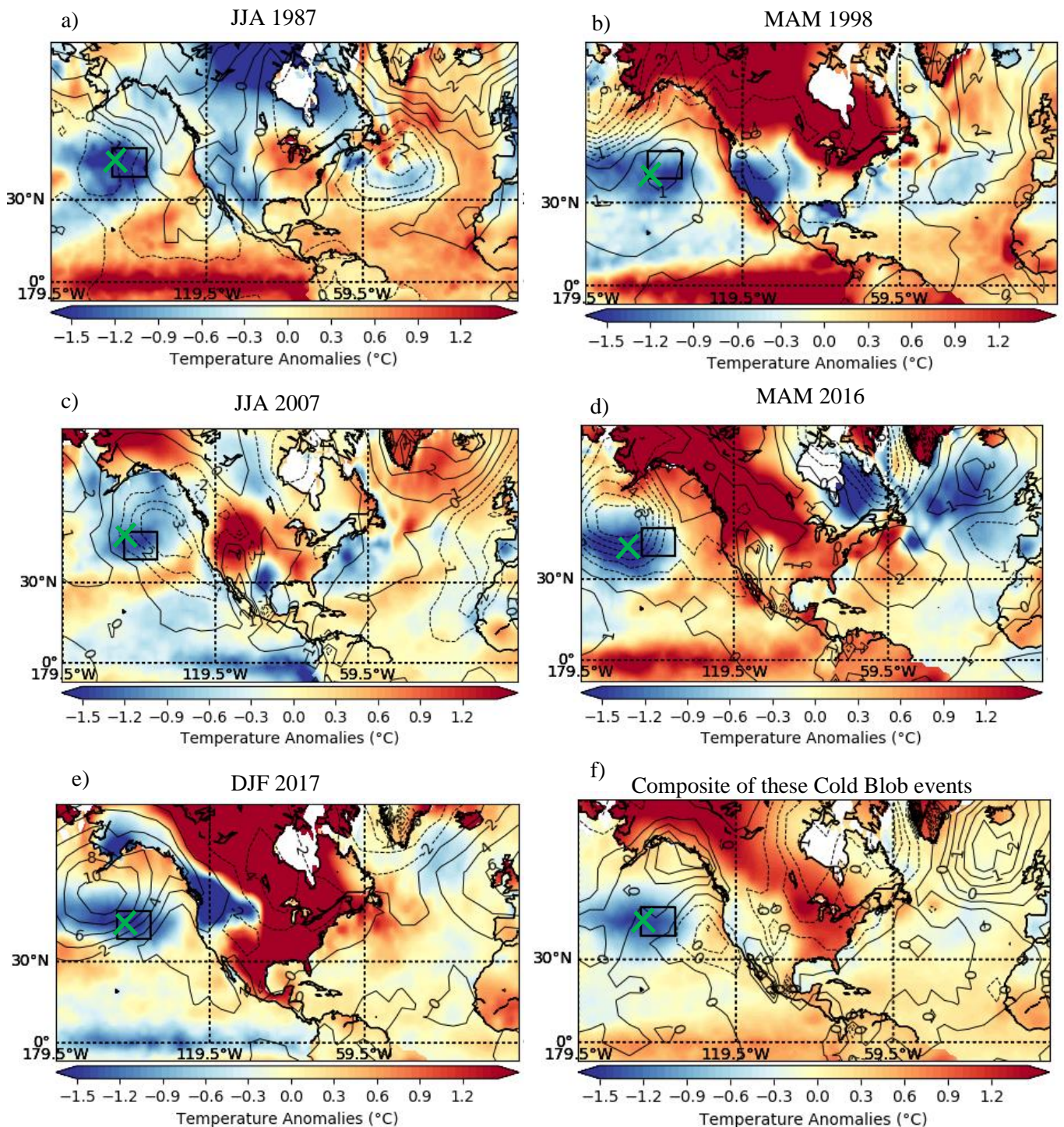


Figure 12: Subplots to show the characteristics of the Cold Blob in maximum SST negative anomaly years. Both land and SST anomaly data are calculated using a base period of 1981-2020. The SSTs are calculated using HadISST1 minus the global temperature anomaly HadSST SST data. The land temperature anomalies are calculated using the Berkeley dataset. Mean Sea Level Pressure contours have also been added using HadSLP2r data. Each map identifies a different timeframe of seasonally averaged data: a) Winter 1987 b) Spring 1998 c) Summer 2007 d) Summer 2016 e) Winter 2017 and f) A composite image of all 5 events averaged. The green crosses represent the centre of the anomalously large Cold temperatures. The black box indicates the region bound by 155-142.5°W and 37.5-45.5°N.

Using data from Figure 12 it can be concluded that the Cold Blob's location and characteristics change between timeframes. This is evident from the movement of the green cross in Figure 12. Figure 12 also shows that the Blob varies significantly in width. In Figure 12b the negative SSTs cover a large longitudinal stretch. This is also the case in Figure 12d, suggesting that the Cold Blob is less homogenous in shape than the Warm Blob. Although Cold Blobs appear to cover a much larger area than bounded by the box, the largest anomalies are located near to or within the box region. Overall, it appears that the Cold Blob has largest magnitude anomalies ($<-1.5^{\circ}\text{C}$), similar to the Warm Blob, the largest anomalies are located in the centre of the Blobs.

In corroboration with the winter Warm Blobs appearing to have warm land temperature anomalies, the Cold Blob event that occurred in the winter of 2017 (Figure 12e) was coupled with cold land temperatures inland (-1.5°C along the western coast and in the Gulf of Alaska). This could suggest that the land is more susceptible to temperature influences of the Blob in the winter months. However, Figure 10 shows cold anomalies in this region prior to 2017, meaning that the land had already been cooled through the transportation of these cold anomalies along the North Pacific current.

The Cold Blobs which occur in the spring (shown in Figures 12b and 12d) have very similar anomalies for both the SSTs and the land. This could suggest the ENSO does impact the Cold Blob, as both 1998 and 2016 are El Niño years (Jin *et al.*, 2008). The Niño3.4 can be highlighted in these Figures as anomalously warm SSTs located around the equator. Land temperature anomalies exceed $+1.5^{\circ}\text{C}$ in the north and the east coast is also warm ($>1.2^{\circ}\text{C}$). The effects of the 2016 Cold Blob appear to be warmer and more extensive than the 1998 Blob; however, the 1998 Cold Blob influences a larger area of cold SST anomalies within the North Pacific.

It is evident from these maps that the Cold Blob is less homogenous than the Warm Blob. It is not primarily circular in shape and appears to have a more elliptical shape in spring (MAM 1998 and 2016) and winter (DJF 2017). The composite image in Figure 12f shows that the Cold Blob extends more laterally from $\sim 140^{\circ}\text{W}$ to 180°W , whereas the Warm Blob does not appear to extend this far ($\sim 140^{\circ}\text{W}$ to 165°W). This could be evidence that the drivers of the Cold and Warm Blob, although similar, may involve slightly different mechanisms which alter the area experiencing these extremes.

The appearance of the North Atlantic Cold Blob appears to be less consistent with the North East Pacific Cold Blob in comparison to the Warm Blob. From these images there is very little evidence to suggest that the Atlantic Blob appears in unison with the Pacific Cold Blob, as temperatures in the Atlantic appear to be highly fluctuating.

Focussing on the MSLP patterns, 4 out of the 5 time frames display an anomalous pressure pattern located near to the region. Figure 12e (winter 2017) demonstrates that a significantly low-pressure centre was observed over the Cold Blob in 2017, with anomalies of -10hPa . Figure 12d (spring 2016)

shows a positive anomaly of +6hPa in the centre. Comparatively, in 2007 a low-pressure centre anomaly was observed reaching a low centre of -3hPa (summer 2007). This supports the conclusion that pressure relates to the occurrence of the Cold Blob differently depending on season and that the effects of pressure incur different impacts seasonally. The composite image (Figure 12f) shows negligible pressure anomalies, which could suggest that pressure plays no part. Alternatively, the negligible pressure anomalies could be a result of large positive and large negative anomalies cancelling each other out.

Table 3: A table to summarise the frequency and intensity of the Warm and Cold Blobs from 1950-2020 using the raw SST anomalies (using a base period of 1981-2020). It should be noted that this table includes persistent events, not just the season the Blob was first identified in.

| | Warm Blob (>+1°C) | | Cold Blob (<-1°C) | |
|---------|---|---|---|---|
| | Frequency of events in this period (Total=22) | Average magnitude of events in this period (°C) | Frequency of events in this period (Total=13) | Average magnitude of events in this period (°C) |
| Autumn | 2 | +1.23 | 7 | -1.25 |
| Winter | 6 | +1.20 | 2 | -1.25 |
| Spring | 5 | +1.21 | 0 | 0 |
| Summer | 9 | +1.18 | 4 | -1.55 |
| Average | | +1.21 | | -1.35 |

To assess the seasonality of the Warm and Cold Blobs a raw SST timeseries was used and Cold and Warm Blobs were identified based on anomalies >+1°C and <-1°C (see methods for details). The raw SSTs were used because the timeseries with the effects of global temperature removed (as seen in Figures 9 and 10) shift the temperature values, meaning that a very low frequency of Cold Blobs occur.

Table 3 demonstrates that more Warm Blob events were recorded in comparison to Cold Blob events in the period of 1950-2020. The Warm Blob has the highest frequency of events in summer, with an average anomaly value of +1.18°C. This average magnitude is the lowest of all the seasons. This may be due to climatology, as temperatures are already warm in summer. This means that there will be less discrepancies between average temperature and anomalies.

It was found that autumn incurs the largest average anomaly (+1.23°C) in relation to Warm Blobs. However, the Blob only occurs twice in this season and the average anomalies of the Warm Blobs are very similar with an average of +1.21°C. If the average anomalies in Table 3 were rounded to 1 decimal place, each seasonal average anomaly would be +1.2°C. This supports the statement that the Warm Blob is homogenous.

The Cold Blob data is more limited due to a lower frequency of events. It appears that over half of the events occur in the autumn (54%), with an average anomaly of -1.25°C and the largest anomaly values occur in summer -1.55°C . This is as expected, as the warm average climate experienced in summer would need to deviate more from climatology in order to show a significantly Cold Blob. No Cold Blob events between 1950-2020 occurred in the spring and very few in the winter.

On average, the intensity of the Cold Blobs are higher than that of the Warm Blob, by an average of 0.14°C . However, this value is relatively small, and the anomalies are very similar, corroborating the fact that these Blobs are very similar.

3.6 Comparison of sea surface temperature anomalies and mean sea level pressure

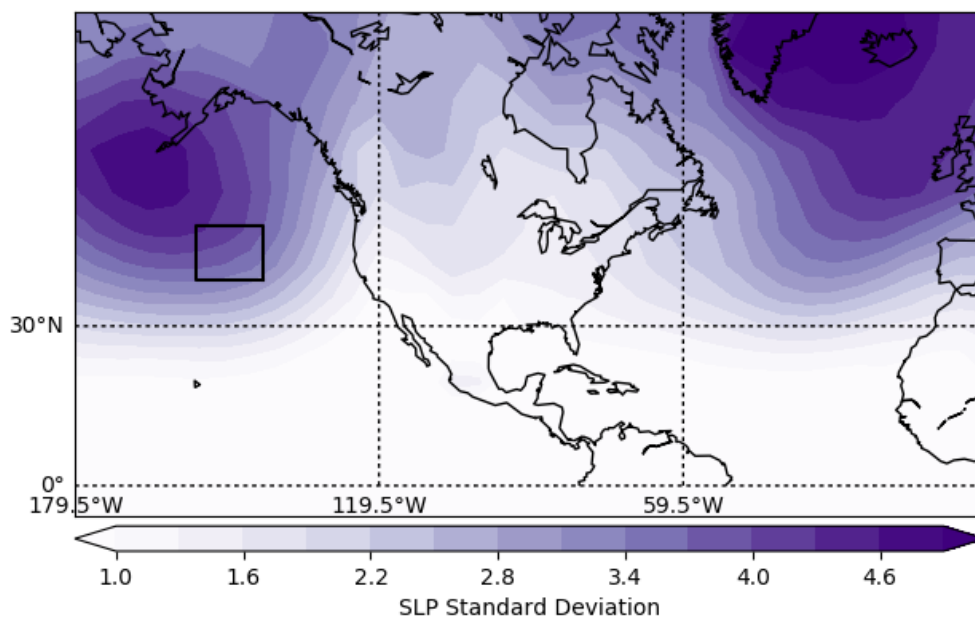


Figure 13: A global map to show the standard deviation of the monthly sea level pressure anomalies (calculated with a base period of 1981-2020) overtime from 1880-2020 for each grid point. This data uses the HadSLP2r dataset.

It is important to assess the standard deviation in this region to see if this highly deviating location of SSTa is related to highly deviating MSLP anomalies. The North East Pacific experiences a very large sea level pressure standard deviation (>3.4 hPa) in comparison to regions in the same latitude in the northern hemisphere. This is conclusive evidence that a large variation of pressures are observed. This suggests that there is some relationship between pressure and the extreme temperatures the Blob experiences. However, this high standard deviation could also be a consequence of the storm track in this area (Hakim, 2003) as America is prone to cyclones and hurricanes, caused by a large range of pressure. Figure 13 shows an even larger MSLP deviation north of the region bounded by the black box. This could suggest that the correlation between the SSTa in the box could have a stronger correlation with MSLPa more northward as deviations are larger here.

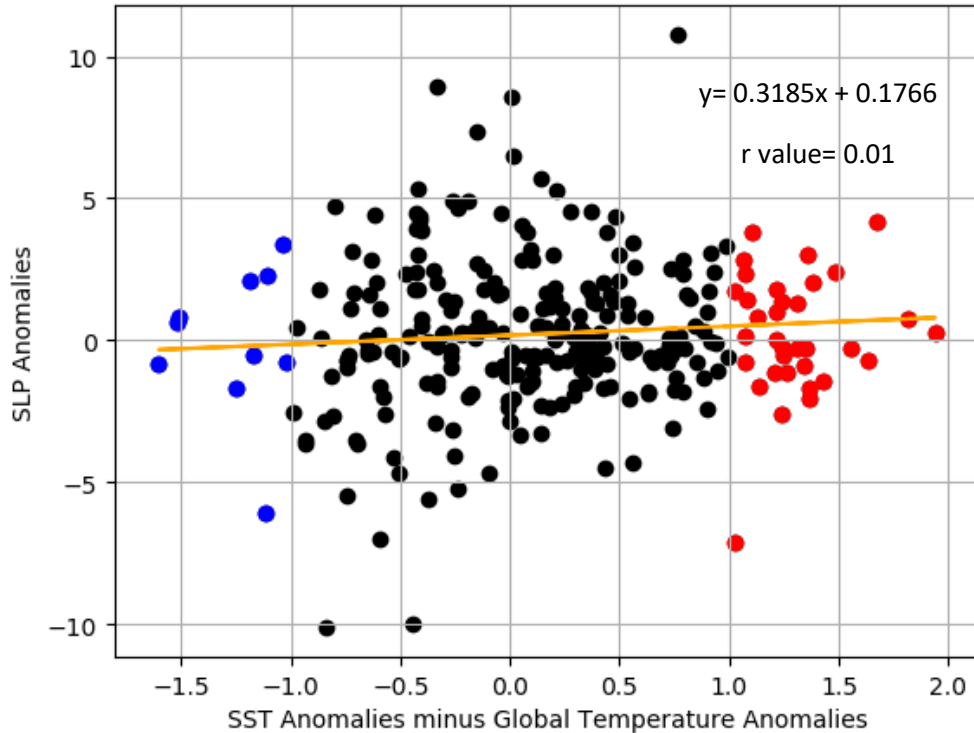


Figure 14: A scatter graph to demonstrate the relationship between the raw SST anomalies ($^{\circ}\text{C}$) and SLP anomalies (hPa) with an added line of best fit (orange line). The blue dots represent a Cold Blob and the red dots represent a Warm Blob. Each time variable was calculated using an average value of the chosen region $155\text{-}142.5^{\circ}\text{W}$ and $37.5\text{-}45.5^{\circ}\text{N}$ for both SST and SLP. The SST anomalies used, come from the HadISST1 dataset and the SLP anomalies used are from the HadSLP2r dataset. This is for the period of 1950-2020.

The SST minus global temperature anomaly dataset was used to successfully compare the mapped SST anomalies shown in Figures 11 and 12 with the correlation between SST and SLP anomalies for the period of 1950-2020. Therefore, Figure 14 has also used the SST minus global temperature anomaly dataset. From this scatter it can be deduced that there is a very minor positive relationship between SST and SLP anomalies ($r = +0.1$). This suggests that as SSTs increase so do SLP anomalies. Through analysing the Warm Blob events, it is evident that the majority of SLP values lie either just below 0 or between 0 to +5. In comparison, during Cold Blob events the SLP anomalies are more scattered around 0.

This weak relationship is not statistically significant and thus can not support the fact that the Warm Blobs occur due to high pressure in this area, such as the ‘ressilient ridge’ 2014 event (Bond *et al.*, 2015). The lack of correlation shown in this graph fails to support the hypothesis that the higher the pressure anomaly, the more likely a Warm Blob will occur in this region. This negligible relationship could be affected by corresponding pressures from other regions. For example the corresponding pressures associated with this warming may not occur in the specific region surrounding the Warm Blob but by pressures located in a region nearby (Overland and Weng, 2016). Figure 13 suggests that the highest deviation is located more north than the location of the box. This means that the relationship

could occur more northerly than the region that was used in the timeseries for the mean SLP anomalies of the box region. This is corroborated by the location of the pressure anomalies in Figures 11a, 11c, 12c, 12d and 12e. This northerly area could be further investigated in future work in comparison to the SST anomalies.

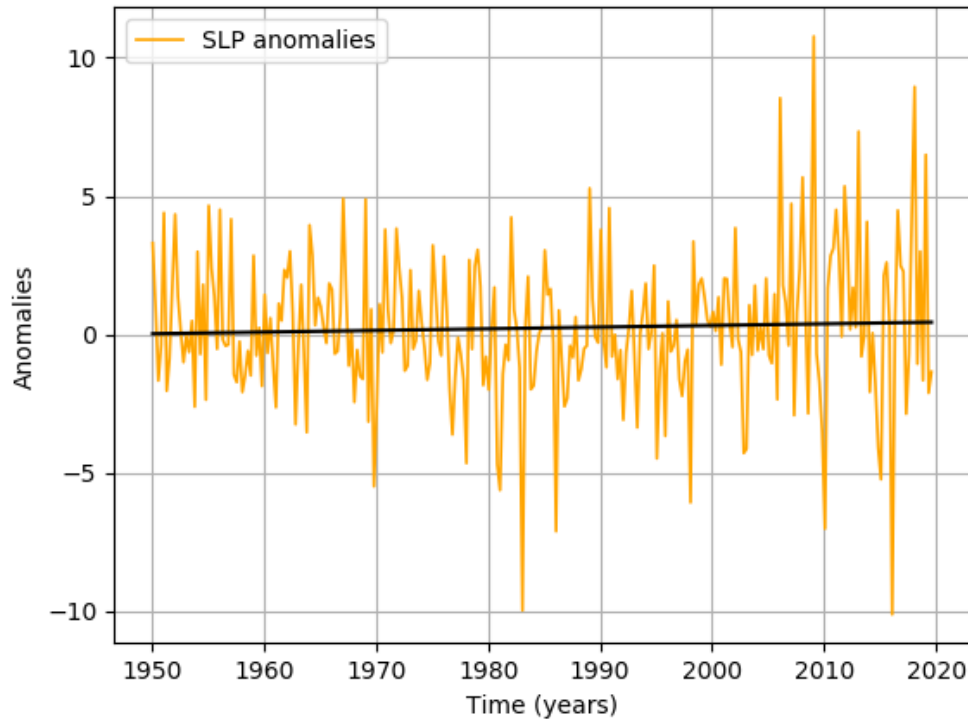


Figure 15: A timeseries to show SLP anomalies (HadSLP2r) between 1950-2020. The anomaly data was calculated using a base period of 1981-2020. Each time datapoint was calculated using an average value of the chosen region 155-142.5°W and 37.5-45.5°N. The black line here shows the trendline of SLP anomalies overtime.

The linear regression relationship between SST and SLP anomalies shows that there is a negligible positive relationship, with an r value of 0.002. This value demonstrates that there is no correlation between SLP anomalies and time.

The timeseries between 2000-2020 shows a large variation between both anomalies. When comparing the standard deviation between 1980-2000 and 2000-2020, it was found that the more recent period has a larger deviation. The years 2000-2020 had a standard deviation of 4.88hPa compared to 3.64hPa in the earlier period of. This corroborates the statement that recently SLP anomalies have been more anomalous. The 2014 Warm Blob event was said to be a result of a resilient ridge of high pressure (Bond *et al.*, 2015), this was supported by the analysis shown in Figure 15. The 2014 peak SST anomaly (+1.4°C) also experiences an SLP anomaly peak (+7hPa). Whereas, the identified Cold Blob year of 2017, saw a trough in the SLP dataset as low as -10hPa. These values support the link between Blob events and the high and low- pressure systems found in Figures 11e and 12e.

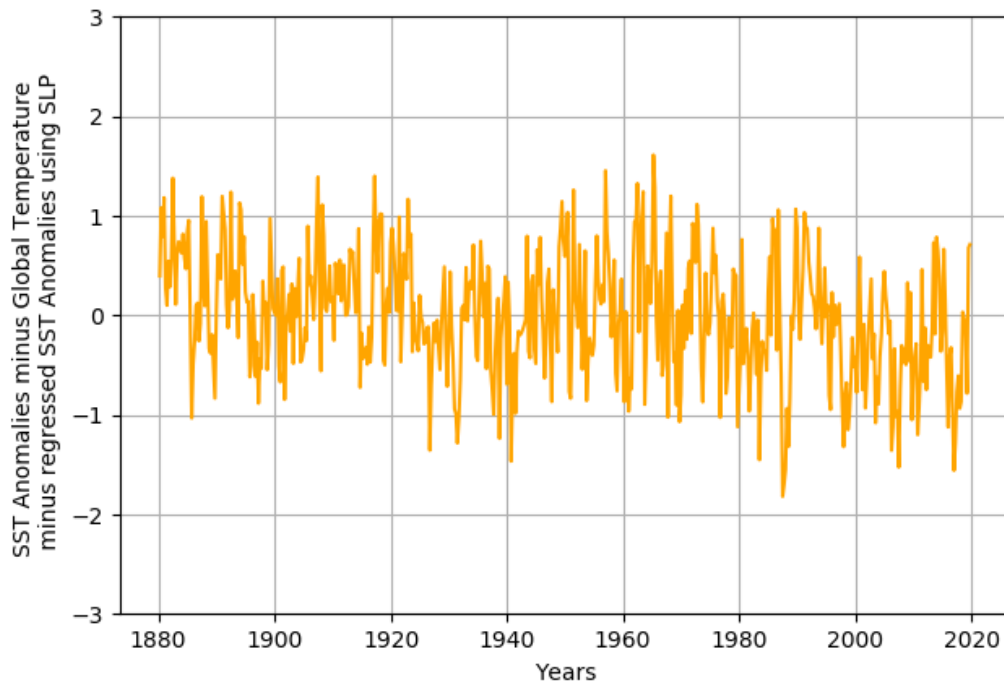


Figure 16: A timeseries to show the raw SST anomalies ($^{\circ}\text{C}$) (with the effects of global temperature removed) minus the modelled SST anomalies calculated using linear regression with the Sea Level Pressure variable. All the raw anomaly data was calculated using a base period of 1981-2020. Each datapoint was calculated using an average value of the chosen region $155\text{-}142.5^{\circ}\text{W}$ and $37.5\text{-}45.5^{\circ}\text{N}$. The SST minus global temperature data used the HadISST1 minus HadSST and the SLP anomalies used are from the HadSLP2r dataset.

Figure 16 shows the SST anomaly timeseries with the linearly regressed SST anomalies, modelled using SLP anomalies, removed. From this Figure it would appear that in recent years, the removal of SLP effects has reduced the peak experiences (i.e. in 2013-2014, 2000, 1991 and 1989) however, the peak observed in 1964 was not affected by the removal of SLP effects. For the period between 1940-1960, the SST anomaly values do not seem to have significantly changed in comparison with Figure 14. This would suggest that the high anomalies seen around this time did not occur as a result of SLP; however, as previously stated it could be SLP in a different region from the Blob which has a larger influence.

The removal of the effects of SLP has also reduced the intensity of the cold anomalies, with some exceptions. The 1987 and 2017 cold anomaly seems to have slightly increased in negativity. This cannot be explained through the trendline shown in Figure 14, where a negligible, marginally positive trend is seen with an r value of $+0.1$.

3.7 Frequency and intensity of Warm and Cold Blobs

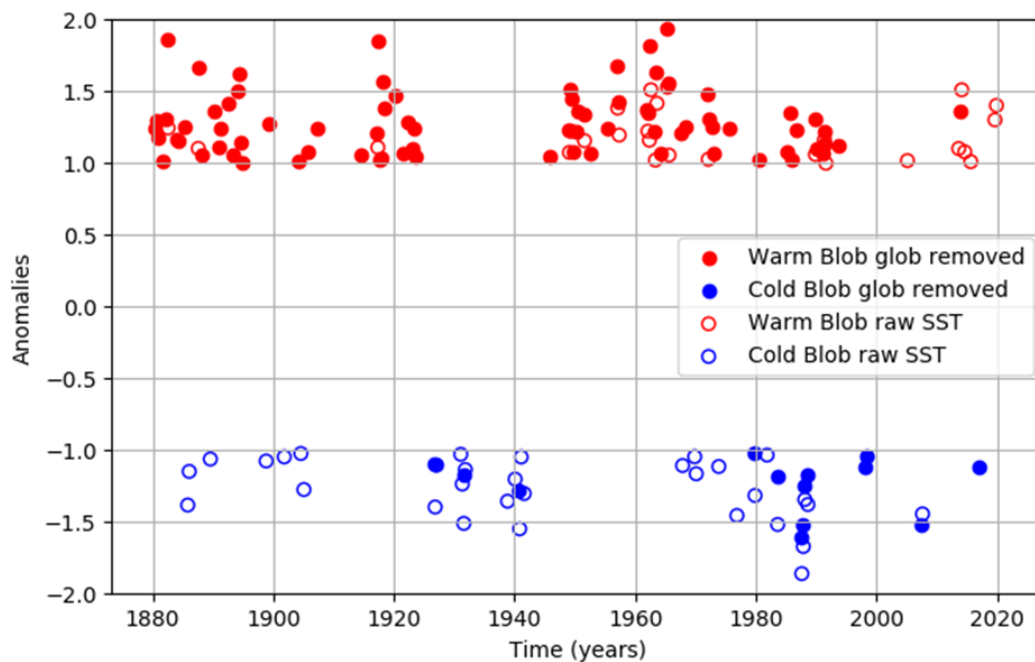


Figure 17: A timeseries to show the occurrence of the Cold and Warm Blobs and their associated intensities for the time period 1880-2020. In this circumstance a Warm Blob has been defined as $>+1^{\circ}\text{C}$ and a Cold Blob $<-1^{\circ}\text{C}$. Each time datapoint was calculated using an average value of the chosen region $155\text{-}142.5^{\circ}\text{W}$ and $37.5\text{-}45.5^{\circ}\text{N}$. The raw SST Blobs are displayed as unfilled circles and the SST minus global temperature dataset used (HadISST1 minus the HadSST data) Blobs are shown as filled circles.

This timeseries shows the Warm and Cold Blobs for both the raw SST data (no fill) and the SST data with the global temperature removed (filled), identified using the method stated in Section 2.2.2. It can be deduced from this timeseries that the occurrence of Cold and Warm Blobs changes significantly between the raw SST anomaly dataset and the dataset with the effects of global temperature anomalies removed. By removing global temperature effects, these results would suggest that both the warm and cold events have experienced warming. This has resulted in more warm events than the raw dataset and less cold events. This could mean that an artificial trend has been added in both these datasets and is a limitation of the method using in this project.

Figure 17 shows that the Warm Blobs do not appear to have any recurring pattern on which they evolve over time. From 1922-1942 there was a large period where no Warm Blobs occurred in either of the datasets however, numerous Cold Blobs appeared. Between 1980 and 1995 many Warm Blobs and Cold Blobs occur, suggesting the marine climate of the North East Pacific, at this point, was unsettled.

Since 1970 the Cold Blob has been more recurrent as evident from the raw SST anomaly data. As mentioned previously, the occurrence of the Cold Blobs appears to associate with ENSO years. Between the period of 1970-1990, where these Cold Blobs appear most frequently, major ENSO events occurred from 1972-73 and 1982-83 (An and Jin, 2004). The 1987 Cold Blob was also thought to be a result of

the rebound from the extreme low ENSO index which occurred in 1986 (McPhaden and Picant, 1990). The importance of the ENSO in this time period could be essential in predicting future Cold Blobs.

3.8 Links to atmospheric circulation patterns

As discussed, the link between SST anomalies and various teleconnections has been investigated in order to see if the combined impacts of these phenomena can be used as an explanation of appearance of the Warm and Cold Blobs. This has been done using linear regression to investigate both the monthly and seasonal r coefficient values and to depict the significance of the relationship (i.e. to see whether the relationship is positive or negative). Additionally, certain teleconnections have been compared to the SSTs using a lag time to explore whether this region has a delayed response to these phenomena.

To investigate the correlation coefficient between the SST timeseries and the variable timeseries, the raw SST data was used in place of the dataset with the effect of global temperature anomalies removed. This was chosen as otherwise the datasets would not be comparable as the teleconnection variable will incur this underlying global temperature warming.

Table 4: A summary table to show the r correlation coefficient values found using linear regression for each teleconnection variable in comparison to the SST-global temperature anomaly dataset. These values are all representative of a 0-month time lag.

| Variable | Data Set | r value using raw SST Anomalies (monthly) for the period 1950-2020 | r value using raw SST Anomalies (monthly) for the period 1979-2020 | r value using raw SST Anomalies (seasonal) for the period 1950-2020 | r value using raw SST Anomalies (seasonal) for the period 1979-2020 |
|------------------------------|----------|--|--|---|---|
| El Niño Southern Oscillation | iHadist1 | 0.05 | 0.08 | -0.00 | 0.03 |
| Pacific Decadal Oscillation | SWFSC | -0.20 | -0.20 | -0.30 | -0.28 |
| Arctic Oscillation | CPC | 0.07 | 0.06 | 0.10 | 0.08 |
| Madden Julian Oscillation | CPC | | -0.09 | | -0.14 |
| North Atlantic Oscillation | CPC | 0.07 | 0.06 | 0.024 | -0.02 |

Table 3 suggests that the monthly relationship between the SSTa and the AO and NAO is negligible with almost no statistical significance (0.06 for period 1979-2020). The monthly relationship between the MJO and the SST anomalies is also very small, with an r value -0.09 (1979-2020). Although, the NAO is a phenomenon located in the Atlantic basin as opposed to the Pacific, it is thought that the

North Atlantic Cold Blob and the North East Pacific Warm Blob could be linked. This would suggest that there would be a more significant relationship between the SSTa representing the Warm Blob and the NAO (Rahmstorf *et al.*, 2015). This is because it is predicted that the NAO, accompanied by the AMOC, is the main mechanism for driving the North Atlantic Cold Blob. A likely explanation that these relationships appear negligible is that a phenomenon occurring in the Atlantic basin that affects the Pacific basin incurs a time lag. This will be further investigated later in this study.

Using data from Table 3 it can be concluded that the SST anomalies have the most significant seasonal relationship with the Pacific Decadal Oscillation with an average r value of -0.3. This value suggests that there is a negative relationship between the PDO and the anomalies, meaning that when the PDO decreases the SST anomalies increase and vice versa. This is was expected, since in the negative phase of the PDO, warm SST anomalies are usually apparent in the interior of the northeast Pacific Ocean, while the coastal regions cool (Mantua, 1999). This negative phase is often accompanied by above average sea level pressures over the North Pacific and could in turn be the reason why these high-pressure ridges have become apparent when this Warm Blob has been identified.

With reference to the literature one would expect the relationship between the ENSO and the SSTa to be more statistically significant. A seasonally averaged r coefficient of 0.08 shows no statistically significant relationship.

Tseng *et al.*, 2017 also investigated this relationship by analysing the r values between these variables to test for a statistically significant relationship. A much stronger relationship was observed between the two teleconnections and the SST anomalies. This investigation also used the HadISST1 SST dataset however, it used a base period of 1958-2016. Using this analysis, it was found that after the removal of monthly mean climatology the Niño3.4 index correlation coefficient was 0.88. The PDO also showed a very strong relationship of 0.67. These differentiating values would suggest that in more recent years the PDO and the Niño3.4 index have played a lesser role in the development of the warm and Cold Blobs than in previous time periods.

3.8.1 El Niño Southern Oscillation

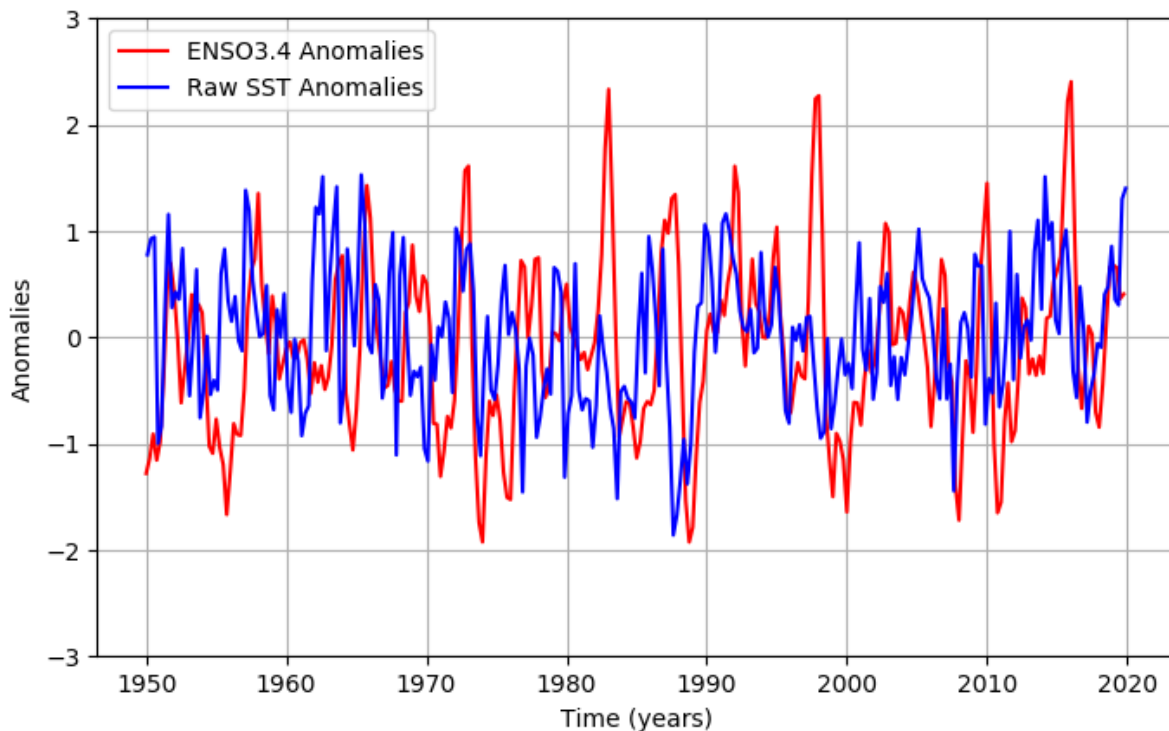


Figure 18: A seasonal timeseries to show the raw SST anomaly data (blue) (HadISST1) as well as the Niño3.4 index (red) (the HadISST1 Niño3.4 index dataset) for the period of 1950-2020. The anomaly timeseries data was averaged for the chosen location of 155-142.5°W and 37.5-45.5°N and have units of °C. The anomaly variables both use a base period of 1981-2020.

Overall, the relationship between ENSO and SST anomalies overtime can be quantified by an r value of 0.08, suggesting there is almost no relationship. Peaks and troughs shown in Figure 18 do not align suggesting that these variables do not intensify simultaneously. This could mean a time lag between the two occurs. These two datasets assess the relationship between the SST anomalies in the Blob region, 155-142.5°W 37.5-45.5°N, with the SST anomalies in the Niño3.4 region, 170-120°W -5-5°N. Due to the distance between these location, it is assumed that a time lag will incur due to the distance the water mass would need to travel.

A proposed time lag between these two variables has been investigated by Feng *et al.* (2014) who argued that the SST anomalies in this chosen Warm Blob region could act as a possible precursor of ENSO instead of a response to ENSO. This is thought to occur through the PDO dynamics (Feng *et al.*, 2014). Capotondi *et al.*, (2019), also investigated a time lag between ENSO index and the SST anomalies in this region, to investigate why in some periods, SST anomalies respond very sensitively to ENSO events and others do not. It was concluded from this investigation that the optimal correlation ($r=0.66$) occurred for a time lag of 7 months (Capotondi *et al.*, 2019). Figure 19 shows that the peak SST anomaly in 2014 (1.4°C) is located around 6-months before and after a peak in the Niño3.4 index (2010=1.4°C,

2016=1.6°C). A lag time investigation was performed to assess if whether either of these are related to the 2014 event.

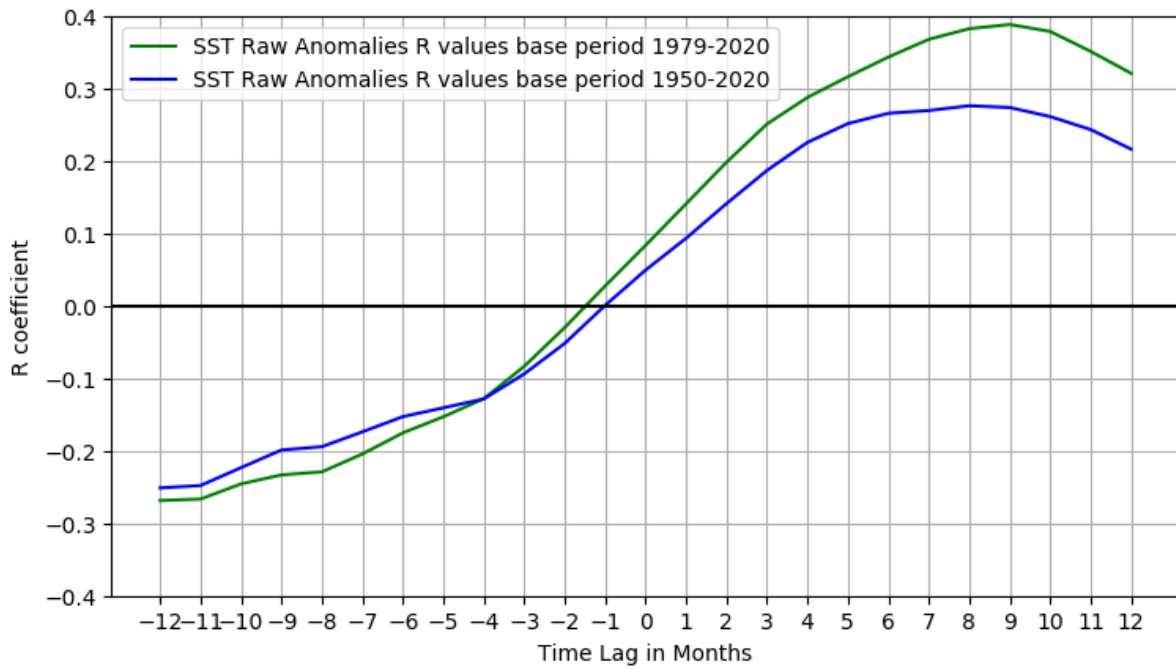


Figure 19: A graph to show the tropospheric temperature time lag between the Niño3.4 index and the raw SST anomalies which are constructed using a base period of 1981-2020. The linearly regressed are coefficient is calculated monthly using the period of 1950-2020 (blue) and 1979-2020 (green). The raw SST anomaly data is from the HadISST1 dataset and the Niño3.4 index from the HadISST1 Niño3.4 index.

A time lag between the raw SST anomalies and the Niño3.4 index was investigated by shifting the time series by 1 month at a time and computing the r correlation value between the time series. In Figure 19 a negative lag would mean that the SST anomalies lead the ENSO and a positive lag would mean that the ENSO leads. This dataset looked at all months from 1950-2020.

It appears that the strongest relationship between ENSO and the SST anomalies arises when there is a positive lag, which the ENSO leads by 9 months (r value= 0.39). This would imply that the ENSO is a precursor of the SST anomalies and indicates that a 9-month temporal lag occurs in the SST pattern as a response to ENSO related forcing in the tropical Pacific.

Lau and Nath (2001) suggest that a time lag occurs in respect to the Niño3.4 variable as important atmospheric circulation changes over the North Pacific and Atlantic occur under ENSO forcing during midwinter. These teleconnection patterns alter the exchange of heat across the local ocean-atmosphere interface.

Through a correlation investigation between the two variables, it is evident that the North Pacific SST anomalies have more statistical significance when they lag the ENSO index (Lau and Nath, 2001). In an experiment by Lau and Nath (2001), an ENSO lead of 2 months was compared to no lag time and to an SST lead of 2 months. It was concluded that the ENSO 2 month lead had the strongest correlation

with the SSTs in the North Atlantic when compared to the other two-time frames. Although this lead is 7 months smaller than the results obtained in Figure 19, there is corroboration that the ENSO leads the SST anomalies. It should be noted that this experiment was in relation to the North Pacific basin and not specifically the Blob region.

The data presented in Table 4 assessed a more refined period of 1979-2020. In this data the overall r value with no time lag was higher than that for 1950-2020 (0.08). However, the time lag investigation shown for the later period was lower than for 1950-2020.

Using the base period 1979-2020, the results show corroborating r values to those seen in 1950-2020. The maximum r value can be seen when the SST anomalies are delayed 8 months after the ENSO. This r value (0.28) is lower than the maximum values for the previous base period (1950-2020, maximum r value = 0.39) and incurs a reduced lag by one month.

Additionally, a high r value (in relation to this magnitude) was also observed when the ENSO occurs at a 12-month time lag after the SST anomalies (r value = -0.25). Although this value is not as high as the positive 8-month time lag, the values are close. This means that this relationship is difficult to assess, and that it is inconclusive which variable is a precursor.

Although the r values found in these two experiments do differ, the lag relationship appears to show a very similar arc shape increase of a relatively similar magnitude, suggesting that this time lag is significant.

To conclude, it appears that the ENSO is weakly associated with SST anomalies and has the highest correlation coefficient value when the ENSO precedes the SST anomalies by 8/9 months. This suggests that the Niño3.4 associated warm SSTs, take 8/9 months to influence the Blob region.

3.8.2 Pacific Decadal Oscillation

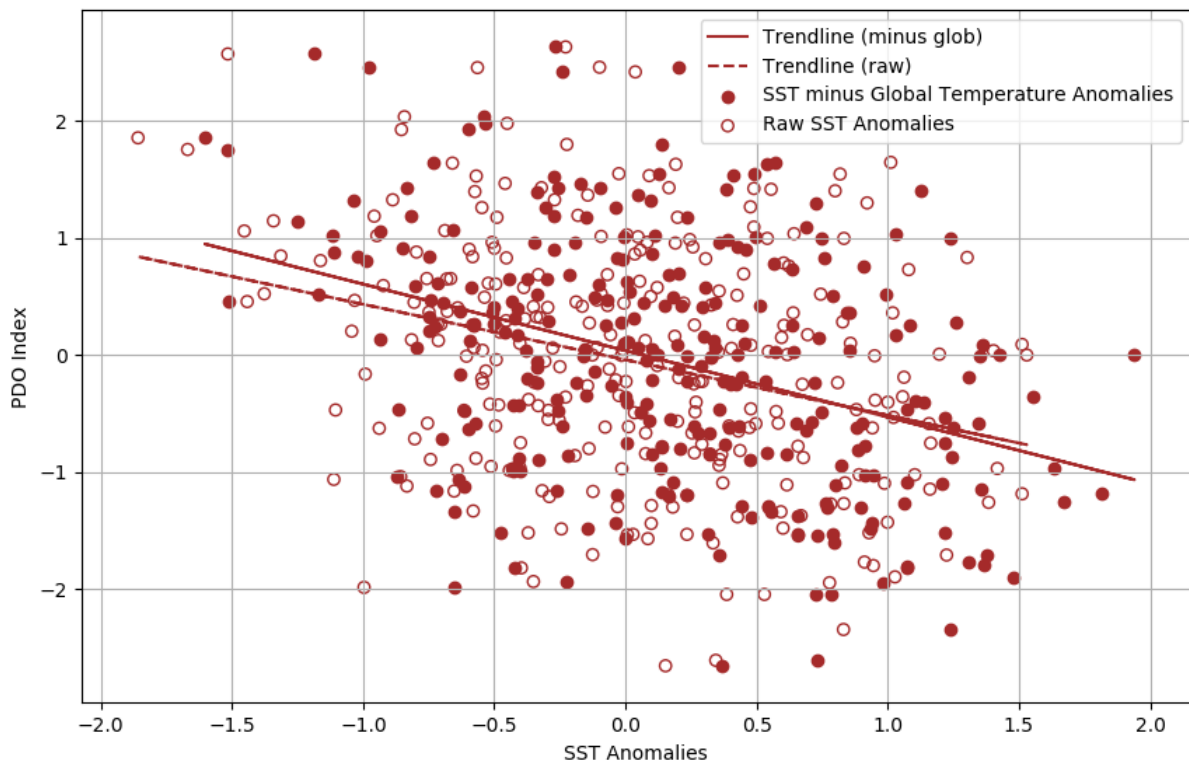


Figure 20: A scatter to show the relationship between the PDO index (SWFSC) and the raw SST anomalies ($^{\circ}\text{C}$) (filled circle- HadISST1 data) as well as the PDO and the SST anomalies with the effects of global temperature removed ($^{\circ}\text{C}$) (HadISST1-HadSST), for the period of 1950-2020. Each variable is representative of averaged data for the chosen location of 155-142.5 $^{\circ}\text{W}$ and 37.5-45.5 $^{\circ}\text{N}$. Lines of best fit using linear regression have been added to demonstrate a relationship. Anomalies have been calculated with a base period of 1982-2020.

Data in Figure 20 highlights that there is a negative relationship between the PDO and SST anomalies (for both datasets). This is supported by Table 4, which demonstrates that the seasonal correlation coefficient is -0.3. This means that as the PDO index increases anomalies become more negative and that the lower PDO values are indicative of higher positive anomalies. This supports the description of the PDO given by Mantua *et al.*, (1997) which states that the PDO has a positive value when SSTs are anomalously cool offshore in the North Pacific. This is also supported by the negative SST anomalies, on average, having a larger PDO index. Alternatively, the PDO has a negative index when SST anomalies are warm offshore in the North Pacific (Mantua *et al.*, 1997). This relationship implies that the location bounded by 155-142.5 $^{\circ}\text{W}$ and 37.5-45.5 $^{\circ}\text{N}$ (Blob region) follows the generic SST relationship with the PDO for the larger region of the offshore North Pacific basin.

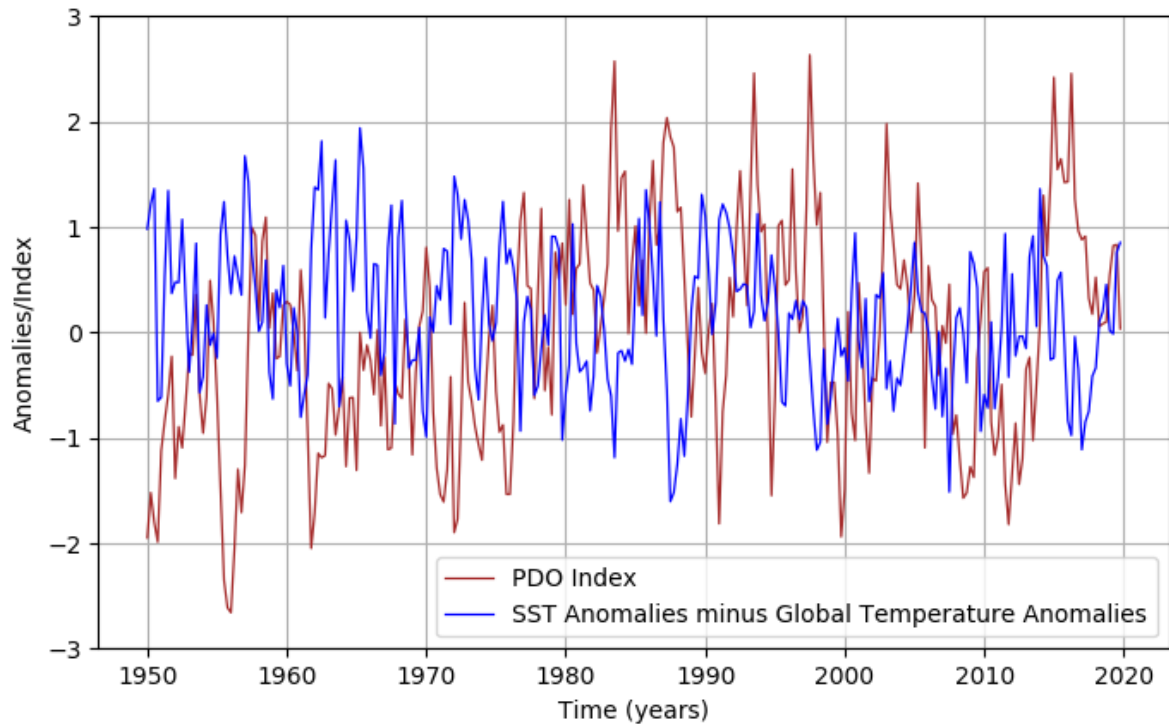


Figure 21: A timeseries to show the SST anomaly data ($^{\circ}\text{C}$) (blue) (minus the effects of global temperature anomalies- HadSST1 minus HadSST) as well as the PDO index (brown) (SWFSC dataset) for the period of 1950-2020. Each variable is representative of averaged data for the chosen location of $155\text{-}142.5^{\circ}\text{W}$ and $37.5\text{-}45.5^{\circ}\text{N}$. The SSTa data uses a base period of 1981-2020.

Figure 21 supports the negative relationship observed in Figure 20, that there is an inverse correlation between the PDO index and the SST anomalies. This means that positive temperature anomalies are correlated with a negative PDO and negative SSTa have a positive PDO.

In 1987 a clear peak in the PDO index at +2 incurs a clear trough in SST anomaly at -1.6°C . This can be seen later in the timeseries. In 2017 a substantial peak in the PDO is accompanied by a drop in SST anomalies (-1.1°C). As noted in previous results (Figure 12), 2017 is identified as a Cold Blob year. This suggests that this Cold Blob was accompanied by a high PDO index of +2.3. Between 1976-1986, this relationship is less evident as well as between 2000-2010.

Although the r coefficient depicts a relatively weak seasonal relationship of -0.3, it would appear that within specific time frames this relationship is much stronger. A time lag was investigated for the relationship between the PDO and the SST anomalies however, it was concluded that the correlation was maximised where there was a zero-month lag.

3.8.3 Arctic Oscillation

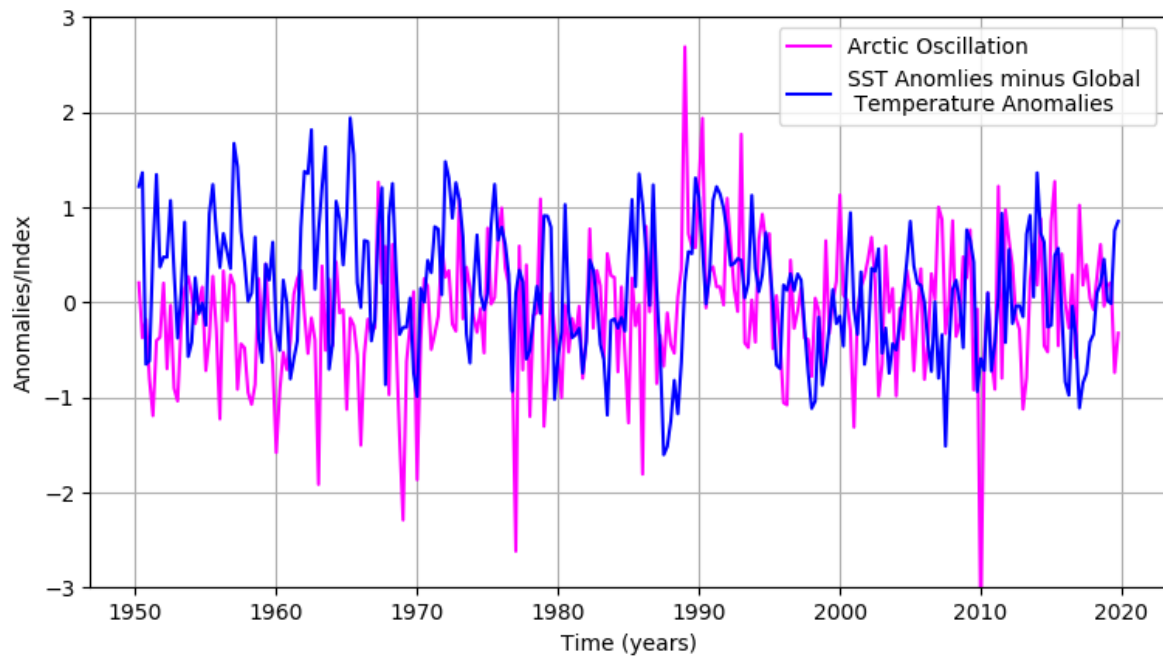


Figure 22: A timeseries to show the SST anomaly data ($^{\circ}\text{C}$) (blue) (minus the effects of global temperature anomalies- HadSST1 minus HadSST) as well as the AO index (magenta) (CPC dataset) for the period of 1950-2020. Each variable is representative of averaged data for the chosen location of $155\text{-}142.5^{\circ}\text{W}$ and $37.5\text{-}45.5^{\circ}\text{N}$. The SSTa data uses a base period of 1981-2020.

Figure 22 demonstrates that at different time frames in the timeseries, opposing relationships can be seen. From 1950-1970, it appears that the AO and the SST anomalies are of opposite sign (when the SSTa peaks there is generally a trough in the AO index). This occurred in 1966 where a peak in SST anomalies of $+1.9^{\circ}\text{C}$ was accompanied by a trough in the AO index -1.5 . From 1970-2010, this relationship continued however, it was weaker than the relationship identified between 1950-1970. The relationship also dissipates between 2010-2020, and a lack of correlation is apparent.

Table 5: The r values for decadal seasonally averaged data to demonstrate the relationship between the SST anomalies and the Arctic Oscillation Index during specific time frames. Produced using the data from Figure 22.

| Year | r Value |
|-----------|---------|
| 1950-1960 | -0.04 |
| 1960-1970 | +0.25 |
| 1970-1980 | +0.41 |
| 1980-1990 | -0.02 |
| 1990-2000 | +0.29 |
| 2000-2010 | -0.08 |
| 2010-2020 | +0.07 |

Table 5 shows that the relationship between the AO and the SST anomalies changes on a decadal scale. The most significant relationship occurred between 1970-1980 with an r value of +0.41. In certain decadal periods a negative correlation is observed.

A significant trough in the AO was identified in 2010 and reached -3 however, its corresponding SST anomaly value remained weak at -0.9°C. The difference in magnitude of these two variables at this time corroborates with the weak relationship seen in this period of -0.08 however, the 2010 relationship is positive. The range in values can be seen in Table 5. The lack of consistency in this data can be used to explain why the seasonally averaged r value is low (0.07).

3.8.4 Madden Julian Oscillation

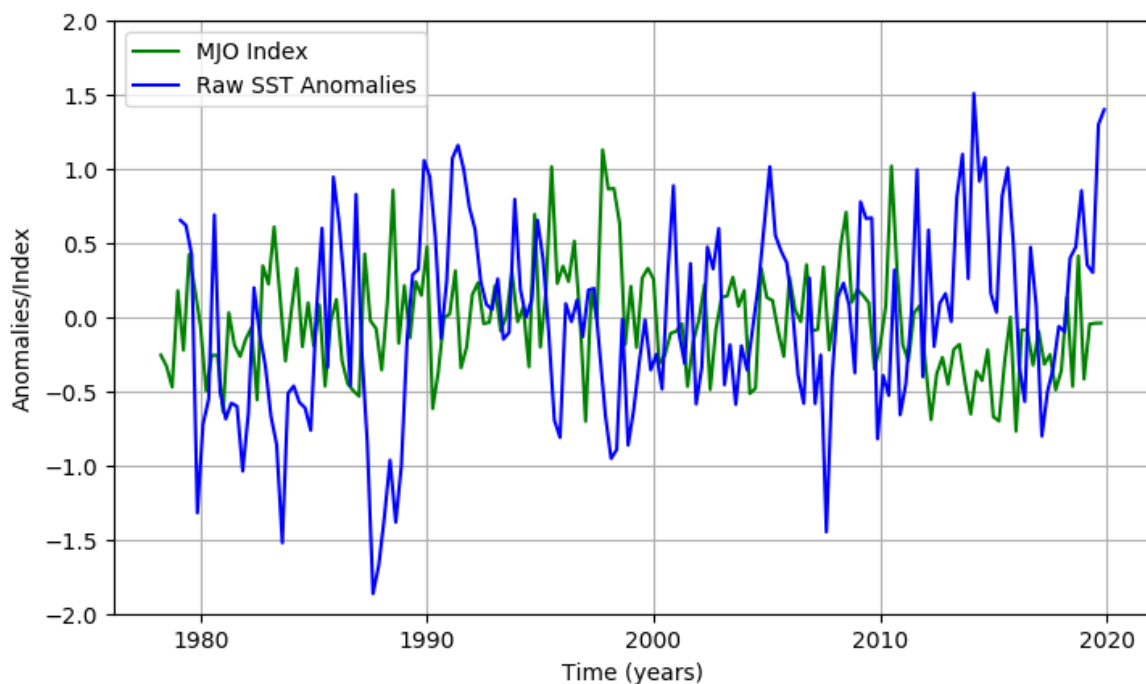


Figure 23: A timeseries to show the SST anomaly data (°C) (blue) (minus the effects of global temperature anomalies- HadSST1 minus HadSST) as well as the MJO index (green) (CPC dataset) for the period of 1979-2020. Each variable is representative of averaged data for the chosen location of 155-142.5°W and 37.5-45.5°N. The SSTa data uses a base period of 1981-2020.

Table 4 shows that the correlation between SST anomalies and the MJO is insignificant, with a r value of -0.1. Although the data for this variable is limited within this timeseries, different correlation patterns can be identified. A significant negative relationship can be seen in certain aspects of the timeseries. Meaning that a peak in SST anomalies is often accompanied by a trough in the MJO. In 2014 there is a peak in SST anomalies (+1.5°C), representing the Warm Blob, and a trough in the MJO (-0.6). Figure 23 shows that peaks in one variable are accompanied by troughs in the other, however, the magnitude of these peaks and troughs do not match. Although a positive SST anomaly is normally accompanied by a negative MJO index, the magnitude of these values were highly differentiating with little obvious pattern. This could explain why the r value is so low.

3.8.5 North Atlantic Oscillation

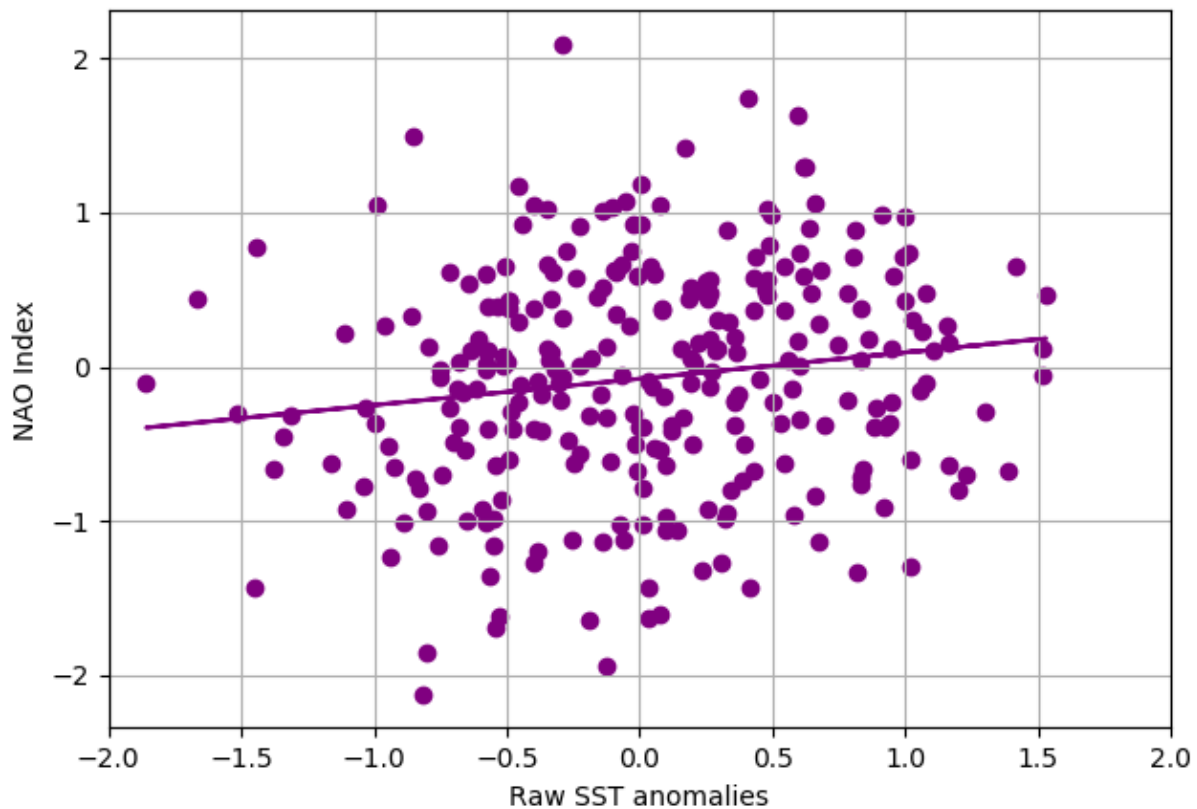


Figure 24: A scatter to show the relationship between the NAO index (CPC) and the raw SST anomalies ($^{\circ}\text{C}$) (HadISST1 data), for the period of 1950-2020. Each variable is representative of averaged data for the chosen location of $155\text{-}142.5^{\circ}\text{W}$ and $37.5\text{-}45.5^{\circ}\text{N}$. A line of best fit using linear regression have been added to demonstrate a relationship. Anomalies have been calculated with a base period of 1982-2020.

Figure 24 shows a small positive correlation between the SSTa and NAO index. This positive relationship supports the r value for the NAO that was included in Table 4 (r value = $+0.07$), suggesting that the relationship between the NAO and SST anomalies in this region is negligible. As this phenomenon primarily influences the North Atlantic, there may be a delay before the effect of this teleconnection reaches the North Pacific. For this reason, a time lag investigation was undertaken.

According to Seager *et al.* (2015), the effect the NAO has on the Pacific basin is likely delayed. This is because the changes in pressure associated with the NAO are located at near to 0°W . Consequently, for this climatic phenomenon to reach this region it must travel a large distance, as jets travel from west to east. Barry *et al.* (2004), state that there is a significant relationship between the ENSO index and NAO where the $r = -0.66$ however, the two are out of phase with a suggested time lag on a decadal scale. The relationship between the ENSO, NAO and SSTa could be further investigated using multi-linear regression in future work.

After investigating this time lag relationship, the r value was unstable, fluctuating month on month. The maximum r value of $+0.15$ demonstrates a negligible relationship between the SSTa and the NAO.

3.9 How will the Blob respond to climate change?

Cavole *et al.*, (2016) states that the Warm Blob represents an indication of things to come, as SSTs are predicted to rise with increasing global temperature. To assess whether this scenario is realistic Cavole *et al.*, compared predicted SST anomalies off the Gulf of Alaska, from 2050 to 2099 with the averages of 1956 to 2005 (using data from Riahi *et al.* (2011) and NOAA, (2016)).

In this model, the anomalies ranged from +1.5°C–4°C above the historical temperature values. These temperature anomalies were comparable to those observed throughout the Warm Blob in extreme SST anomaly years such as 2014 (Figure 5). This supports the argument that the Warm Blob could be an optimal representation of future ocean conditions (Cavole *et al.*, 2016; Kintish, 2020).

In the future, the entire water column is expected to warm, and anomalies are to be less focused to the surface layer and develop deeper, warming the water column more evenly. This will alter the characteristics of future SSTs and will improve stratification in the vertical profile. A process that can already be observed in the North Pacific in subarctic regions (Larsen *et al.*, 2007). Increased ocean stratification reduces the freshening of interior waters which could potentially lead to waters being deoxygenated (Cavole *et al.*, 2016). This will have severe knock-on impacts to both the environment and economy as fisheries would deplete. The consequences would be similar to that of the Warm Blob.

In December 2014, Peterson *et al.*, (2015) suggested that the El Niño event, which was developing at the equator, would induce another Warm Blob event in 2015/2016. However, this ENSO feature was also apparent in 2013 but the El Niño never materialised. The equatorial waters became anomalously cool during much of the summer of 2014, whilst the North Pacific was anomalously warm. Peterson *et al.* also suggest that ‘a canonical pattern of positive phase’ PDO from 2014 would be seen in North Pacific SST charts. This would have indicated that things are returning to normal SST patterns, however, a Warm Blob has developed in 2020 (Figure 3) meaning that SST patterns have not normalised.

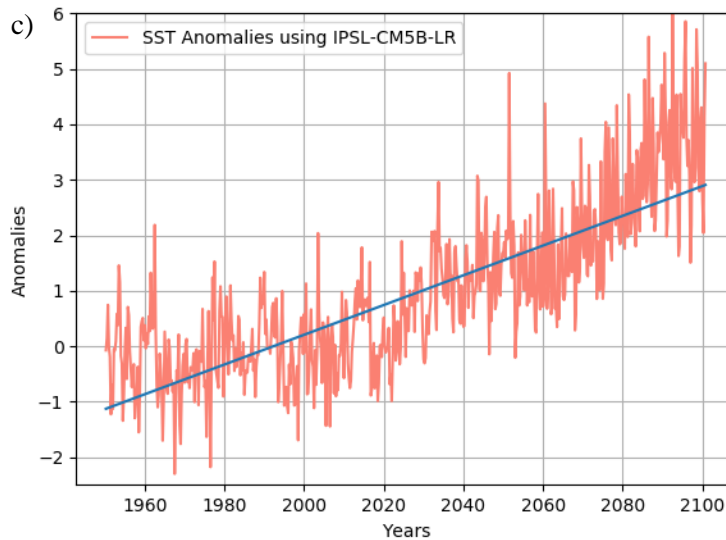
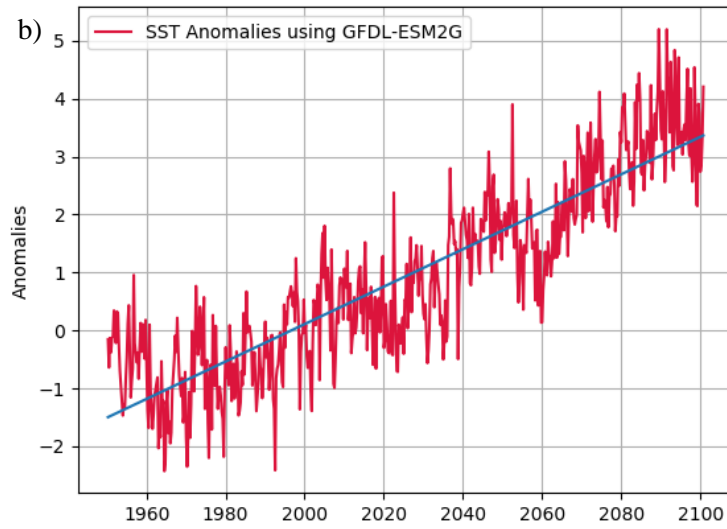
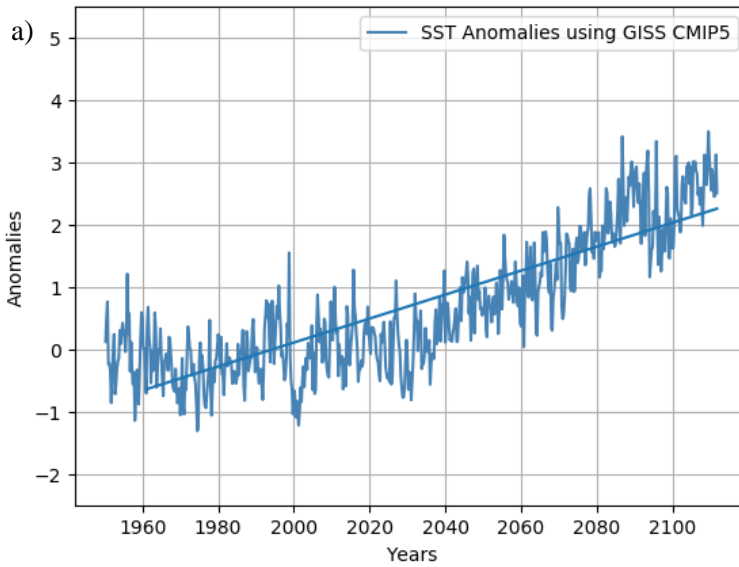


Figure 25: An SST timeseries constructed using CMIP5 RCP8.5 models which demonstrate concentration pathway that lead to concentrations in 2100 that produces a change in forcing of 8.5W/m^2 . These raw seas surface temperature anomaly values were calculated with a base period of 1981-2020 for the region bounded by $155\text{-}142.5^\circ\text{W}$ and $37.5\text{-}45.5^\circ\text{N}$. The blue in each plot represents the trendline overtime. Each Figure is representative of a different CMIP5 model: a) GISS-E2-H b) GFDL-ESM2G c) IPSL-CM5B-LR.

Figure 25 predicts that SST anomalies will increase significantly over time in the region bounded by 155-142.5°W and 37.5-45.5°N.

When comparing the three models, it was found that the most extreme anomalies were evident in the IPSL-CM5B-LR dataset, reaching a maximum anomaly of $>+6^{\circ}\text{C}$ between 2080-2100. The GFDL-ESM2G model forecasts anomalies with a similar size, between 2080-2100, and show a maximum of $+5.2^{\circ}\text{C}$. The GISS-E2-H data set shows values that are approximately 50% of the magnitude seen in the IPSL-CM5B-LR dataset and has a maximum SST anomaly value of $+3.5^{\circ}\text{C}$. With the future impacts of global temperature warming, the values in this particular timeseries seem to be low, especially under the RCP8.5 conditions, which were explained in Section 2.1.3.

The IPSL-CM5B-LR dataset shows increased fluctuation between 2050-2100, suggesting that a sudden increase in SSTa will occur and that extremes will become more frequent. This also occurs in the GFDL-ESM2G dataset, where an increase in fluctuations can be seen from 2080. This can also be seen in the GISS-E2-H dataset from 2080.

This can be quantified by assessing the standard deviation value in each model between the years 2080-2100. The largest value is 1.08°C , in the IPSL-CM5B-LR model, followed by a value of 0.70°C in the GFDL-ESM2G model and finally 0.53°C for the GISS-E2-H model. All trendlines demonstrate a clear positive trend, which will be the evidence of global warming with increasing CO_2 concentrations (Riahi *et al.*, 2011). The correlation coefficient values with time are as follows; GISS-E2-H =0.701, GFDL-ESM2G =0.773, IPSL-CM5B-LR =0.624.

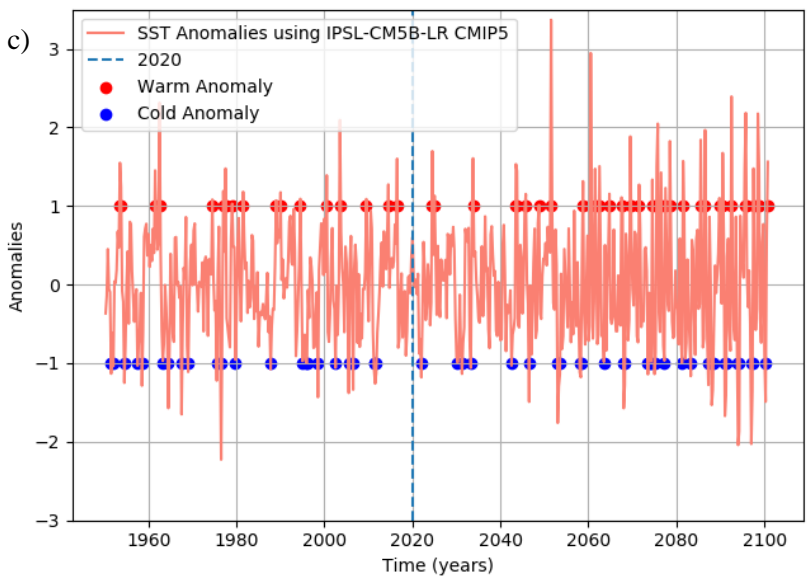
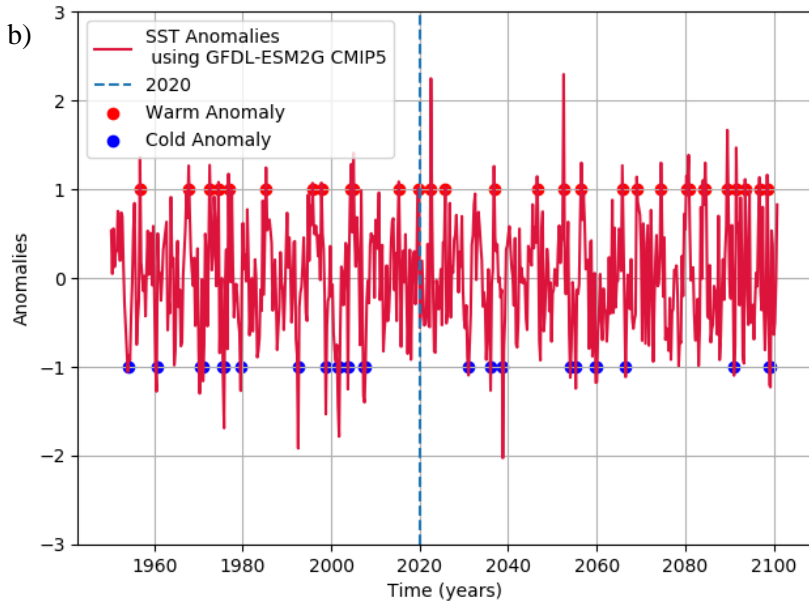
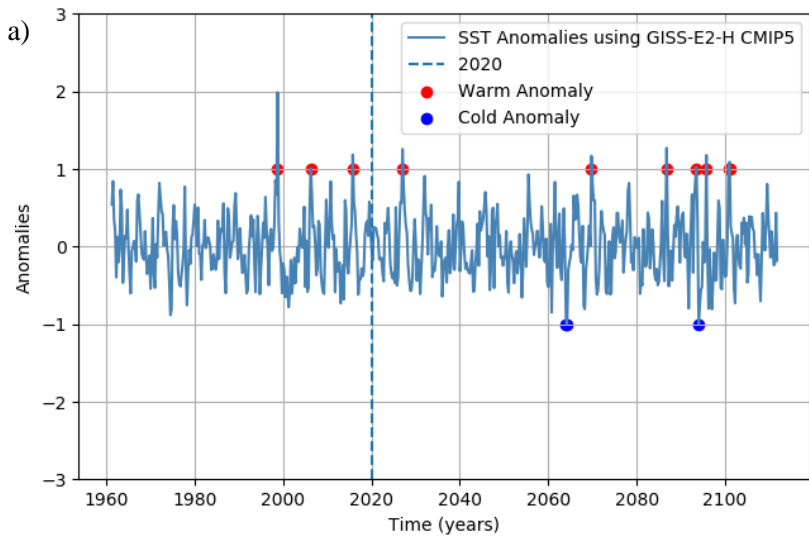


Figure 26: An SST timeseries constructed using CMIP5 RCP8.5 models which demonstrate concentration pathway that lead to concentrations in 2100 that produces a change in forcing of 8.5W/m^2 . These sea surface temperature anomaly values were calculated with a base period of 1981-2020 for the region bounded by $155\text{-}142.5^\circ\text{W}$ and $37.5\text{-}45.5^\circ\text{N}$. An individual five-year average value was removed from its corresponding time period in each model, with an incentive to remove the effects of global warming. Each Figure is representative of a different CMIP5 model: a) GISS-E2-H b) GFDL-ESM2G c) IPSL-CM5B-LR. The red circles demonstrate a suspected Warm Blob ($>1^\circ\text{C}$) and a blue circle indicates a suspected Cold Blob ($<-1^\circ\text{C}$).

Figure 26 was constructed using the same three raw timeseries observed in Figure 25; however, for each individual model a 5-year mean value was removed to its corresponding time period. This was done in an attempt to remove the effects of global warming.

Overall, Figure 26 demonstrates that, under RCP8.5, the frequency of Warm Blobs are expected to increase from 2020. Figures 26b and 26c also suggest that the frequency of Cold Blobs will increase. The largest increase in frequency and intensity of the SST anomalies is observed in the IPSL-CM5B-LR model however, some of these circles may just represent a prolonged period, not separate events.

This increase in frequency can be quantified by assessing the standard deviation value for the period of 2080-2100 in each model. The largest value is 0.88°C in the IPSL-CM5B-LR model, followed by a value of 0.63°C in the GFDL-ESM2G model and finally 0.46°C for the GISS-E2-H. In comparison to the deviation between 1990-2010 are; IPSL-CM5B-LR $=0.59^{\circ}\text{C}$, GFDL-ESM2G $=0.59^{\circ}\text{C}$, GISS-E2-H $=0.45^{\circ}\text{C}$. This demonstrates that in the GISS model the variance of values do not largely differ between the two time periods however, for the IPSL-CM5B-LR and GFDL-ESM2G model, the standard deviation is higher in the later period. This suggests that the intensity and/or frequency of the Warm and Cold Blobs will increase in the period of 2080-2100 when compared to 1990-2010.

The intensity of the Blobs appears to vary significantly in the models with anomaly peaks as large as $+3^{\circ}\text{C}$ even with the effects of the 5-year warming removed. A few spikes in Warm Blob events show a much larger maximum anomaly than is previously observed (Figure 5). The IPSL model shows a peak anomaly of $+3.2^{\circ}\text{C}$, whilst the GFDL model shows peaks of $+2.3^{\circ}\text{C}$. This means that these warm and cold anomalies could increase in intensity in addition to there being in an overall warmer climate. This means that the knock-on impact of the Blob could be more detrimental.

Changes in future morphology

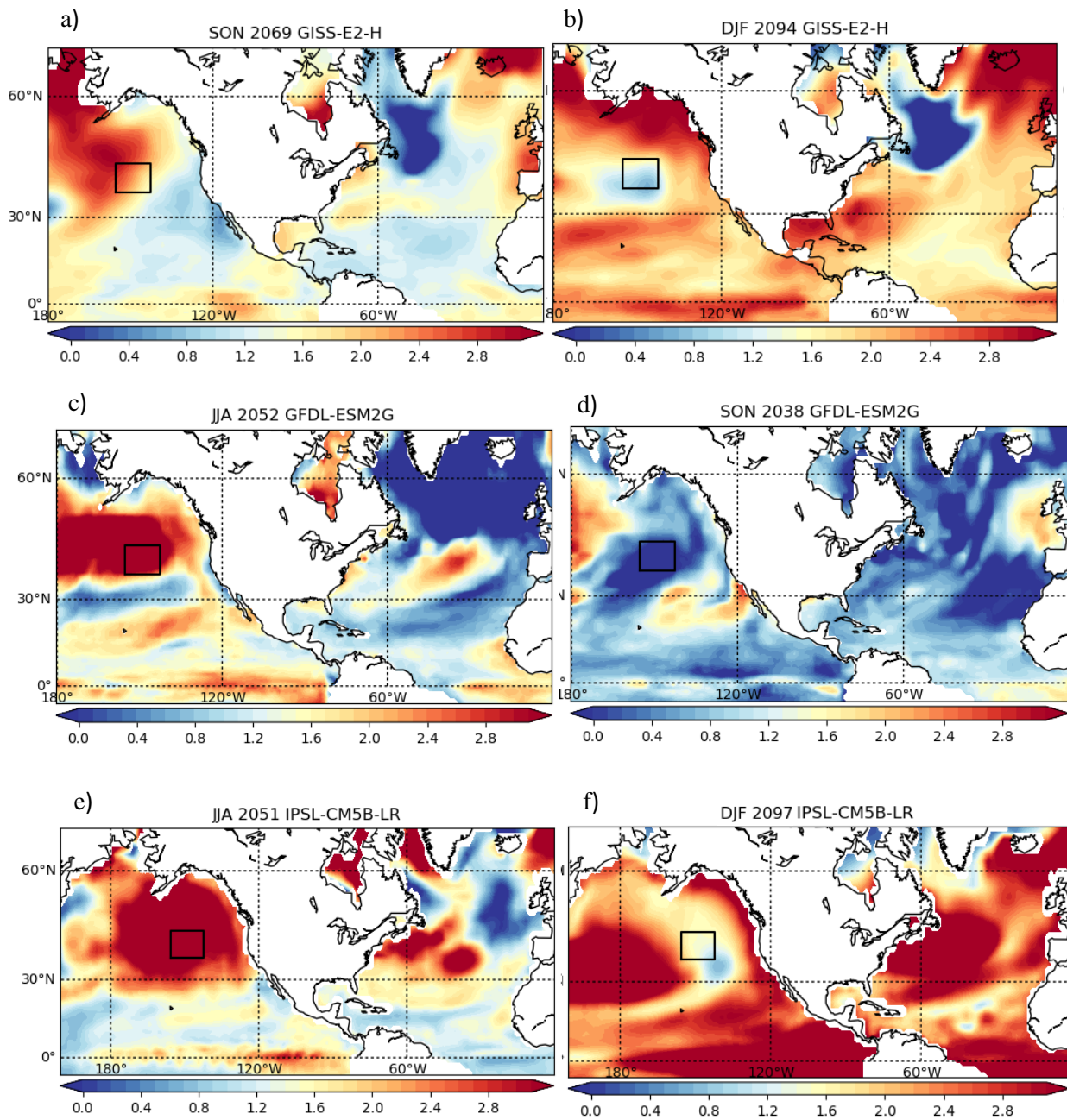


Figure 27: Mapped anomalies to identify future Warm Blobs (a,c,e) and Cold Blobs (b,d,f). These time frames have been identified using Figure 26 highlighting the largest positive and negative values. These Figures use the raw SST data ($^{\circ}\text{C}$) so therefore include the global warming trend. For this reason, negative anomalies are not seen as the base period is set to 1881-2020. Therefore, the lower values are representative of that of a colder anomaly. Each row is representative of a different model: a) GISS-E2-H b) GFDL-ESM2G and c) IPSL-CM5B-LR. The black box marks the region 155-142.5 $^{\circ}$ W and 37.5-45.5 $^{\circ}$ N.

Figure 27 demonstrates that all three model runs found that the Warm Blob will increase in size in the future (Figure 27 a,c,e). The Blob is seen to stretch into the more coastal regions. This characteristic is especially evident from the IPSL-CM5B-LR dataset analysis shown in Figure 27e. It is also expected that the Warm Blob will increase in intensity. Figures 27c and 27e show that temperatures in the centre of the Blob will be greater than +3°C. This intensity is not restricted to the centre of the Blob but affects the entire region. It can also be seen that the Blob is located more northerly than the black box suggested the Warm Blob location has shifted.

In comparison the Cold Blob is less identifiable in Figures 27 b, d and f. Although a Cold Blob can be identified in Figures 27b and f, this region of low SST anomalies is very small. In comparison to the 2094 North Atlantic Cold Blob displayed in Figure 27f, the North Pacific Cold Blob is not as cold. The lower the anomaly the colder the region. Temperature anomalies in the North Atlantic are near to 0 whereas in the North Pacific they are +0.8°C. This could signify that in the future Cold Blobs in this region will weaken and shrink. Figure 27d appears to show anomalies representative of a Warm Blob to the left of the black box. This supports the statement that the location of the Blob has changed and that the centre is perhaps located more westerly. The area bounded by Figure 27d, is most representative of a Cold Blob however, in this year the whole image displays low anomaly values suggesting this is due to climatology rather than the existence of a Cold Blob.

Having mapped these CMIP5 datasets it is noticeable that the GISS-E2-H Figures (27 a and b) are lower resolution than the other datasets. Having assessed Figures 25, 26 and 27, the model deemed most appropriate for this particular study is the IPSL-CM5B-LR. Although the magnitudes in Figure 26 are the largest, having mapped a particular peak magnitude anomaly, it would appear this is most representative of a Warm Blob. The magnitude of the events shown in the timeseries are similar between the GFDL-ESM2G model and the IPSL-CM5B-LR model (Figures 25 and 26), however, as demonstrated by Figure 27d, the suspected Cold Blob event is in fact just a homogeneously cold time period. Unfortunately, only one suspected Warm and Cold Blob were mapped using these models, making it difficult to complete a reliable analysis of future trends.

4.0 Conclusions

4.1 Summary

In addition to identifying several Warm Blob events, this study has identified a corollary Cold Blob off the Gulf of Alaska within the location 155-142.5°W and 37.5-45.5°N. Since 1950, the study found that the Warm Blob has occurred 22 times whereas, the Cold Blob has only occurred 13 times seasonally. This suggests that the Cold Blob is less common than the Warm Blob. The analysis of the SST anomaly timeseries, found that the Warm and Cold Blobs occurred frequently before the 2013/2014 event however, this has not been previously discussed in the literature.

During Warm Blob events the centre of the Blob generally exceeds an SST anomaly of $\sim +1.25^{\circ}\text{C}$. The peak anomaly also occurs in the centre of the Cold Blob with a value $< -1.20^{\circ}\text{C}$. The Warm Blobs occur more often in the summer (41%) however, Warm Blob events that occur in the summer also have the lowest average seasonal anomaly value ($+1.18^{\circ}\text{C}$). One explanation for this could be the climatology in this period, as summer in this region generally experiences warmer SSTs. With this addition of climatology, the temperatures in the centre of the Blob will still be as high as in other seasons respectively. Alternatively, the Cold Blob occurs most frequently in the autumn (54%). However, the Cold Blobs are largest in intensity in the summer, with an average SST anomaly of -1.55°C .

A comparison between the Warm Blob composite image (Figure 11f) and the Cold Blob (12f) demonstrates that the Warm Blob is more homogenous in shape and size whereas, the Cold Blob is more stretched in the longitudinal direction and not as concentrated to the region bounded by the box (155-142.5°W and 37.5-45.5°N).

The relationship between anomalous SSTs in this region and atmospheric teleconnection indices are weak. It was conclusive that the Pacific Decadal Oscillation had the largest seasonal correlation value ($r = -0.3$ for the period 1950-2020), suggesting that the PDO and SST anomalies incurred a negative relationship. With a zero time lag the relationship between ENSO and the SST anomalies were weak (r value close to 0). Therefore, a time lag relationship was tested with the El Niño Southern Oscillation, as it takes time for global teleconnections to alter the atmosphere and ocean circulation and for SSTs to warm or cool in response. It was found that the highest r value incurred an SST anomaly lag of 8/9 months after to the Niño3.4 index ($r = 0.39$).

Coupled climate model simulations demonstrating the historical and future predictions under the RCP8.5 high emissions scenario, were compared to investigate how the Blob region will change in the future. A 5-year mean was removed from its correlated time period in order to minimise the effects of global warming, so the data was more comparable to the observational data. In comparison, it was concluded that Warm Blob events will increase in frequency from 2050-2100 in comparison to 1950-2000. Additionally, with estimated global temperature warming removed the intensity of these Blobs

will increase in comparison to observations significantly, potentially reaching as large as +3°C. The maximum recorded in the observations peaked at +1.9°C. This means that with the addition of the underlying global warming trend, these temperatures could exceed +6°C. This occurrence will also be mirrored in negative temperature anomalies, where the frequency of Cold Blobs will also increase however the magnitude will not (remains with a maximum negative anomaly value of -2.0°C) in comparison to observations. However, in this warmer climate these negative anomalies will be warm values in comparison to the climate observed in 2020. The morphology of the Blob is also seen to change. It is apparent that Warm Blobs will increase in size and stretch into the more coastal regions. In comparison, Cold Blobs will significantly decrease in size.

4.2 Limitations

A limitation of this study is that the SST anomaly dataset differed between raw SST anomaly data and SST anomaly data with the effects of global temperature warming removed. The global temperature dataset is a monthly average anomaly for the northern hemisphere ocean which intends to represent global warming. However, this may not be representative of the change within this specific region.

In this study it was difficult to determine whether to use the raw or modified dataset. When assessing teleconnection patterns the raw dataset was used as these indices were relative. This means that they included global warming trends. However, when assessing mapped SST anomalies, global temperature was removed to identify the largest events independently of global warming.

As demonstrated in Figure 17, the Warm and Cold Blob occurrences differ largely between the raw SST dataset and the modified SST dataset. This is attributed to the method used, which means that each dataset incurs a bias. The raw data set has an underlying cold bias, displaying more Cold Blobs and less Warm Blobs. The other dataset incurs a warm bias, which occurs due to the fact that the mean global temperature effect is not location specific. This reduces the number of cold events and significantly increases the number of warm events.

Future research could analyse absolute teleconnection indices and SST anomalies with a location-based warming removed. If this experiment was to be further developed, instead of using a global dataset, the removal of the 5-year running mean could more accurately determine the warming trend, as was done in Figure 26,.

Another limitation in the methods is the classification of a Warm and Cold Blob. The criteria for identifying a Blob event was determined following an analysis of the HadISST1 data, as criteria had not been created in any previous studies. The Warm Blob is universally defined as a large mass of water in the North Pacific, which has anomalously warm temperatures in relation to climatology and its surrounding region. However, this definition does not define the magnitude of the Blob. To encompass the largest anomalous events, this investigation defined the Blob as the largest 15% of anomaly values

for the period 1880-2020. This was determined using the SST anomaly dataset minus the global temperature anomalies. This ensured that only the largest 15% of anomalies were selected to demonstrate the most intense events above the 85th percentile. This definition could exclude Blob events where less extreme SSTa were observed. Additionally, as no previous research has been done into the Cold Blob, it was assumed that the characteristics of the Cold Blob mirror that of the Warm Blob. Another issue with this method is that the temperature range ($\pm 1^{\circ}\text{C}$) was determined using values between 1880-2020. Alternatively, the majority of the timeseries in this investigation focus on 1950-2020. This could mean that temperature changes in the largest 15% differ from the temperature range used to define these events.

Aforementioned the process of locating the area of focus is limited as the method used is relatively basic. The region was defined using the standard deviation of each grid point overtime for the period 1880-2020. To validate the region chosen (155-142.5°W and 37.5-45.5°N), a standard deviation using only the selected time frames in which the Warm and Cold Blob events are noted to have occurred using Figure 17 (anomalies $>1^{\circ}\text{C}$ and $<-1^{\circ}\text{C}$) could be mapped and cross-referenced to test for similarity. However, as previously mentioned, this timeseries is limited by the dataset used and the warm and cold biases observed.

A limitation of this study also includes the lack of focus on surface energy fluxes. In understanding and quantifying these changes a better explanation of these events could be interpreted as well as a better prediction of the mechanisms. Lau and Nath (2001), investigate the Blob with highlighted attention on atmosphere-ocean fluxes identifying alterations between the ocean through changes in energy and momentum across the sea-air interface. Additionally, they investigate changes in shortwave radiative fluxes associated with variations in cloud cover which further effect the Warm Blob region. The Warm and Cold Blobs could have links with relatively large wind and heat anomalies, these variables should be further investigated.

The correlation between the ENSO index and SST anomalies was investigated to test for a time lag between the two variables. The relationship between teleconnection patterns and the SST anomalies may incur a delay as the atmosphere and ocean can take time in responding to this alteration and be subsequently influenced. Although, this test did identify a time lag of 9 months (the SST anomalies after ENSO), without fundamental evidence of ocean mechanisms, energy budgets of the upper mixed layer, heat advection by ocean currents, and mechanisms which demonstrate how heating alters atmospheric circulation, this time lag cannot be explained.

Additionally, obtaining a longer timeseries of the teleconnection variables may increase the statistical significance of the relationship between the Blob and the atmospheric patterns. The datasets used here only date back as far as 1950; however, data from 1920 may highlight a more robust relationship.

Obviously earlier observations could be less reliable due to the systematic error explained in the methods section of this report.

The linear regression statistical significance test is just one way to assess a correlation between two or more datasets. Through using linear regression, a large assumption of linearity between the dependent and the independent variable is made. However, a non-linear relationship may be more likely if Warm and Cold Blobs are driven by the same mechanisms,. In relation to climate, data is rarely linearly separable due to the chaotic nature of the atmosphere. This linear assumption is a significant limitation in the results section. A T-Test could have been used to examine the statistical difference between the means of two variables. This T-Test could be used determine a correlation between two datasets. Additionally, the phenomena assessed are interconnected and interdependent, each influencing each other in the climate system. This means that a multiple- regression could have been used to test for a relationship between the SST anomalies and all the teleconnections. This test would examine whether the extent of anomalies could be explained by a combination of the phenomena which are deemed to influence this region.

4.3 Future work

Further work is required to investigate a correlation offset between the SSTa of the Blob and SLP anomalies. This should be investigated at each grid point to create a correlation map, showing where the SLP deviation is largest (between the years 1950-2020). Figure 13 shows that the largest deviation of SLP occurs more northward of the box. This is also reflected in the pressure systems that occur during Warm and Cold Blob events. Indicating that the largest SLP anomalies are likely to occur north of the box. Additional research should focus on regions north of the box, to determine whether a correlation exists between the SST anomalies within this box region and SLP anomalies within the largest deviation area.

As identified in Figure 11, the Warm Blob is more homogenous than the Cold Bob. The Cold Blob appears to spread significantly in a longitudinal direction between timeframes and deviates more from the bounded region. The displacement of the Cold Blob should be examined in relation to the location of the bounded region. Further research should identify time frames in which the Cold Blob is furthest from the study area and when it is closest. The seasonality of this displacement could also be assessed to evaluate whether a certain season is susceptible to this spreading characteristic. The corresponding intensity of the anomaly should be noted, to establish if a more intense anomaly associates with more or less spreading from the identified region.

Aforementioned in limitations (Section 4.1), the result from the ENSO time lag investigation cannot answer the question: is the Warm/Cold Blob a consequence of the teleconnection pattern, or do the anomalies induce the teleconnection? Further studies should build on the ENSO time lag results, from Figure 19, to assess ocean and atmosphere mechanisms. This will provide an explanation for the ENSO

time lag results. This analysis should investigate variables such as; cloud cover (to understand the radiation budget), heat content (to understand the transportation of heat overtime from the teleconnection region), wind speed/direction, and wind stress (to develop an understanding of how the atmosphere circulates these warmer temperatures). All these variables are available via the KNMI explorer and would support the results of this project. A further time lag analysis, investigating SST anomalies, should be completed for other teleconnections such as; the PDO, NAO and AO.

A greater number of CMIP5 models would provide a more significant simulation of future Blobs under RCP8.5. Assessing more models would develop the understanding of changes this region could experience approaching the year 2100. This will better allow for the identification of Warm and Cold Blob events and their corresponding magnitude.

The use of multiple CMIP5 models and observations would also allow for the comparison between models and observations. This would enable the identification of the optimum simulation and would minimise any limitations caused by one specific model. Through this assessment, a composite of the 5 models deemed most appropriate to this investigation could be created and the frequency and intensity of Warm and Cold Blobs with time could be determined.

In future work that uses the CMIP5 models, the global warming signal would need to be removed to allow for a more reliable comparison between the dataset and observations. This could be done by removing a running mean of a chosen timeframe (i.e. 5, 7 or 10 years). Analysis should then be completed to compare the effect of the removal of the running mean at different timeframes. From this analysis the most similar time series to the observational run should be identified and used in future studies.

In addition to this further CMIP5 investigation, it may be of interest to examine CMIP5 model runs of average land temperature anomalies and associated sea level pressure anomalies under RCP8.5. These variables should be compared to the SST anomalies to test for a relationship at different time frames. This will enable a greater understanding of how the Blob will characteristically change with time, and the impacts of the Blob on the surrounding climate. These variable simulations could also be compared to observational datasets to test for corroboration. From this analysis, we can identify the characteristics and effects of the Blob in the past, present and future.

iii) References

- Alexander, M. A., D. J. Vimont, P. Chang, and J. D. Scott, 2010: The impact of extratropical atmospheric variability on ENSO: Testing the seasonal foot printing mechanism using coupled model experiments. *J. Climate*, **23**(11), 2885–2901
- Allan, R. and T. Ansell, 2006: A New Globally Complete Monthly Historical Gridded Mean Sea Level Pressure Dataset (HadSLP2): 1850–2004. *J. Climate*, **19**, 5816–5842, doi:10.1175/JCLI3937.1
- Amaya, D.J., A.J. Miller, S. Xie, *et al.* 2020: Physical drivers of the summer 2019 North Pacific marine heatwave. *Nat Commun*, **11**, 1903, <https://doi.org/10.1038/s41467-020-15820-w>
- An, S., and F. Jin, 2004: Nonlinearity and Asymmetry of ENSO. *J. Climate*, **17**, 2399–2412, [https://doi.org/10.1175/1520-0442\(2004\)017<2399:NAAOE>2.0.CO;2](https://doi.org/10.1175/1520-0442(2004)017<2399:NAAOE>2.0.CO;2)
- Bakker, P., A. Schmittner, J.T.M. Lenaerts, A. Abe-Ouchi, M. Van den Broeke and J. Yin, 2016: Fate of the Atlantic Meridional Overturning Circulation: Strong decline under continued warming and Greenland melting. *Geophysical Research Letters*, **43**, 12,252–12,260. <https://doi.org/10.1002/2016GL070457>
- Barnston, A. G., and R. E. Livezey, 1987: Classification, seasonality, and persistence of low-frequency atmospheric circulation patterns. *Mon. Wea. Rev.*, **115**, 1083–1126
- Barry D. Keim, R.A. Muller, Gregory W. Stone, 2004: Spatial and temporal variability of coastal storms in the North Atlantic Basin. *Marine Geology*, **210**, Issues 1–4, <https://doi.org/10.1016/j.margeo.2003.12.006>.
- Benesty, J., J. Chen, Y. Huang, and I. Cohen, 2009: Pearson correlation coefficient. In Noise reduction in speech processing, *Springer*, 37–40
- Bond, N. A., M. F. Cronin, H. Freeland, and N. Mantua, 2015: Causes and impacts of the 2014 warm anomaly in the NE Pacific, *Geophys. Res. Lett.*, **42**, 3414–3420, doi:10.1002/2015GL063306.
- Bylhouwer, B., D. Ianson, and K. Kohfeld, 2013: Changes in the onset and intensity of wind-driven upwelling and downwelling along the North American Pacific coast. *J. Geophys. Res. Oceans*, **118**, 2565–2580, doi:10.1002/jgrc.20194.
- Capotondi, A., P.D. Sardeshmukh, E. Di Lorenzo, 2019: Predictability of US West Coast Ocean Temperatures is not solely due to ENSO. *Sci Rep* **9**, **10993**, <https://doi.org/10.1038/s41598-019-47400-4>.
- Cavole, L. M. *et al.*, 2016: Biological impacts of the 2013–2015 warm-water anomaly in the Northeast Pacific: winners, losers, and the future. *Oceanography*, **29**, 273–285.

- Chan, J. C. L., 2000: Tropical cyclone activity over the western North Pacific associated with El Niño and La Nina events. *J. Climate*, **13**, 2960–2972.
- Chen, D.K, T. Lian, C.B.Fu, M.A.Cane, Y.M.Tang, R.Murtugudde, X.S.Song, Q.Y.Wu and L.Zhou, 2015: Strong influence of westerly wind bursts on El Niño diversity. *Nat Geosci*, **8(5)**, 339–345
- Cheng, L., and Coauthors, 2020: Record-setting ocean warmth continued in 2019. *Adv. Atmos. Sci.*, **37(2)**, 137–142, <https://doi.org/10.1007/s00376-020-9283-7>.
- Cohen, J., Furtado, J. C., Jones, J., Barlow, M., Whittleston, D. & Entekhabi, D, 2014: Linking Siberian snow cover to precursors of stratospheric variability. *J. Clim.* **27**, 5422–5432.
- Cohen, J., Furtado, J., Barlow, J. M., Alexeev, V. & Cherry, J, 2012: Arctic warming, increasing fall snow cover and widespread boreal winter cooling. *Environ. Res. Lett.* **7**, 014007.
- Delworth, T. L., and F. Zeng, 2016: The impact of North Atlantic Oscillation on climate through its influence on the Atlantic Meridional Overturning Circulation, *J. Climate*, **29**, 941-962, doi:10.1175/JCLI-D-15-0396.1.
- Di Lorenzo, E., and N. Mantua, 2016: Multi-year persistence of the 2014/15 North Pacific marine heatwave. *Nat. Climate Change*, **6**, 1042–1047, doi:10.1038/nclimate3082.
- Di Lorenzo, E., N.Schneider, K.M.Cobb, P.J.S. Franks, K.Chhak, A.J. Miller and P.Rivière, 2008: North Pacific Gyre Oscillation links ocean climate and ecosystem change. *Geophysical Research Letters*, **35**, <https://doi.org/10.1029/2007GL032838>
- Feldstein, S. B., and C. Franzke, 2006: Are the North Atlantic Oscillation and the Northern Annular Mode Distinguishable?. *J. Atmos. Sci.*, **63**, 2915–2930, <https://doi.org/10.1175/JAS3798.1>.
- Feng, J., Z. Wu, and X. Zou, 2014: Sea Surface Temperature Anomalies off Baja California: A Possible Precursor of ENSO. *J. Atmos. Sci.*, **71**, 1529–1537, <https://doi.org/10.1175/JAS-D-13-0397.1>.
- Folland C.K., M.J. Salinger, N. Jiang and N.A. Rayner, 2003: Trends and variations in South Pacific island and ocean surface temperatures. *J. Climate*.
- Freeland and Ross, 2019: ‘The Blob’ - or, how unusual were ocean temperatures in the Northeast Pacific during 2014-2018, *Deep Sea Research Part I: Oceanographic Research Papers*, 10.1016/j.dsr.2019.06.007.
- Freeland, H. and F. Whitney, 2014: Unusual warming in the Gulf of Alaska. *PICES Press*, **22(2)**, 51-52.

- Frölicher, T. and C. Laufkötter, 2018: Emerging risks from marine heat waves. *Nature Communications*, **9**, 650, 10.1038/s41467-018-03163-6.
- Gastineau, G., and C. Frankignoul, 2015: Influence of the North Atlantic SST variability on the atmospheric circulation during the twentieth century. *J. Climate*, **28**, 1396-1416, doi:10.1175/JCLI-D-14-00424.1.
- Grossi, D., M. Monim, and A. Gangopadhyay, 2017: Global Climate Patterns: An Overview of Arctic Oscillation, Pacific Decadal Oscillation, Pacific/North American Pattern, and El Niño Southern Oscillation, *School for Marine Science & Technology Technical Report SMAST*, **17**, 4-10
- Hakim, G. J., 2003: Developing wave packets in the North Pacific storm track. *Mon. Wea. Rev.*, **131**, 2824–2837.
- Hare, S. R., and N. J. Mantua, 2000: Empirical evidence for North Pacific regime shifts in 1977 and 1989. *Progress in Oceanography*, **47**, 103–145
- Hartmann, D. L., 2015: Pacific sea surface temperature and the winter of 2014, *Geophys. Res. Lett.*, **42**, doi:10.1002/2015GL063083.
- Hickey, B. M. and T. Royer, 2001: California and Alaskan Currents. *Encyclopedia of Ocean Sciences. Academic Press*, 368–379
- Hoell, A., and C. Funk, 2013: The ENSO-Related West Pacific Sea Surface Temperature Gradient. *J. Climate*, **26**, 9545–9562, <https://doi.org/10.1175/JCLI-D-12-00344.1>
- Hong, C., Hsu, H., Tseng, W. *et al.*, 2017: Extratropical Forcing Triggered the 2015 Madden–Julian Oscillation–El Niño Event. *Sci Rep* **7**, **46692**, <https://doi.org/10.1038/srep46692>
- Hu, Z.-Z., A. Kumar, B. Huang, J. Zhu, and Y. Guan, 2014: Prediction skill of North Pacific variability in NCEP Climate Forecast System version 2: Impact of ENSO and beyond. *J. Climate*, **27**, 4263–4272, doi:<https://doi.org/10.1175/JCLI-D-13-00633.1>.
- Hu, Z.-Z., A. Kumar, B. Jha, J. Zhu, and B. Huang, 2017: Persistence and predictions of the remarkable warm anomaly in the northeastern Pacific Ocean during 2014–16. *J. Climate*, **30**, 689–702, doi:<https://doi.org/10.1175/JCLI-D-16-0348.1>
- Hu, Z.-Z., and B. Huang, 2006: On the significance of the relationship between the North Atlantic Oscillation in early winter and Atlantic sea surface temperature anomalies. *J. Geophys. Res.*, **111**, doi:<https://doi.org/10.1029/2005JD006339>
- Huyer, A, 1983: Coastal upwelling in the California current system. *Prog. Oceanogr.* **112**, 259–284.

- Jacox, M.G., D. Tommasi, M.A. Alexander, G. Hervieux and C.A. Stock, 2019: Predicting the Evolution of the 2014–2016 California Current System Marine Heatwave From an Ensemble of Coupled Global Climate Forecasts. *Front. Mar. Sci.* **6**(497), doi: 10.3389/fmars.2019.00497
- Jin, E. K., and Coauthors, 2008: Current status of ENSO prediction skill in coupled ocean–atmosphere models. *Climate Dyn.*, **31**, 647–664.
- Jo, H.S., S.W. Yeh and C.H. Kim, 2013: A possible mechanism for the North Pacific regime shift in winter of 1998/1999. *Geophysical Research Letters*, **40**, 4380–4385. <https://doi.org/10.1002/grl.50798>
- Johnson, N. C., D. C. Collins, S. B. Feldstein, M. L. L’Heureux, and E. E. Riddle, 2014: Skillful Wintertime North American Temperature Forecasts out to 4 Weeks Based on the State of ENSO and the MJO. *Wea. Forecasting*, **29**, 23–38, <https://doi.org/10.1175/WAF-D-13-00102.1>
- Jones, C. D., M. Collins, P. M. Cox, and S. A. Spall, 2001: The Carbon Cycle Response to ENSO: A Coupled Climate–Carbon Cycle Model Study. *J. Climate*, **14**, 4113–4129
- Kalnay E and Coauthors, 1996: The NCEP/NCAR 40-year reanalysis project. *Bull. Amer. Meteorol. Soc.*, **77**, 437–471.
- Kennedy J.J., Rayner, N.A., Smith, R.O., Saunby, M. and Parker, D.E, 2011a: Reassessing biases and other uncertainties in sea-surface temperature observations since 1850 part 1: measurement and sampling errors. *J. Geophys. Res.*, **116**, D14103, >doi:10.1029/2010JD015218
- Kennedy J.J., Rayner, N.A., Smith, R.O., Saunby, M. and Parker, D.E, 2011b: Reassessing biases and other uncertainties in sea-surface temperature observations since 1850 part 2: biases and homogenisation. *J. Geophys. Res.*, **116**, D14104, doi:10.1029/2010JD015220
- Kintisch, E., 2015: ‘The Blob’ invades Pacific, flummoxing climate experts. *Science*, **348**, 17–18.
- Larsen, C.F., R.J. Motyka, A.A. Arendt, K.A. Echelmeyer, and P.E. Geissler. 2007: Glacier changes in southeast Alaska and northwest British Columbia and contribution to sea level rise. *Journal of Geophysical Research*, **112**, F0100
- Lau, N., and M. J. Nath, 2001: Impact of ENSO on SST Variability in the North Pacific and North Atlantic: Seasonal Dependence and Role of Extratropical Sea–Air Coupling. *J. Climate*, **14**, 2846–2866, [https://doi.org/10.1175/1520-0442\(2001\)014<2846:IOEOSV>2.0.CO;2](https://doi.org/10.1175/1520-0442(2001)014<2846:IOEOSV>2.0.CO;2)
- Lee, T., I. Fukumori, and B. Tang, 2004: Temperature advection: Internal versus external processes, *J. Phys. Oceanogr.*, **34**, 1936–1944.
- Liang, Y., J. Yu, E. S. Saltzman, and F. Wang, 2017: Linking the Tropical Northern Hemisphere Pattern to the Pacific Warm Blob and Atlantic Cold Blob. *J. Climate*, **30**, 9041–9057, <https://doi.org/10.1175/JCLI-D-17-0149.1>.

- Lima, F. P. and D.S. Wethey, 2012: Three decades of high-resolution coastal sea surface temperatures reveal more than warming. *Nat. Commun.* **3**, 1–13, DOI: 10.1038/ncomms1713.
- Loeb *et al.*, 2012: New Generation of Climate Models Track Recent Unprecedented Changes in Earth's Radiation Budget Observed by CERES, *Geophys. Res. Lett.*, **47**, doi:10.1029/2019GL086705.
- Lyu, M., M. Wen and Z. Wu , 2018: Possible contribution of the inter-annual Tibetan Plateau snow cover variation to the Madden–Julian oscillation convection variability. *Int J Climatol.* **38**, 3787–3800. <https://doi.org/10.1002/joc.5533>
- Maloney, E. D., and D. L. Hartmann, 2000: Modulation of Eastern North Pacific Hurricanes by the Madden–Julian Oscillation. *J. Climate*, **13**, 1451–1460, [https://doi.org/10.1175/1520-0442\(2000\)013<1451:MOENPH>2.0.CO;2](https://doi.org/10.1175/1520-0442(2000)013<1451:MOENPH>2.0.CO;2)
- Mantua, N.J. and S.R. Hare, Y. Zhang, J.M. Wallace, and R.C. Francis, 1997: A Pacific interdecadal climate oscillation with impacts on salmon production. *BAMS*, **78**, 1069-1079.
- McPhaden, M. J., and J. Picaut, 1990: El Niño-Southern Oscillation displacements of the western equatorial Pacific warm pool, *Science*, **250**, 1385-1388.
- Miller, L. and R.E. Cheney, 1990: Large-scale meridional transport in the tropic Pacific Ocean during the 1986–87 El Niño from GEOSAT. *J. Geophys. Res.* **95**, 17 905–17 919.
- Newman, M., G. P. Compo, and M. A. Alexander, 2003: ENSO-Forced Variability of the Pacific Decadal Oscillation. *J. Climate*, **16**, 3853–3857, [https://doi.org/10.1175/1520-0442\(2003\)016<3853:EVOTPD>2.0.CO;2](https://doi.org/10.1175/1520-0442(2003)016<3853:EVOTPD>2.0.CO;2).
- NOAA, 2017: Climate Prediction Centre Monthly(CPC)Arctic Oscillation Index, Accessed: 10th August 2020, <https://catalog.data.gov/dataset/climate-prediction-center-monthlycpcarctic-oscillation-index>
- NOAA, 2016: Visualize NOAA High-Resolution Blended Analysis Data, Accessed: 10th August 2020, <http://www.esrl.noaa.gov/psd>.
- Oldenborgh, G.J. van and G. Burgers, 2005: Searching for decadal variations in ENSO precipitation teleconnections, *Geophys. Res. Lett.*, **32**, 15, L15701, doi:10.1029/2005GL023110
- Overland, J.E, Wang, M., 2005, The Arctic climate paradox: The recent decrease of the Arctic Oscillation, *Geophysical Research Letters*, **32**, L06701, doi:10.1029/2004GL021752
- Oyler J.W, Ballantyne, A., Jencso, K., Sweet ,M., Running, S.W., 2014: Creating a topoclimatic daily air temperature dataset for the conterminous United States using homogenized station data and remotely sensed land skin temperature. *RMets. Wiley*, **35**, 2258-2279, DOI: 10.1002/joc.4127

- Peterson, W., M. Robert and N. Bond, 2015: The Warm Blob continues to dominate the ecosystem of the northern California current. *PICES Press*, **23(2)**, 44-46.
- Rahmstorf, S., J. E. Box, G. Feulner, M. E. Mann, A. Robinson, S. Rutherford, and E. J. Schafersicht, 2015: Exceptional twentieth century slowdown in Atlantic Ocean overturning circulation. *Nat. Climate Change*, **5**, 475-480, doi:10.1038/NCLIMATE2554.
- Rayner, N. A., Parker, D. E., Horton, E. B., Folland, C. K., Alexander, L. V., Rowell, D. P., Kent, E. C., Kaplan, 2003: A. Global analyses of sea surface temperature, sea ice, and night marine air temperature since the late nineteenth century. *J. Geophys. Res.* **108**, 14-4407, DOI:10.1029/2002JD002670
- Riahi, K. and Coauthors, 2011: RCP 8.5—A scenario of comparatively high greenhouse gas emissions. *Climatic Change* *109*, **33**, <https://doi.org/10.1007/s10584-011-0149-y>
- Riddle, E. E., M. B. Stoner, N. C. Johnson, M. L. L'Heureux, D. C. Collins, and S. B. Feldstein, 2013: The impact of the MJO on clusters of wintertime circulation anomalies over the North American region. *Climate Dyn.*, **40**, 1749–1766
- Rohde, R. and Coauthors, 2013: Berkeley Earth Temperature Averaging Process. *Geoinfor Geostat*, **1**, 1-13, <http://dx.doi.org/10.4172/gigs.1000103>
- Seager, R., M. Hoerling, S. Schubert, H. Wang, B. Lyon, A. Kumar, J. Nakamura, and N. Henderson, 2015: Causes of the 2011–14 California drought. *J. Climate*, **28**, 6997–7024, doi:<https://doi.org/10.1175/JCLI-D-14-00860.1>.
- Serreze, M. C., Barrett, A. P., Stroeve, J. C., Kindig, D. M. & Holland, M. M., 2009: The emergence of surface-based Arctic amplification. *Cryosphere*, **3**, 11–19
- Sheppard, C. and Rayner, N., 2002: Utility of the Hadley Centre sea ice and sea surface temperature data set (HadISST1) in two widely contrasting coral reef areas. *Marine Pollution Bulletin*, **44**, 303-308, [https://doi.org/10.1016/S0025-326X\(02\)00059-0](https://doi.org/10.1016/S0025-326X(02)00059-0).
- Shindell, D. T. and Coauthors, 2013: Interactive ozone and methane chemistry in GISS2 historical and future climate simulations. *Atmos. Chem. Phys.*, **13**, 2653–2689
- Sippel, S., N. Meinshausen, A. Merrifield, F. Lehner, A. G. Pendergrass, E. Fischer, and R. Knutti, 2019: Uncovering the Forced Climate Response from a Single Ensemble Member Using Statistical Learning. *J. Climate*, **32**, 5677–5699, <https://doi.org/10.1175/JCLI-D-18-0882.1>
- Swain, D.L., M. Tsiang, M. Haugen, D. Singh, A. Charland, B. Rajaratnam, and N.S. Diffenbaugh, 2014 : The extraordinary California drought of 2013/2014: character, context, and the role of climate change. *Bull. Am. Meteorol Soc.*, **95(9)**, 553-597.

- Taylor, K. E., R. J. Stouffer, and G. A. Meehl, 2012: An Overview of CMIP5 and the Experiment Design. *Bull. Amer. Meteor. Soc.*, **93**, 485–498, <https://doi.org/10.1175/BAMS-D-11-00094.1>.
- Thompson, D. W. J., and J. M. Wallace, 1998: The Arctic Oscillation signature in the wintertime geopotential height temperature fields. *Geophys. Res. Lett.*, **25**, 1297–1300.
- Tseng, Y.H, Ding, R., Huang, X., 2017: The Warm Blob in the northeast Pacific—the bridge leading to the 2015/16 El Niño, *Environ. Res. Lett.*, **12**, 54-119, doi: 10.1088/1748-9326/aa67c3
- Wang, S.-Y., L. Hips, R. R. Gillies, and J.-H. Yoon, 2014: Probable causes of the abnormal ridge accompanying the 2013–2014 California drought: ENSO precursor and anthropogenic warming footprint, *Geophys. Res. Lett.*, **41**, 3220–3226, doi:10.1002/2014GL059748.
- Wen, C., Y. Xue, and A. Kumar, 2012: Seasonal prediction of North Pacific SSTs and PDO in the NCEP CFS hindcasts. *J. Climate*, **25**, 5689–5710, doi:<https://doi.org/10.1175/JCLI-D-11-00556.1>
- Xue, Y., M. Chen, A. Kumar, Z.-Z. Hu, and W. Wang, 2013: Prediction skill and bias of tropical Pacific sea surface temperatures in the NCEP Climate Forecast System version 2. *J. Climate*, **26**, 5358–5378, doi:<https://doi.org/10.1175/JCLI-D-12-00600.1>.
- Xue, Yan, R. W. Higgins, H.-K. Kim and V. Kousky, 2002: Impacts of the Madden Julian Oscillation on U.S. Temperature and Precipitation during ENSO Neutral and Weak ENSO Winters. 26th Climate Diagnostics and Prediction Workshop. [Available at <http://www.cpc.ncep.noaa.gov/products/outreach/CDW26.html>]
- Yang, Q. and Coauthors, 2019: How “The Blob” affected groundfish distributions in the Gulf of Alaska. *Fish Oceanogr.*, **28**, 434–453, <https://doi.org/10.1111/fog.12422>
- Ying, J., P. Huang, and R. H. Huang, 2016: Evaluating the formation mechanisms of the equatorial Pacific SST, *Institute of Atmospheric Physics*, **33**, 433-441, doi: 10.1007/s00376-015-5184-6.
- Zhang, Y., J.M. Wallace and D.S. Battisti, 1997: ENSO-like interdecadal variability: 1900–93 *J. Clim.*, **10**, 1004–1020.
- Zhang, Q., J. Gottschalck, and Y. Xue, 2007: Extension of the CPC MJO Index to Forecast Mode. *American Meteorological Society 16th Conference on Applied Climatology*, **4**, doi: 10.1.1.554.3172
- Zhi, H., P. Lin, R. Zhang, F. Chai and H. Liu, 2019: Salinity effects on the 2014 warm “Blob” in the Northeast Pacific. *Acta Oceanol. Sin.* **38**, 24–34. <https://doi.org/10.1007/s13131-019-1450-2>